Technische Universität München

II. Medizinische Klinik und Poliklinik

Klinikum rechts der Isar

Dual-recombination system for time- and host-specific targeting of pancreatic ductal adenocarcinoma

Kathleen Schuck

Vollständiger Abdruck der von der Fakultät für Medizin der Technischen Universität München zur Erlangung des akademischen Grades eines

Doktors der Naturwissenschaften

genehmigten Dissertation.

Vorsitzender:	Prof. Dr. Marc Schmidt-Supprian
Prüfer der Dissertation:	1. apl. Prof. Dieter K.M. Saur
	2. Prof. Angelika Schnieke, Ph.D.

Die Dissertation wurde am 21.12.2016 bei der Technischen Universität München eingereicht und am 12.07.2017 durch die Fakultät für Medizin angenommen.

I List of Contents

II List of Figures

III List of Tables

IV Abbreviations

°C	degree Celsius
2-ME	2-mercaptoethanol
4-OHT	4-hydroxytamoxifen
5-FU	5-fluorouracil
A	adenine
ADM	acinar-to-ductal metaplasia
AFL	atypical flat lesion
AFN	Atipamezole-Flumazenil-Naloxone
APS	ammonium persulfate
BRCA2	breast cancer 2
BrdU	5-bromo-2'-deoxyuridine
BSA	bovine serum albumin
C	cytosine
CAF	cancer-associated fibroblast
CDKN2A	cyclin-dependent kinase Inhibitor 2A
CK19	cytokeratin 19
cm	centimeter
CO_2	carbon dioxide
Cpa3	carboxypeptidase A3
ddH2O	bidistilled water
D-MEM	Dulbecco's modified eagle medium
DMSO	dimethylsulfoxide
DNA	deoxyribonucleic acid
DPC4	deleted in pancreatic cancer locus 4
DTT	dithiothreitol
ECM	extracellular matrix
EDTA	ethylenediaminetetraacetic acid
eGFP	enhanced green fluorescent protein
EGFR	epidermal growth factor receptor
EMT	epithelial-mesenchymal transition

ER	estrogen receptor
Erk	mitogen-activated protein kinase kinase kinase 1
et al.	et alii
EtOH	ethanol
FAP	fibroblast activating protein
FCS	fetal calf serum
FcεRI	high-affinity IgE receptor
FGFR	fibroblast growth factor receptor
frt	Flippase recognition target
FSF	frt-STOP-frt
FSP	fibroblast-specific protein
g	gram
G	guanine
GAP	GTPase-activating protein
GEF	guanine nucleotide exchange factors
GEMM	genetically engineered mouse model
GFAP	glial fibrillary acidic protein
GTP	guanosine triphosphate
h	hours
H&E	hematoxylin and eosin
H_2O_2	hydrogen peroxide
HCl	hydrochloric acid
HEPES	4-(2-hydroxyethyl)-1-piperazineethanesulfonic acid
hGFAP	human glial fibrillary acidic protein
i.p.	intraperitoneal
IgE	immunoglobulin E
IGF	insulin-like growth factor
IPMN	intraductal papillary mucinous neoplasm
kb	kilobase pairs
KC	*Pdx1-Cre;LSL-Kras$^{G12D/+}$*
KF	*Pdx1-Flp;FSF-Kras$^{G12D/+}$*
KPC	*Pdx1-Cre;LSL-Kras$^{G12D/+}$;LSL-p53$^{R172H/+}$*

KPF	*Pdx1-Flp;FSF-Kras$^{G12D/+}$;p53$^{frt/+}$*
Kras	v-Ki-ras2 Kirsten rat sarcoma viral oncogene homolog
L	liter
LBD	ligand-binding domain
LKB1/STK11	liver kinase B1 / serine/threonine kinase 11
LOH	loss of heterozygosity
loxP	locus of X-over of P1
LSL	loxP-stop-loxP
LSM	Laser scanning microscope
M	mol / molar
MAPK	mitogen-activated protein kinase
MCN	mucinous cystic neoplasm
Mek	mitogen-activated protein kinase kinase
mg	milligram
mGFAP	murine glial fibrillary acidic protein
min	minutes
mL	milliliter
mM	millimol / millimolar
MMF	Midazolam, Medetomidine, Fentanyl
MMP	matrix metalloproteinase
MTT	3-(4,5-deimethylthiazol-2-yl)-2,5-diphenyl tetrazolium bromide
mut	mutated
NG2	neuron glial antigen-2
nM	nanomol / nanomolar
nm	nanometer
OD	optical density
p	phospho
PanIN	pancreatic intraepithelial neoplasia
PBS	phosphate buffered saline
PCR	polymerase chain reaction
PDAC	pancreatic ductal adenocarcinoma
PDGFR	platelet-derived growth factor receptor

Pdk1	3-phosphoinositide-dependent protein kinase 1
Pdx1	pancreatic and duodenal homeobox 1
PFA	paraformaldehyde
PI3K	phosphoinositide 3-kinase
pp	base pairs
PSC	pancreatic stellate cells
Ptf1a	pancreas transcription factor subunit alpha
PVDF	polyvinylidene fluoride
R26	Rosa26
RNA	ribonucleic acid
rpm	rounds per minute
RT	room temperature
SCF	stem cell factor
SDS	sodium dodecyl sulfate
sec	seconds
SHH	Sonic hedgehog
Sm22	smooth muscle protein 22 alpha
SMAD4	mothers against decapentaplegic homolog 4
T	thymine
TAE	tris acetate EDTA
TAF	tumor-associated fibroblast
TAM	tamoxifen
TEMED	N,N,N',N'-tetramethylethylenediamine, 1,2-bis(dimethylamino)-ethane
TGFβ	transforming growth factor β
TIMP	tissue inhibitor of metalloproteinases
TP53 / p53	transformation related protein 53
Tris	tris-(hydroxymethyl)-aminomethan
U	unit
V	volt
VDR	vitamin D receptor
VEGF	vascular endothelial growth factor
WT	wild type

αSMA	alpha smooth muscle actin
µg	microgram
µL	microliter
µM	micromol / micromolar

1 INTRODUCTION

1.1 PANCREATIC DUCTAL ADENOCARCINOMA (PDAC)

Cancer is currently the second leading cause of death in the US. Pancreatic cancer is the fourth leading cause of cancer-related death (Siegel et al., 2015) and is predicted to be the second leading cause of cancer-related death in the US in 2030 (Rahib et al., 2014). Whereas incidence rates are declining for most cancer types, the incidence rates are increasing for pancreatic cancer (48.960 new cases estimated in 2015 in the US) as well as the rates of death for pancreatic cancer (40.560 deaths estimated in 2015 in the US) (Siegel et al., 2015). No early symptoms, no available blood or urine biomarker and late unspecific symptoms lead to late diagosis by abdominal ultrasound scans, magnetic resonance imaging or computed tomography. The treatment did not improve much and the 5-year survival rate has not changed over the last decades and is still around 7 %. In case of late diagnosis the 5-year survival rate decreases to 2 % (Siegel et al., 2015).

Pancreatic ductal adenocarcinomas (PDAC) account for over 90 % of pancreatic cancer (Feldmann and Maitra, 2008; Gopinathan et al., 2015) and the median survival is about 6 months. For most cases, PDAC arises in the head of the pancreas (Andea et al., 2003; Kozuka et al., 1979). Most patients are diagnosed at a late stage of the disease, have often developed metastases and are therefore not suitable candidates for surgery (Neesse et al., 2015). Only up to 20 % of patients with pancreatic cancer are fitting for surgery and the resection of the pancreas (Butturini et al., 2008; Chames et al., 2010). Of those patients who underwent surgery only about 20 % survive 5 years (Schneider et al., 2005). The cause for the development of pancreatic cancer is still not fully answered. There are known risk factors like smoking, long-standing diabetes mellitus, obesity, non-O blood type, and chronic pancreatitis (Amundadottir et al., 2009; Everhart and Wright, 1995; Fuchs et al., 1996; Gapstur et al., 2000; Lowenfels and Maisonneuve, 2006; Stolzenberg-Solomon et al., 2005; Stolzenberg-Solomon et al., 2001; Wolpin et al., 2009). Furthermore, age is a risk factor since the disease is rare in people under an age of 40 and the median age of diagnosis is 71 years (http://seer.cancer.gov/). Another known risk factor is the family history of pancreatic cancer but only 5 – 10 % of the cases have a history for this disease (Klein et al., 2004; Shi et al., 2009). Gemcitabine was the first-line therapy for nearly two decades (Burris et al., 1997). The survival is prolonged by roughly one month with the treatment of gemcitabine. Studies for new therapies by combination of gemcitabine and a second cytotoxic drug all failed to reach an overall survival benefit. An

exception is the combination of gemcitabine with Erlotinib, a small molecule inhibitor of the epidermal growth factor receptor (EGFR), which resulted in a weak improvement of median survival from 5.9 months to 6.2 months (Gupta and El-Rayes, 2008; Moore et al., 2007). The combination of gemcitabine with 5-fluorouracil (5-FU), capecitabine, oxaliplatin, cisplatin or irinotecan could not provide any survival benefit and did not enter clinical routine (Berlin et al., 2002; Herrmann et al., 2007; Louvet et al., 2005; Poplin et al., 2009). Furthermore, some prognostic markers have been identified to predict the responsiveness towards gemcitabine treatment but unfortunately most pancreatic cancers do not respond to a treatment of gemcitabine alone (Vincent et al., 2011). In 2011, the treatment of metastatic PDAC with FOLFIRINOX was shown to improve the overall survival compared to the treatment with gemcitabine (prolongation from 6.8 months up to 11.1 months) (Conroy et al., 2011). FOLFIRINOX is a combination treatment of folinic acid, fluorouracil, irinotecan and oxaliplatin. Another study from 2013 showed that the combined treatment of gemcitabine with nab-paclitaxel extended the survival by 1.5 months compared to gemcitabine alone (Von Hoff et al., 2013). Therefore, FOLFIRINOX and gemcitabine/nab-paclitaxel are currently the standard of care treatment regimens for advanced and metastatic PDAC.

Although over the last years the knowledge of this disease increased enormously, there is still a need for better understanding the initiation and progression as well as improvement and optimization of treatment options.

1.1.1 MODELS OF PDAC DEVELOPMENT AND PROGRESSION

Compared to other human malignancies, the genetics of pancreatic ductal adenocarcinoma are complex and very heterogeneous (Cowley et al., 2013; Jones et al., 2008). So far no targetable molecular mutation/alteration, driving tumor progression and proliferation of tumor cells, has been identified yet with a possible exception of BRCA. Some patients with mutations in the BRCA pathway responded to platinum therapy (Waddell et al., 2015). This heterogeneity is one of the factors for the aggressiveness of the PDAC and its poor responsiveness towards treatment. Mutations of various oncogenes, tumor suppressors and many other genes involved in various cellular processes have been discovered in pancreatic ductal adenocarcinoma (Bailey et al., 2016; Jones et al., 2008; Witkiewicz et al., 2015; Zavoral et al., 2011).

PDAC usually evolves from benign, non-invasive precursor lesions which stepwisely progress to severe dysplastic lesions. There are different types of precursor lesions described for PDAC. The most common form are the pancreatic intraepithelial neoplasia (PanINs)

(Klimstra and Longnecker, 1994). Other described precursor lesions are intraepithelial papillary mucinous neoplasia (IPMN), mucinous cystic neoplasia (MCN) and atypical flat lesions (AFL) (Aichler et al., 2012; Brugge et al., 2004; Esposito et al., 2012; Maitra et al., 2005). Recently, the transdifferentiation of pancreatic acinar cells to ductal cells was suggested to be an initiation event of pancreatic cancer (Aichler et al., 2012; Guerra et al., 2007; Hruban et al., 2006; Reichert and Rustgi, 2011; Strobel et al., 2007). PanINs are grouped by their morphological alterations into type I, II and III (Hruban et al., 2000a). The normal ductal and ductular epithelium is characterized by cuboidal to low-columnar epithelium and the absence of mucin in the cytoplasm. The low grade PanIN lesions PanIN1a and PanIN1b are flat to papillary, micropapillary or basally pseudostratified epithelial lesions with abundant cytoplasmic mucin. The cells are usually tall columnar cells with their nuclei orientated at the basal membrane (Hruban et al., 2001). In adults above 50 years of age these low grade lesions make up to 40 % of non-malignant pancreata (Hruban et al., 2004; Schneider et al., 2005). Progression to higher grade PanIN lesions is accompanied by nuclear alterations like loss of polarity, nuclear crowding, and hyperchromatism. PanIN2 lesions are mucinous epithelial lesions mostly of papillary structure although they can be flat lesions as well. High-grade PanIN3 lesions are papillary or micropapillary and consist of dystrophic goblet cells. Intraepithelial lumen formation (cibriforming) can be observed. PanIN3 lesions are present in 30 – 50 % of invasive PDACs and are therefore considered to be direct precursors of invasive carcinomas although the invasion of the basement membrane is still absent (Hezel et al., 2006; Hruban et al., 2004).

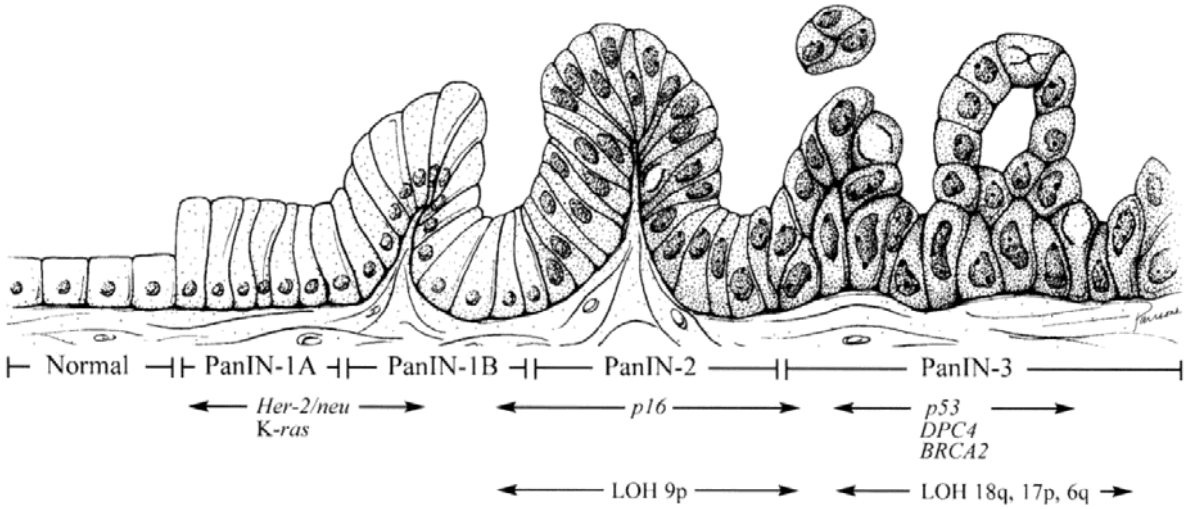

Fig.1 PanIN progression model.
Normal epithelial cells progress to low-grade PanIN1a and PanIN1b lesions and acquire an activation mutation of Kras. Cells of the early lesions also start to overexpress Her-2/neu. (Figure legend continued on next page)

When progressing to higher grade PanIN2 and PanIN3 lesions additional mutations accumulate like mutations or loss of p16, p53 and SMAD4 (DPC4). In the late stage of PanIN3 and pancreatic carcinoma also mutations in the BRCA2 gene occur. Reprinted with permission from the American Association for Cancer Research (Hruban et al., 2000b).

Similar to the multi-step process of PanIN lesion progression (Fig.1), genetic alterations occur and accumulate during carcinogenesis. In general, in pancreatic cancers genomic changes like chromosomal aberrations, copy number changes, inactivation of tumor suppressor genes, and activating mutations of oncogenes are frequently detected (Feldmann and Maitra, 2008).

One of the first mutations which was identified in pancreatic cancer is an activating point mutation in KRAS (Kirsten rat sarcoma) (Almoguera et al., 1988; DiGiuseppe et al., 1994b; Klimstra and Longnecker, 1994). This mutation in codon 12 of the oncogene KRAS is already present over 90 % in low-grade PanIN lesions (92.0 % in PanIN1a and 92.3 % in PanIN1a). It was detected in even higher amounts in PanIN2 (93.3 %) and PanIN3 (95.4 %) (Kanda et al., 2012). KRAS belongs to the family of small GTPases and is involved in many cellular processes like proliferation, survival, and differentiation. For efficient activation, it requires GTPase activating proteins (GAPs) resulting in GTP hydrolysis and attenuation of the downstream signal. The RAF/MEK/ERK (RAF-mitogen-activated kinase, MAPK), the phosphoinositide-3-kinase (PI3K) and the Ral guanine nucleotide exchange factor (RalGEFs) pathways are the three major downstream signaling pathways of KRAS (Collisson et al., 2012; Eser et al., 2013; Feldmann et al., 2010; Lim et al., 2005). The most common mutations of KRAS are an exchange of glycine to valine or aspartate (G12V or G12D). This substitution leads to a decreased intrinsic rate of GTP hydrolysis (Malumbres and Barbacid, 2003) and therefore makes KRAS insensitive for GAPs resulting in a constitutive active form of KRAS. The activation is independent of the stimulation by growth factors (Hezel et al., 2006). Not only KRAS mutations but also telomere shorting was already detected in the low-grade lesions (van Heek et al., 2002).

During progression more alterations accumulate, e. g. Her-2/neu is already overexpressed in early lesions (Hruban et al., 2000a) and in 80 % of invasive PDAC the function of $p16^{INK4A}$ and $p14^{ARF}$ in humans ($p19^{ARF}$ in mice) is lost either due to deletion, mutation or promoter hypermethylation (Rozenblum et al., 1997; Wilentz et al., 1998; Yamano et al., 2000) and often occur subsequent to the KRAS mutation. $p16^{INK4A}$ and $p19^{ARF}$ are both encoded by the *Cyclin-dependent kinase inhibitor 2A* (*CDKN2A*) locus but having distinct first exons and different reading frames of shared exons. In pancreatic cancer, $p16^{INK4A}$ seems to be more important as a tumor suppressor since so far mutations have only been identified in this protein

but not in $p14^{ARF}$ ($p19^{ARF}$ in mice) (Bardeesy et al., 2006). Another important tumor suppressor is the *TP53* gene, which often is mutated in advanced stages of PanIN lesions. DiGiuseppe et al. showed that p53 is overexpressed in PDAC (DiGiuseppe et al., 1994a). Often missense mutations in the DNA-binding domain of *TP53* occur and in 50 – 75 % of pancreatic tumors TP53 is inactivated (Feldmann and Maitra, 2008; Redston et al., 1994; Rozenblum et al., 1997). Mutations in the TP53 gene are often accompanied by loss of heterozygosity (LOH) and therefore the wild type allele is lost (Luttges et al., 2001). This loss of wild type p53 leads to uncontrolled cell growth and proliferation and further genomic instability since wild type p53 has functions in cell cycle control, DNA damage response, and apoptosis (Feldmann and Maitra, 2008).

Furthermore, the transcription factor SMAD4 (DPC4, deleted in pancreatic carcinoma, locus 4) is found to be lost in PanIN3 lesions and pancreatic cancer. This inactivation results from mutation in one allele and LOH of the second allele or from biallelic mutation (Hahn et al., 1996; Luttges et al., 2001; Wilentz et al., 2000). SMAD4 has a central role in the transforming growth factor β (TGFβ) signaling pathway which regulates cell growth inhibition, differentiation, and migration. Deletion or inactivation of SMAD4 therefore leads to uncontrolled cell proliferation by decreased inhibition of cell growth and selective growth advantages. This pathway plays an important role in tumorigenesis and metastases e. g. via tumor-stroma interactions or via its capability to induce epithelial-to-mesenchymal transition (Bardeesy and DePinho, 2002; Massague et al., 2000; Oft et al., 1998; Siegel and Massague, 2003).

Additionally to these quite frequently mutated genes, more rare mutations are found in BRCA2 and LKB1/STK11 tumor suppressor genes (Hezel et al., 2006). Moreover, increased expression of various growth factor receptors and/or their ligands have been described for pancreatic cancer (Hezel et al., 2006) like EGFR, insulin-like growth factor (IGF-I), Met receptor, vascular endothelial growth factor (VEGF) and variants of fibroblast growth factor receptor (FGFR). Recently, platelet-derived growth factor receptor β (PDGFRβ) was described to be necessary for mutant p53-driven metastasis formation in PDAC (Weissmueller et al., 2014).

1.1.2 MOUSE MODELS TO INVESTIGATE PDAC IN VIVO

The identification of mutations occurring in human cancers helps not only to understand the disease but also gives the opportunity to develop models for analysis of cancer development and its progression. Generation of genetically engineered mouse models has improved the knowledge of carcinogenesis. In 2003, Hingorani et al. developed a mouse model which resembles the human PDAC (Hingorani et al., 2003). Endogenous, oncogenic $Kras^{G12D}$

expression at physiological levels induces progression of PDAC from low-grade to high-grade PanIN lesion formation finally resulting in invasive and metastatic disease. Jackson et al. generated a mouse line which harbors the mutant $Kras^{G12D}$ in the endogenous *Kras* locus (Jackson et al., 2001). They silenced the expression of mutant Kras by introducing a STOP cassette flanked by loxP-sites to prevent expression in the whole organism. This lox-STOP-lox cassette can be excised by Cre recombinase leading to constant expression of oncogenic Kras in recombined cells. The Cre/loxP system was and is used to study many cancers (Jonkers et al., 2001; Marino et al., 2000; Orban et al., 1992). To direct oncogenic Kras expression to the pancreas, the Cre recombinase was introduced under the control of promoter of the pancreas-specific transcription factors Pdx1 (Pancreatic and duodenal homeobox gene 1) and the Ptf1a (pancreatic transcription factor 1a). Pdx1 (homeodomain-containing transcription factor) is already expressed at embryonic day 8.5 and in adult pancreata it is found to be expressed mainly in the islets (Kim and MacDonald, 2002; Offield et al., 1996). Shortly after expression of Pdx1, the expression of the Ptf1a transcription factor can be detected (embryonic day 9.5) (Krapp et al., 1996) and is still present in acinar cells in adult pancreata. In 2002, Kawaguchi et al. generated a mouse line expressing Cre recombinase under control of the *Ptf1a* promoter. They introduced the recombinase in the endogenous locus of *Ptf1a* (Kawaguchi et al., 2002). Mice expressing oncogenic $Kras^{G12D}$ either upon recombination by $Ptf1a^{Cre}$ or transgenic *Pdx1-Cre* develop PanINs and invasive PDAC mimicking the human disease (Hingorani et al., 2003). Similar to human pancreatic cancer, which metastasizes to the liver, lung, and lymph node, these mice displayed metastases in lung and liver tissue as well as in lymphatics. These $Ptf1a^{Cre/+}$;$LSL\text{-}Kras^{G12D/+}$ and *Pdx1-Cre*;$LSL\text{-}Kras^{G12D/+}$ mice (*KC*) develop PDAC within roughly a year. As mutations accumulate during progression in the human PDAC, various alterations of tumor suppressor genes were introduced to the *KC* mouse model. E.g. a missense mutation in the *p53* gene leads to acceleration of the cancer formation if expressed in the *KC* model (Hingorani et al., 2005). The expression of the activating mutation of p53 ($p53^{R172H}$) promotes tumor formation and the development of the metastatic disease.

1.1.2.1 The dual-recombination system

Pancreatic ductal adenocarcinoma is a multi-step process in which alterations occur sequentially. The well-established mouse models help to understand the development and progression of PDAC but so far a time-specific manipulation of oncogenes or tumor suppressors was not possible. To circumvent this, the common Cre/loxP system was altered to allow inducible site-specific recombination. The Cre recombinase was fused to the ligand-binding

domain (LBD) of the human estrogen receptor (ER) preventing the activation of the recombinase (Metzger et al., 1995). Only upon binding of either estradiol or tamoxifen (estrogen analogue) the Cre recombinase is active. To prevent activation of the Cre recombinase in mice by the hormone, a point mutation was introduced in the LBD. The exchange of glycine to arginine at position 521 (G521R) in the LBD resulted in sensitivity only towards tamoxifen or 4-hydroxytamoxifen (4-OHT; fusion protein named $CreER^T$). This mutant does not bind the estradiol anymore and therefore the activity of the Cre recombinase is only dependent on the administration of tamoxifen (Feil et al., 1996). If the ligand is not present, the fusion protein $CreER^T$ is localized in the cytoplasm where it is bound to the heat shock protein HSP90. Upon ligand binding the $CreER^T$ dissociates from the HSP90 and can translocate to the nucleus where the $CreER^T$ is active and can recognize loxP sites (Fig.2). The chimeric $CreER^T$ was improved by introducing a triple mutant in the LBD of the estrogen receptor (G400V/M543A/L540A) (Feil et al., 1997). Due to these three mutations, the affinity of $CreER^{T2}$ towards 4-OHT is increased by four times. Not only the human estrogen receptor was used to direct Cre activity in a time-specific manner but other steroid hormone receptors as well like the murine estrogen receptor (Zhang et al., 1996) or the progesterone receptor which can be activated by administration of RU486, a synthetic steroid (instead of the physiological hormone progesterone) (Kellendonk et al., 1999).

To recapitulate the multi-step carcinogenesis of the human disease, a novel dual-recombination system was generated, which allows the combination of the Cre/loxP system and the Flp/frt recombination system. The Flp/frt recombination system is analogous to the Cre/loxP system. LoxP sites are derived from the *bacteriophage P1* whereas frt sites are derived from yeast *saccharomyces cerevisiae*. The expression of the Flippase (Flp) recombinase is driven by the Pdx1 promoter targeting its activation to the pancreas (Schonhuber et al., 2014). Oncogenic $Kras^{G12D}$ expression is silenced by an frt-flanked STOP cassette (FSF) which can be cut by the Flp. *Pdx1-Flp;FSF-Kras*$^{G12D/+}$ (*KF*) mice develop precursor lesions and PDAC similar to *KC* mice. Overall survival is comparable to survival of *KC* mice (401 days for *KF* vs 383 days for *KC*, (Schonhuber et al., 2014)). For secondary time- and site-specific genetic manipulation, a Flp-dependent $CreER^{T2}$ mouse line is used (*FSF-R26*$^{CAG\text{-}CreERT2}$). Upon tamoxifen administration, secondary targets can be activated or inactivated and their role in tumor progression and maintenance can be analyzed.

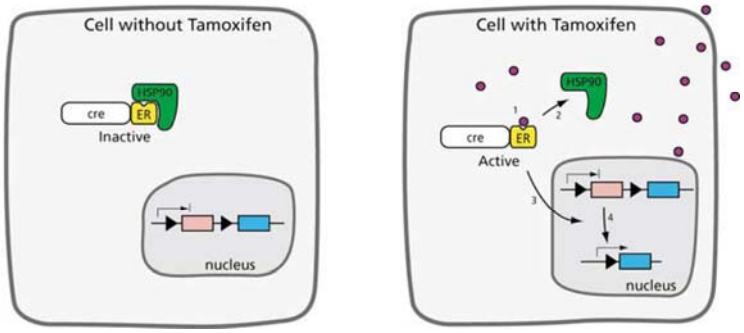

Fig.2 Scheme of CreER^{T2} system.
Left panel shows the CreER^{T2} fusion protein which is bound to the heatshock protein HSP90 in the absence of Tamoxifen. CreER^{T2} is located in the cytoplasm and inhibited from entering the nucleus. Right panel depicts upon administration of Tamoxifen (violet circles) and its binding to ER^{T2} domain. HSP90 dissociates from the fusion proteins CreER^{T2} and the tamoxifen-bound complex translocates to the nucleus where the Cre mediates recombination of loxP-flanked DNA sequences. Reprinted with permission from Elsevier (Leone et al., 2003)

1.2 TUMOR MICROENVIRONMENT

For almost two decades it has been known that in carcinomas a drastic change of cellular organization occurs and the surrounding stroma is extensively altered and remodeled (Ronnov-Jessen et al., 1996). One of the characteristics of PDAC is the dense fibrotic stromal reaction. For years the stroma was believed to be just a bystander in cancer development and tumor progression (Stoker et al., 1966). The tumor microenvironment was suggested to be involved in the tumor initiation and progression (Hanahan and Weinberg, 2011; Korc, 2007; Neesse et al., 2011). Development of reactive stroma occurs early in cancer progression and co-evolves with the tumor. It can create a niche for cancer cells mediating a pro-tumorigenic environment by secretion of growth factors and chemokines. In healthy tissues reactive stroma is usually found during wound repair to generate pro-growth conditions. After repair is completed the reactive stroma returns to normal state without promoting tissue growth. Dvorak et al. described cancer as wounds which do not heal (Dvorak, 1986) and eventually the stroma induces continuous tissue growth. Pathological tumor microenvironment of carcinomas resembles the histopathology of inflamed or wounded tissue. Due to these similarities, studies of inflammation, fibrosis, or wound healing brought insights into the cancer pathology (McAllister and Weinberg, 2014).

In general, the tumor stroma is heterogeneous and varies in its composition depending on its location and cancer type (Chu et al., 2007). Formation of tumor microenvironment is influenced by the interaction of non-malignant cells, tumor cells, and extracellular matrix (ECM)

components. In stroma-rich tumors like PDAC, cancer cells are often outnumbered by stromal cells implying the importance of the tumor microenvironment (Feig et al., 2012). The stroma surrounding the tumor cells consists of vascular cells, fibroblasts and myofibroblasts, macrophages, mast cells, and other immune cells as well as stellate cells (Apte et al., 2004; Bachem et al., 2005; Esposito et al., 2004; Kalluri and Zeisberg, 2006; Otranto et al., 2012). The ECM composes of proteins like collagen type I and III, fibronectin, proteoglycans, hyaluronic acid, and laminin as well as soluble proteins like matrix metalloproteinases (MMPs) and their inhibitors (TIMPs) (Chu et al., 2007; Feig et al., 2012). Secretion of proteases can help to remodel the tumor microenvironment e.g. by cleavage of ECM proteins and thereby promoting the availability of growth factors (Chu et al., 2007). Progression of the cancer is enhanced by remodeling of the stroma supporting invasion of tumor cells to other organs.

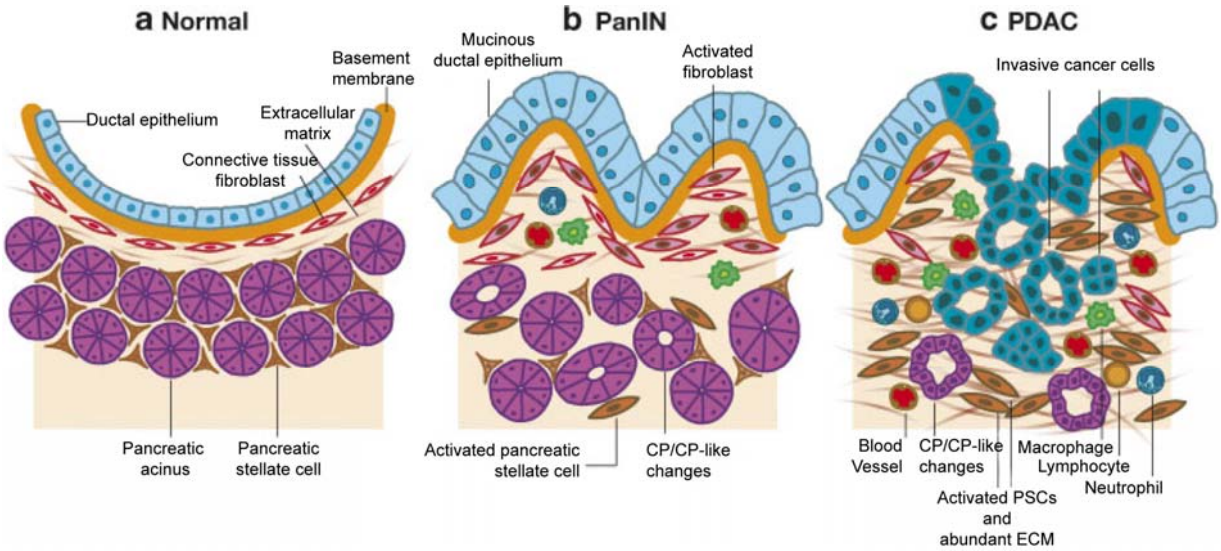

Fig.3 Model of tumor-stroma interactions in PDAC.
(**a**) In normal pancreatic tissue, ductal epithelium is separated from the connective tissue which consists of fibroblast and ECM. Pancreatic acini are enwrapped by pancreatic stellate cells (PSCs). (**b**) During development of PanIN lesions ductal epithelium is replaced by columnar mucin-containing cells which also exhibit nuclear atypia. Basement membrane separating the epithelium from connective tissue remains intact. Already stromal alterations are observed including activation of fibroblasts and PSCs, and beginning vascular proliferation. Acini develop chronic pancreatitis-like (CP/CP-like) changes e.g. ductal metaplasia. (**c**) In PDAC, the basement membrane is breached and invasion of tumor cells in surrounding tissue occurs. Cancer cells can form duct-like structures. Stromal reaction is extensive including activated PSCs (exhibiting myofibroblast-like pehontype) and abundant ECM. Infiltration of immune cells like macrophages, leukocytes and neutrophils is detected. Reprinted with permission of Wiley-Liss, Inc. (Chu et al., 2007).

Due to abundant stroma, the vasculature of PDAC is altered resulting in poor diffusion of the tumor. The blood vessels are disordered and unregularly organized (Feig et al., 2012; Xu et al., 2014). Affecting the vasculature in PDAC the extensive desmoplastic reaction leads to

insufficient perfusion as well as to hypoxic areas. A high metabolic rate contributes to the development of hypoxia in pancreatic tumor. There is evidence that hypoxia can induce collagen and VEGF production by pancreatic stellate cells and migration thereby promoting invasion and metastases (Erkan et al., 2009; Masamune et al., 2008; Xu et al., 2014). Hypoxic cells are shown to be more resistant towards radiotherapy as well as chemotherapy leading to a more aggressive disease (Feig et al., 2012). So far, there is no direct evidence that hypoxia results from the hypovascularity of PDAC. Reduced perfusion decreases not only the supply of metabolites but also drug delivery (Olive et al., 2009).

The tumor microenvironment of the PDAC is under suspicion to not only mediate tumor growth and proliferation, invasion and early metastasis but also therapeutic resistance (Neesse et al., 2013). Recently, studies analyzed whether targeting the tumor stroma is improving treatment options. New developed antistromal therapies inhibiting MMPs which underwent clinical trials phase II and III failed so far and were not approved for clinical routine (Bramhall et al., 2001; Bramhall et al., 2002; Moore et al., 2003). Also inhibition of sonic hedgehog (SHH) signaling using IPI-926 (saridegib) and GDC-0449 (vismodegib) in combination with gemcitabine failed in clinical trials phase II (Neesse et al., 2013). Hedgehog (Hh) signaling involves secretion of the Hh ligand by epithelial cells and its binding to the Hh receptor Pathed1 expressed by mesenchymal cells. This activates smoothened (seven trans-membrane domain protein) and induces nuclear localization of the transcription factor Gli (Pasca di Magliano and Hebrok, 2003). The SHH pathway is active during pancreas organ development and is re-expressed during carcinogenesis (Thayer et al., 2003). This activation of the SHH during pancreatic cancer development results in expansion of stromal cells leading to desmoplasia (Bailey et al., 2008; Neesse et al., 2013; Tian et al., 2009). Currently, clinical trials combining FOLFIRINOX or gemcitabine-nab-paclitaxel with sonic hedgehog inhibitors are ongoing (Sclafani et al., 2015). In PDAC many receptor tyrosine kinases (RTKs) are expressed, not only in cancer cells but in stromal cells as well. Therefore, targeting RTKs is proposed for treatment of PDAC patients. A multi-tyrosine kinase inhibitor, dovitinib (TKI-258), which targets PDGFR, VEGFR and FGFR, results in reduction of cancer cell motility as well as for stromal cells and leads to an increased therapeutic effect of gemcitabine resulting in growth inhibition of MiaPaCa2 cells (Sclafani et al., 2015; Taeger et al., 2011). Clinical trials for treatment options of dovitinib are currently ongoing. Also proteins of the extracellular matrix are considered as new targets for therapy of PDAC. The depletion of hyaluronic acid using recombinant hyaluronidase which is PEGylated (PEGPH20) showed promising results in mouse models (Jacobetz et al., 2013; Provenzano et al., 2012) and is now in clinical trials to analyze the safety and activity of PEGPH20 in combination with gemcitabine or FOLFIRINOX (Lowery and O'Reilly, 2015; Sclafani et al., 2015). First results of a

clinical phase Ib study indicated that the combined treatment of gemcitabine and PEGPH20 was well tolerated and could be a therapy option, especially in patients with a high hyaluronan levels in the tissue (Hingorani et al., 2016). The tumor microenvironment and its role in tumor progression still need to be investigated for better understanding. So far the options as possible new therapeutic targets are discussed controversy.

1.2.1 MAST CELLS

The link between inflammation and the development of pancreatic cancer has been known for years. In 1993, Lowenfels and colleagues could show that chronic pancreatitis patients have a higher risk to develop pancreatic cancer (Lowenfels et al., 1993). As reviewed by Hanahan and Weinberg tumors need to evade immune destruction but on the other side they remodel the immune response creating a pro-tumorigenic environment (Hanahan and Weinberg, 2011). Macrophages, leukocytes, lymphocytes, and mast cells are some of the tumor-infiltrating immune cells and are suggested to promote proliferation by secretion of various growth factors, cytokines and chemokines. They also rearrange the tumor microenvironment and its extracellular matrix by expression of proteolytic enzymes like matrix metalloproteinases (Hanahan and Coussens, 2012).

Mast cells are part of the immune system and are found in almost all tissues but are undetectable in bone marrow and peripheral blood of healthy tissues (Rodewald and Feyerabend, 2012). They play a role as initiators of the IgE-dependent allergic reactions (Gilfillan and Beaven, 2011) via IgE-binding to the high-affinity receptor FcεRI which is present on mast cells (Galli, 2000). Besides the role of mast cells in the immune system, new data suggest their contribution to tumor-promoting or –suppressing inflammatory responses. Mast cells can release several enzymes and cytokines from their granules like serine proteases (Galinsky and Nechushtan, 2008).

Human mast cells develop from CD34-positive stem cells from the bone marrow and the spleen (Gilfillan and Beaven, 2011; Hodges et al., 2012). After differentiation along the myeloid pathway mast cell progenitors migrate into the varying tissues. Growth, differentiation, and survival of mast cells are mainly dependent on the activation of the receptor tyrosine kinase Kit by binding its ligand the stem cell factor SCF (Gilfillan and Beaven, 2011). The Kit receptor is present on mast cells throughout their differentiation. Mutations in the *Kit* gene lead to mast cell deficiency and result in white spots of the coat color of animals. Therefore, the *Kit* allele is referred to the *white-spotted* (*W*) allele. The hypomorphic $Kit^{W/Wv}$ and the $Kit^{W\text{-}sh/W—sh}$ mutants are common models to study the function of mast cells (Berrozpe et al., 1999; Kitamura et al., 1978).

Since Kit signaling is not only restricted to mast cells, mutations in this gene affect other cell lineages as well, like hematopoietic stem cells, red blood cells, intestinal pacemaker cells, and germ cells. Recently, a new mast cell-deficient mouse model was established where the expression of Cre recombinase under the control of the *mast cell carboxypeptidase A* (*Cpa3*) promoter which results in mast cell depletion independent from Kit (Feyerabend et al., 2011).

The role of mast cells in tumors is still under investigation and there are contradictory data suggesting either a tumor-promoting or tumor-suppressing role (Galinsky and Nechushtan, 2008). Chang and colleagues could show that mast cell infiltration in the tumor microenvironment occurs at an early stage of PDAC using the $Kras^{G12V}$ mouse model (Chang et al., 2011). In mast cell-deficient $Kit^{w\text{-}sh/w\text{-}sh}$ mice the tumor growth was suppressed compared to mast cell-proficient mice and PDAC patients with a higher mast cell count were associated with a worse prognosis. Strouch et al. correlated a higher mast cell count in patient-derived tissue samples with higher grade tumors and decreased survival (Strouch et al., 2010). Furthermore, they observed tumor-cell growth in mast cell-conditioned medium. Mast cells are proposed to be required for angiogenesis and tumor growth in Myc-induced β-cell tumor model (Soucek et al., 2007). Although they could not identify the molecules which induced angiogenesis in this model and subsequently, it is not clear whether angiogenesis was really an effect of mast cells (Theoharides, 2008). Inhibiting mast cell migration and function resulted in reduced PDAC growth suggesting that targeting mast cells could improve therapy of pancreatic cancer (Ma et al., 2013). However, so far the role of mast cells in tumorigenesis is not clarified. The secretion of cytokines and proteolytic enzymes could have antitumor effects like induction of apoptosis (Gooch et al., 1998). The role of mast cells in cancerogenesis needs to be further investigated.

1.2.2 PANCREATIC STELLATE CELLS

In PDAC pancreatic stellate cells (PSCs) and fibroblasts share the most prominent role in the desmoplastic reaction (Moir et al., 2015). PSCs were first isolated in 1998 (Apte et al., 1998; Bachem et al., 1998). In healthy pancreatic tissue PSCs are quiescent and characterized by vitamin A storage lipid droplets which are found in the cytoplasm. They regulate the synthesis and degradation of ECM components and thereby have an influence on the healthy tissue architecture (Moir et al., 2015). By secretion of matrix degrading enzymes (matrix metalloproteinases, MMPs) and their inhibitors (tissue inhibitors of matrix metalloproteinases, TIMPs) PSCs have the capability to turnover and remodel the normal ECM (Phillips et al., 2003). Upon injury of the pancreas these cells get activated and lose their vitamin A stores. Activated pancreatic stellate cells acquire a myofibroblast-like phenotype and express α-smooth muscle

actin (αSMA) (Apte et al., 2011; Apte et al., 2004). Another identified marker for activated PSCs is nestin which is expressed at higher levels compared to quiescent stellate cells. In general, pancreatic stellate cells are characterized by the expression of GFAP (glial fibrillary acidic protein), vimentin, and desmin (Omary et al., 2007). Once activated, PSCs produce large amounts of ECM proteins which subsequently lead to fibrosis. Therefore, PSCs play an important role in chronic pancreatitis which is a known risk factor for pancreatic cancer. Not only in pancreatitis but also in pancreatic cancer PSCs seem to be important since abundant stromal reaction is one the characteristics of PDAC. Apte et al. could demonstrate the presence of pancreatic stellate cells in desmoplastic regions of pancreatic cancer by immunohistochemical staining (Apte et al., 2004). Furthermore, they could show that PSCs are responsible for the fibrosis in pancreatic cancer. Pancreatic cancer cells produce and secrete mitogenic and growth factors which influence PSCs to produce and release cytokines and growth factors. The interaction with cancer cells and cancer-promoting properties of stellate cells were shown by orthotopic transplantation of pancreatic cancer cells with isolated human PSCs. The mixture of both cell types resulted in acceleration of tumor growth and increased metastasis formation (Apte and Wilson, 2012; Bachem et al., 2005; Hwang et al., 2008; Vonlaufen et al., 2008). Pancreatic stellate cells were shown to promote the hapto-migration of cancer cells which indicates a role of PSCs in the migration/invasion of cancer cells (Lu et al., 2014). Kikuta and colleagues could demonstrate that cancer cells have a more fibroblast-like phenotype if co-cultured with pancreatic stellate cells, suggesting a role of PSCs in epithelial-mesenchymal-transition (EMT) (Kikuta et al., 2010). EMT is the process of epithelial cells changing their morphology towards mesenchymal state. Cells lose their cell-cell adhesion and cell polarity and gain migratory and invasive characteristics to become mesenchymal. EMT is suggested to be responsible for metastasis formation and therapy resistance (Arumugam et al., 2009; Pandol and Edderkaoui, 2015).

Recently, the pro-tumorigenic role of PSCs is questioned as depletion of cancer-associated fibroblasts and fibrosis lead to an acceleration of PDAC growth and decreased survival (Ozdemir et al., 2014). Less αSMA-positive myofibroblast-like cells in tumor samples were associated with a reduced survival of PDAC patients. Rhim et al. observed upon genetic targeting of sonic hedgehog (Shh), pancreatic tumors showed less stroma content but tumors were less differentiated. The deletion of Shh decreased survival in mice (Rhim et al., 2014). More studies are necessary to understand the role of pancreatic stellate cells in the tumorigenesis.

1.2.3 FIBROBLASTS

Not only PSCs contribute to the characteristic dense stroma of PDAC, fibroblasts are involved as well. First described by Virchow in 1858, fibroblasts are cells of the connective tissue (Kalluri and Zeisberg, 2006). They appear as elongated, spindle-like shaped cells and are embedded in the fibrillary matrix of the connective tissue. These non-vascular, non-inflammatory and non-epithelial cells are one of the main source of ECM components. Fibroblasts synthesize and deposit various types of collagen like type I, type III and type IV, and fibronectin as well as laminin (Chang et al., 2002; Rodemann and Muller, 1991). Furthermore, fibroblasts are involved in ECM turnover and tissue remodeling by producing ECM-degrading proteases like matrix metalloproteases (MMPs) (Kalluri and Zeisberg, 2006). Fibroblasts are not only important in healthy tissue but are important for wound healing as well. In the process of wound repair, fibroblasts get activated and proliferate more compared to non-activated fibroblasts. These activated cells also produce and secrete more ECM components (Castor et al., 1979; Kalluri and Zeisberg, 2006). The excessive production and deposition of ECM is referred to as tissue fibrosis and fibroblasts are thought to be the main origin besides PSCs. Fibrosis and excessive stroma production is one of the features of PDAC and subsequently activated fibroblasts are abundant in the PDAC microenvironment. Activated fibroblasts present in tumor stroma are called cancer-associated fibroblasts (CAFs) or tumor-associated fibroblasts (TAFs). Those activated fibroblasts are described as myofibroblasts since they express the smooth muscle cell marker α-smooth-muscle actin (αSMA) and resemble in their morphology smooth muscle cells (Kalluri and Zeisberg, 2006). Other markers, which were described for CAFs, are the fibroblast activation protein (FAP), fibroblast specific protein-1 (Fsp1), vimentin, and desmin. It was also shown that CAFs express neuron glial antigen-2 (NG2) and platelet derived growth factor receptor α and β (PDGFRα and β) (Shiga et al., 2015). The presence of CAFs in PDAC was demonstrated in various studies (Chu et al., 2007; Neesse et al., 2011; Santos et al., 2009) but the origin of these fibroblasts is still under debate. Cancer-associated fibroblasts are suggested to descend from resident fibroblasts, endothelial or epithelial cells, adipocytes as well as from bone marrow derived hematopoietic or bone marrow derived mesenchymal stem cells (Shiga et al., 2015). Hence, it could be that CAFs originate from various cell types and are therefore heterogeneous. Similar to PSCs, CAFs can influence cancer cells by releasing growth factors, chemokines and cytokines. The function of fibroblasts in tissue remodeling is suggested to be important for metastasis formation during tumor progression. CAFs express MMPs, which can rearrange the ECM and therefore facilitate metastasis. To target fibroblasts in PDAC, more studies needs to be done for further characterization.

1.3 AIM OF THIS WORK

PDAC is one of the leading causes of cancer-related death worldwide. Although in the last years many insights of the development and progression were gained, no efficient therapy was found. Established mouse models allow the investigation of the development and progression of PDAC but have some limitations. They cannot reconstitute the accumulation of mutations during cancerogenesis, which is a multi-step process. To simulate the human situation, a dual-recombination system combining two recombinase systems was characterized. Flp-dependent oncogenic $Kras^{G12D}$ expression was directed to the *Pdx1* lineage (*Pdx1-Flp*) using a frt-flanked STOP cassette silencing the $Kras^{G12D}$ expression (*FSF-Kras*$^{G12D/+}$). To recapitulate the multi-step process of cancer progression, a Flp-dependent $CreER^{T2}$ mouse line (*FSF-R26*$^{CAG\text{-}CreERT2}$) was bred with *Pdx1-Flp;FSF-Kras*$^{G12D/+}$ (*KF*) mice. Upon tamoxifen treatment additional tumor suppressor genes can be inactivated or activated at specific time points. Therefore, it is possible to allow a sequential step-wise manipulation. Furthermore, the tumor microenvironment can be studied and characterized using a dual-recombination system. In this work the dual-recombination system was analyzed for its accuracy and efficiency using the Cre recombinase reporter mouse line *R26*$^{mT\text{-}mG}$ (Muzumdar et al., 2007). For examination of the composition and role of specific cell types in the tumor microenvironment, different Cre lines were crossed with *Pdx1-Flp;FSF-Kras*$^{G12D/+}$ mice. Various Cre lines under control of cell-type specific promoter e.g. for fibroblasts, mast cells and pancreatic stellate cells were used. PDACs of these animals were investigated for targeted stromal cell types and analyzed for expression and co-localization of marker proteins to identify which cell type exactly was targeted using the stromal Cre. In addition, the role of mast cells in PDAC initiation was studied using a genetic depletion strategy. The dual-recombination system not only gives the opportunity to reproduce the step-wise process of cancerogenesis but also to characterize and functionally analyze the tumor microenvironment.

2 MATERIALS

2.1 TECHNICAL EQUIPMENT

Table 1 Technical equipment

Device	Source
Analytical balance A 120 S	Sartorius AG, Göttingen
Analytical balance BP 610	Sartorius AG, Göttingen
AxioCam HRc	Carl Zeiss AG, Oberkochen
AxioCam MRc	Carl Zeiss AG, Oberkochen
Centrifuge Rotina 46R	Andreas Hettich GmbH & Co. KG, Tuttlingen
CO_2 incubator HERAcell®	Heraeus Holding GmbH, Hanau
Cryostat Microm HM 560	Thermo Fisher Scientific, Inc., Waltham, MA, USA
Electrophoresis power supply Power Pac 200	Bio-Rad Laboratories GmbH, Munich
Experion® automated electrophoresis station	Bio-Rad Laboratories GmbH, Munich
Experion® vortex station	Bio-Rad Laboratories GmbH, Munich
FACSCalibur™	BD Biosciences, Franklin Lakes NJ, USA
Gel Doc™ XR+ system	Bio-Rad Laboratories GmbH, Munich
Glass ware, Schott Duran®	Schott AG, Mainz
Heated paraffin embedding module EG1150 H	Leica Microsystems GmbH, Wetzlar
HERAsafe® biological safety cabinet	Thermo Fisher scientific, Inc., Waltham, MA, USA
Homogenizer SilentCrusher M with tool 6F	Heidolph Instruments GmbH & Co. KG, Schwabach
Horizontal gel electrophoresis system	Biozym Scientific GmbH, Hessisch Oldenburg
Horizontal shaker	Titertek Instruments, Inc., Huntsville, AL, USA
Laminar flow HERAsafe	Heraeus Holding GmbH, Hanau
Magnetic stirrer, Ikamag® RCT	IKA® Werke GmbH & Co. KG, Staufen
Microcentrifuge 5415 D	Eppendorf AG, Hamburg
Microcentrifuge 5417 R	Eppendorf AG, Hamburg
Microplate reader Anthos 2001	Anthos Mikrosysteme GmbH, Krefeld
Microscope Axio Imager.A1	Carl Zeiss AG, Oberkochen
Microscope Axiovert 25	Carl Zeiss AG, Oberkochen
Microscope DM LB	Leica Microsystems GmbH, Wetzlar

Device	Source
Microscope Leica SP5	Leica Microsystems GmbH, Wetzlar
Microtome Microm HM355S	Thermo Fisher Scientific, Inc., Waltham, MA, USA
Microwave	Siemens, Munich
Mini Centrifuge MCF-2360	LMS Consult GmbH & Co. KG, Brigachtal
Mini-Protean® Tetra Cell	Bio-Rad Laboratories GmbH, Munich
Multipette® stream	Eppendorf AG, Hamburg
Narcotic device	Völker GmbH, Medizintechnik, Kaltenkirchen,
Neubauer hemocytometer, improved	LO-Laboroptik GmbH, Bad Homburg
Odyssey® infrared imaging system	Li-Cor Biosciences, Lincoln, NE, USA
Paraffin tissue floating bath Mircom SB80	Thermo Fisher Scientific, Inc., Waltham, MA, USA
pH meter 521	WTW Wissenschaftlich-Technische Werkstätten GmbH, Weilheim
Pipettes, Reference®, Research®	Eppendorf AG, Hamburg
Pipetus®	Hirschmann Laborgeräte GmbH & Co. KG, Eberstadt
Power Supplies E844, E822, EV243	Peqlab Biotechnologie GmbH, Erlangen
Stereomicroscope Stemi SV 11	Carl Zeiss AG, Oberkochen
Surgical instruments	Thermo Fisher Scientific, Inc., Waltham, MA, USA
Thermocycler T1	Biometra GmbH, Göttingen
Thermocycler TGradient	Biometra GmbH, Göttingen
Thermocycler TPersonal	Biometra GmbH, Göttingen
Thermomixer compact	Eppendorf AG, Hamburg
Tissue processor ASP 300	Leica Mircosystems GmbH, Wetzlar
Tumbling table WT 17	Biometra GmbH, Göttingen
Vevo 2100, ultrasound	FUJIFILM VisualSonics, Amsterdam, Netherlands
Vortex Genius 3	IKA® Werke GmbH & Co. KG, Staufen
Water bath 1003	GFL Gesellschaft für Labortechnik mbH, Burgwedel
Western blot system SE 260 Mighty Small II	Hoefer, Inc., Holliston, MA, USA
Zeiss LSM 510	Carl Zeiss AG, Oberkochen

2.2 CHEMICALS AND ENZYMES

Table 2 Chemicals and enzymes

Chemical	Source
1 kb DNA extension ladder	Invitrogen GmbH, Karlsruhe
1,4-Dithiothreitol (DTT)	Carl Roth GmbH + Co. KG, Karlsruhe
2-Mercaptoethanol, 98 %	Sigma-Aldrich Chemie GmbH, Munich
2-Propanol (isopropanol)	Carl Roth GmbH + Co. KG, Karlsruhe
3-(4,5-deimethylthiazol-2-yl)-2,5-diphenyl tetrazolium bromide (MTT)	Carl Roth GmbH + Co. KG, Karlsruhe
4-hydroxytamoxifen (4-OHT)	Sigma-Aldrich Chemie GmbH, Steinheim
5-Bromo-2'-deoxyuridine *Biochemica* (BrdU)	AppliChem GmbH, Darmstadt
Acetic acid	Carl Roth GmbH + Co. KG, Karlsruhe
Agarose	Sigma-Aldrich Chemie GmbH, Munich
Ammonium persulfate	Sigma-Aldrich Chemie GmbH, Munich
Bovine serum albumin, fraction V	Serva Electrophoresis GmbH, Heidelberg
Bradford reagent	Serva Electrophoresis GmbH, Heidelberg
Bromphenol blue	Sigma-Aldrich Chemie GmbH, Munich
Complete, EDTA-free. Protease inhibitor cocktail tablets	Roche Deutschland Holding GmbH, Grenzach-Wyhlen
Cresol red	AppliChem GmbH, Darmstadt
D(+)-Saccharose	Carl Roth GmbH + Co. KG, Karlsruhe
Dimethyl sulfoxide (DMSO, for MTT)	Carl Roth GmbH + Co. KG, Karlsruhe
dNTP mix (10 mM each)	Fermentas GmbH, St. Leon-Rot
Dodecyl sulfate Na-salt in pellets (SDS)	Serva Electrophoresis GmbH, Heidelberg
Dulbecco´s phosphate buffered saline, powder	Biochrom AG, Berlin
Ethanol (100 %)	Merck KGaA, Darmstadt
Ethidium bromide	Sigma-Aldrich Chemie GmbH, Munich
Ethylenediaminetetraacetic acid (EDTA)	Invitrogen GmbH, Karlsruhe
eye ointment	Vidisc, Gerhad Mann GmbH, Berlin
Forene® isoflurane	Abbott GmbH & Co. KG, Ludwigshafen
GeneRuler™ 100 bp DNA ladder	Fermentas GmbH, St. Leon-Rot

Chemical	Source
Glycerol	Sigma-Aldrich Chemie GmbH, Munich
Glycine	Carl Roth GmbH + Co. KG, Karlsruhe
HEPES	Carl Roth GmbH + Co. KG, Karlsruhe
HotStarTaq DNA polymerase	Qiagen GmbH, Hilden
Hydrochloric acid (HCl)	Merck KGaA, Darmstadt
Isotonic sodium chloride solution	Braun Melsungen AG, Melsungen
Magnesium chloride	Carl Roth GmbH + Co. KG, Karlsruhe
Magnesium sulfate	Merck KGaA, Darmstadt
Methanol	Merck KGaA, Darmstadt
Modified Giemsa Stain (20 x)	Sigma-Aldrich Chemie GmbH, Munich
Mouse chow CreActive TAM400	LASvendi, Soest
Mouse diet Pancrex-Vet, #S2881-S713	ssniff Spezialdiäten GmbH, Soest
N,N-dimethyl formamide	Sigma-Aldrich Chemie GmbH, Munich
Nonidet P40	Roche Deutschland Holding GmbH, Grenzach-Wyhlen
Orange G	Carl Roth GmbH + Co. KG, Karlsruhe
Peanut oil	Sigma-Aldrich Chemie GmbH, Munich
Phosphatase inhibitor mix I	Serva Electrophoresis GmbH, Heidelberg
Precision Plus Protein™ all blue standard	Bio-Rad Laboratories GmbH, Munich
Proteinase K, recombinant, PCR grade	Roche Deutschland Holding GmbH, Grenzach-Wyhlen
Reaction buffer S (PCR)	peqlab, Biotechnologie GmbH, Erlangen
Rotiphorese® gel 30	Carl Roth GmbH + Co. KG, Karlsruhe
Skim milk powder	Sigma-Aldrich Chemie GmbH, Munich
Sodium chloride	Merck KGaA, Darmstadt
Sodium hydroxide solution (NaOH)	Merck KGaA, Darmstadt
Sucrose (PCR)	Sigma-Aldrich Chemie GmbH, Munich
Tamoxifen	Sigma-Aldrich Chemie GmbH, Munich
Taq-DNA-polymerase	peqlab, Biotechnologie GmbH, Erlangen
TEMED	Carl Roth GmbH + Co. KG, Karlsruhe
Tissue-Tek® O.C.T.™ compound	Sakura Finetek Europa B.V, Alphen aan den Rijn,

Chemical	Source
	Netherlands
Tris hydrochloride	J.T.Baker® Chemicals, Phillipsburg, NJ, USA
Tris Pufferan®	Carl Roth GmbH + Co. KG, Karlsruhe
Triton® X-100	Merck KGaA, Darmstadt
Tween® 20	Carl Roth GmbH + Co. KG, Karlsruhe

2.3 ANTIBODIES

Primary antibodies used for immunofluorescence or immunohistochemistry were in general diluted 1:100 (except CK19 which was used at a dilution of 1:75) whereas primary antibodies detecting proteins in immunoblotting were diluted 1:1000.

Table 3 Primary antibodies

Antibodies	Source
αAmylase, A8273	Sigma-Aldrich Chemie GmbH, Munich
αSMA	AbCam plc, Cambridge, UK
αTubulin, T6199	Sigma-Aldrich Chemie GmbH, Munich
c-Kit (C19)	Santa Cruz Biotechnology, Inc., Santa Cruz, CA, USA
c-Kit (M14)	Santa Cruz Biotechnology, Inc., Santa Cruz, CA, USA
Cytokeratin 19 (CK19)	AbCam plc, Cambridge, UK
F4/80	BD Biosciences, Franklin Lakes NJ, USA
FAP	LifeSpan BioSciences Inc., Seattle, WA
GFAP	ThermoFisher Scientific, Inc., Waktham, MA, USA
Insulin	Cell Signaling Technology, Inc., Danvers, MA, USA
p21 (C-19), sc-397	Santa Cruz Biotechnology, Inc., Santa Cruz, CA, USA
p53 (CM5), Novocastra®	Leica Microsystems GmbH, Wetzlar
Phalloidin	ThermoFisher Scientific, Inc., Waktham, MA, USA
Vimentin	Cell Signaling Technology, Inc., Danvers, MA, USA

Secondary anitbodies for immunofluorescence were diluted 1:100 whereas secondary antibodies for immunohistochemistry and immunoblotting were diluted 1:500 and 1:1000, respectively.

Table 4 Secondary antibodies

Antibodies	Source
Alexa Fluor® 680 … anti-goat, IgG	Invitrogen GmbH, Karlsruhe
Alexa Fluor® 680 goat anti-mouse IgG, A21058	Invitrogen GmbH, Karlsruhe
Alexa Fluor® 680 goat anti-rabbit, IgG	Invitrogen GmbH, Karlsruhe
Anti-goat (680)	Invitrogen GmbH, Karlsruhe
Anti-mouse IgG (H+L) (DyLight® 680 Conjugate), #5470	Cell Signaling Technology, Inc., Danvers, MA, USA
Anti-mouse IgG (H+L) (DyLight® 800 Conjugate), #5257	Cell Signaling Technology, Inc., Danvers, MA, USA
Anti-rabbit IgG (H+L) (DyLight® 680 Conjugate), #5366	Cell Signaling Technology, Inc., Danvers, MA, USA
Anti-rabbit IgG (H+L) (DyLight® 800 Conjugate), #5151	Cell Signaling Technology, Inc., Danvers, MA, USA
Anti-rat (680)	Invitrogen GmbH, Karlsruhe
Biotinylated anti-goat IgG (H+L)	Vector Laboratories, Inc., Burlingame, CA, USA
Biotinylated anti-mouse IgG (H+L)	Vector Laboratories, Inc., Burlingame, CA, USA
Biotinylated anti-rabbit IgG (H+L)	Vector Laboratories, Inc., Burlingame, CA, USA
Biotinylated anti-rat IgG (H+L)	Vector Laboratories, Inc., Burlingame, CA, USA

2.4 DISPOSABLES

Table 5 Disposables

Disposable	Source
Amersham Hybond-N+ membrane	GE Healthcare Europe GmbH, Munich
Cell culture plastics	Greiner Bio-One GmbH, Frickenhausen; TPP Techno Plastic, Products AG, Trasadigen, Switzerland; Sarstedt AG & Co., Nümbrecht

Disposable	Source
Cell scrapers	TPP Techno Plastic, Products AG, Trasadigen, Switzerland
Combitips BioPur®	Eppendorf AG, Hamburg
Conical tubes, 15 mL and 50 mL	Sarstedt AG & Co., Nümbrecht
Cover slips	Gerhard Menzel, Glasverarbeitungswerk GmbH & Co. KG, Braunschweig
Cryo embedding tubes	Carl Roth GmbH + Co. KG, Karlsruhe
CryoPure tubes	Sarstedt AG & Co., Nümbrecht
Disposable scalpels	Feather Safety Razor Co., Ltd., Osaka, Japan
Embedding cassettes	AMP Stensved, Denmark
EthilonII	CLS Medizintechnik, Kassel
Filtropur S 0.2 and S 0.45	Sarstedt AG & Co., Nümbrecht
Glass slides Superfrost® Plus	Gerhard Menzel, Glasverarbeitungswerk GmbH & Co. KG, Braunschweig
Microtome blades S35 and C35	Feather Safety Razor Co., Ltd., Osaka, Japan
Para film®	Bemis Company Inc., Oshkosh, WI, USA
Pasteur pipettes	Hirschmann Laborgeräte GmbH & Co. KG, Eberstadt
PCR reaction tubes	Sarstedt AG & Co., Nümbrecht
Petri dishes	Sarstedt AG & Co., Nümbrecht
Pipette tips	Sarstedt AG & Co., Nümbrecht
Reaction tubes, 0.5 mL, 1.5 mL and 2.0 mL	Eppendorf AG, Hamburg
Safe seal pipette tips	Biozym Scientific GmbH, Hessisch Oldendorf
Safe-lock reaction tubes BioPur®	Eppendorf AG, Hamburg
Serological pipettes	Sarstedt AG & Co., Nümbrecht
Single use needles Sterican® 27 gauge	B. Braun Melsungen AG, Melsungen
Single use syringes Omnifix®	B. Braun Melsungen AG, Melsungen
Tissue Embedding cassette system	Medite GmbH, Burgdorf
Transfer membrane Immobilon-P	Millipore GmbH, Schwalbach am Taunus
Wound clips	MEDICON eG, Tuttlingen

2.5 BUFFERS AND SOLUTIONS

All buffers were prepared using bidistilled water.

Table 6 Buffers and solutions

Buffer/solution	Component
10 x Gitschier´s buffer	670 mM Tris, pH 8.8
	166 mM $(NH_4)_2SO_4$
	67 mM $MgCl_2$
5 x Protein loading buffer (Laemmli), pH 6.8	10 % SDS
	50 % Glycerol
	228 mM Tris hydrochloride
	0.75 mM Bromphenol blue
	5 % 2-Mercaptoehtanol
50 x Tris acetate EDTA (TAE) buffer, pH 8.5	2 M Tris
	50 mM EDTA
	5.71 % Acetic acid
PBS-T	1 x PBS
	0.1 % Tween® 20
PCR lysis buffer (Soriano)	0.5 % Triton® X-100
	1 % 2-Mercaptoethanol
	1 x Gitschier´s buffer
	400 µg/mL Proteinase K (add prior use)
Protein lysis buffer, pH 7,9	50 mM HEPES
	150 mM NaCl
	1 mM EDTA
	0.5 % Nonidet P40
	10 % Glycerol
	Phosphatase inhibitor (add prior to use)
	Protease inhibitor (add prior to use)

Buffer/solution	Component
Running buffer	25 mM Tris 192 mM Glycine 0.1 % SDS
Separating gel buffer	1.5 M Tris, pH 8.8 (adjusted with HCl)
Stacking gel buffer	0.5 M Tris, pH 6.8 (adjusted with HCl)
SucRot solution (PCR)	1.5 mg/mL Cresol red 100 mM Tris (pH 9.0) 30 % saccharose
Transfer buffer, pH 8.3	25 mM Tris 192 mM Glycine 20 % Methanol

2.6 PRIMERS

All primers were made by Eurofins MWG (Ebersberg) and dissolved in 5 mM Tris (pH 7.0) to a concentration of 10 mM. For PCR usage primers were further diluted to a concentration of 10 µM.

Table 7 Primers for genotyping

PCR name	Primer name	Sequence (5'-3')
Cpa3-Cre	Cpa3-Cre common forward	GGACTGTTCATCCCCAGGAACC
	Cpa3-Cre WT reverse	CTGGCGTGCTTTTCATTCTGG
	Cpa3-Cre mut	GTCCGGACACGCTGAACTTG
Col1a-CreERT	Col1a-CreERT forward	TCCAATTTACTGACCGTACACCAA
	Col1a-CreERT reverse	CCTGATCCTGGCAATTTCGGCTA
$CreER^{T2}$	$CreER^{T2}$ forward	GAATGTGCCTGGCTAGAGATC
	$CreER^{T2}$ reverse	GCAGATTCATCATGCGGA
E-cadherin	Cdh1 forward	TCAATCTCAGAGCCCCACCTA
	Cdh1 reverse	TGCCATGATTGTCATGGAC

PCR name	Primer name	Sequence (5'-3')
FSF-Kras	Kras common forward	CACCAGCTTCGGCTTCCTATT
	Kras WT reverse	AGCTAATGGCTCTCAAAGGAATGTA
	Kras FSF mut reverse	GCGAAGAGTTTGTCCTCAACC
FSF-STOP	FSF-STOP forward	TGAATAGTTAATTGGAGCGGCCGCAATA
	Cre reverse	CAGGGTGTTATAAGCAATCCC
General Cre (PCR for	Cre forward	CCTGGAAAATGCTTCTGTCCG
Fsp1-Cre; Sm22-Cre;	Cre reverse	CAGGGTGTTATAAGCAATCCC
mGFAP-Cre; C-Cre)	Gabra forward	AACACACACTGGAGGACTGGCTAGG
	Gabra reverse	CAATGGTAGGCTCACTCTGGGAGATGATA
hGFAP-Cre	hGFAP forward	ACTCCTTCATAAAGCCCT
	hGFAP reverse	ATCACTCGTTGCATCGACCG
$p53^{frt}$	p53-frt forward	CAAGAGAACTGTGCCTAAGAG
	p53-frt reverse	CTTTCTAACAGCAAAGGCAAGC
$p53^{LSL}$	p53-WT-forward	CAACTGTTCTACCTCAAGAGCC
	p53-WT-reverse	AGCTAGCCACCATGGCTTGAGTAAGT
	p53-WT-mut	CTTGGAGACATAGCCACACTG
Pdx1-Flp	Pdx1-Flp forward	AGAGAGAAAATTGAAACAAGTGCAGGT
	Flp reverse	CGTTGTAAGGGATGATGGTGAACT
	Gabra forward	AACACACACTGGAGGACTGGCTAGG
	Gabra reverse	CAATGGTAGGCTCACTCTGGGAGATGATA
R26-CAG	R26 common forward	AAAGTCGCTCTGAGTTGTTAT
	R26 WT reverse	GGAGCGGGAGAAATGGATATG
	$R26^{CAG\text{-}CreERT2}$ mut reverse	TCAATGGGCGGGGGTCGTT
$R26^{mT\text{-}mG}$	R26 common forward	AAAGTCGCTCTGAGTTGTTAT
	R26 WT reverse	GGAGCGGGAGAAATGGATATG
	$R26^{mT\text{-}mG}$ mut reverse	GTACTTGGCATATGATACACTTGATGTAC
$Sm22^{Cre}$	Sm22-forward	GGCCCAGGGGTTGTCAAAATAGTC
	Sm22-reverse	CTCCTCCAGCTCCTCGTCATACTTC
	Sm22-mut	CGCCGCATAACCAGTGAAACAG

Table 8 Primer for recombination analysis

Recombination PCR	Primer name	Sequence
FSF-R26-CreER^{T2} recombined	FSF-R26-CreER^{T2} reverse	CGATCCCTGAACATGTCCATC
	FSF-R26-CreER^{T2} forward	GTTCGGCTTCTGGCGTGT
FSF-Kras recombined	FSF-Kras recombined F	AGAATACCGCAAGGGTAGGTGTTG
	FSF-Kras recombined R	TGTAGCAGCTAATGGCTCTCAAA
p53^{frt} recombined	p53-frt forward	CAAGAGAACTGTGCCTAAGAG
	p53-frt recombined R	CTTTCAACAGCAAAGGCAAGC

2.7 CELL CULTURE

Table 9 Reagents for cell culture

Reagents	Source
Collagenase type 2	Worthington Biochemical Corporation, Lakewood, NJ, USA
Dimethyl sulfoxide (DMSO, for cell culture)	AppliChem GmbH, Darmstadt
Dulbecco´s modified medium (D-MEM) with L-glutamine	Invitrogen GmbH, Karlsruhe
Dulbecco´s phosphate buffered saline (PBS)	Invitrogen GmbH, Karlsruhe
Fetal calf serum (FCS)	Biochrom AG, Berlin
Fungizone® antimycotic	Invitrogen GmbH, Karlsruhe
Penicillin(10000 units/mL)-Streptomycin (10000 µg/mL) solution	Invitrogen GmbH, Karlsruhe
Trypsin MycoVIR 10x EDTA (1:250)	Biontex Laboratories GmbH, Munich

Table 10 Cell culture media

Medium	Component
Freezing medium	70 % D-MEM
	20 % FCS
	10 % DMSO

Medium	Component
Tumor cell medium	D-MEM
	10 % FCS
	1 % Penicillin-Streptomycin

2.8 HISTOLOGY

Table 11 Reagents and kits for histological analysis

Reagent/kits	Source
Acetic acid (glacial)	Merck KGaA, Darmstadt
Alcian Blue 8 GX	Sigma-Aldrich Chemie GmbH, Munich
Aluminium sulfate	Honeywell Specialty Chemicals Seelze GmbH, Seelze
Antigen unmasking solution, citric acid based	Vector Laboratories, Inc., Burlingame, CA, USA
Avidin/biotin blocking kit	Vector Laboratories, Inc., Burlingame, CA, USA
Certistain® Nuclear fast red	Merck KGaA, Darmstadt
DAB peroxidase substrate kit, 3, 3'-diaminobenzidine	Vector Laboratories, Inc., Burlingame, CA, USA
Direct Red 80	Sigma-Aldrich Chemie GmbH, Munich
Eosin	Waldeck GmbH & Co KG, Münster
Goat serum G9023	Sigma-Aldrich Chemie GmbH, Munich
Hematoxylin	Merck KGaA, Darmstadt
Hydrogen peroxide 30 %	Merck KGaA, Darmstadt
Pertex mounting medium	Medite GmbH, Burgdorf
Picric acid	Sigma-Aldrich Chemie GmbH, Munich
Roti®Histofix 4 %	Carl Roth GmbH + Co. KG, Karlsruhe
Roti®Histol	Carl Roth GmbH + Co. KG, Karlsruhe
Saponin	Sigma-Aldrich Chemie GmbH, Munich
Toluidine Blue O	Fluka, Sigma-Aldrich Chemie GmbH, Steinheim
Vectashield® mounting medium without Dapi	Vector Laboratories, Inc., Burlingame, CA, USA
Vectastain ® elite ABC kit	Vector Laboratories, Inc., Burlingame, CA, USA

Table 12 Buffers and solutions for histological analysis

Buffer/Solutions	Components
Alcian Blue, pH 2.5	1 % Alcian blue 3 % Acetic acid
Blocking solution for immunofluorescence	3 % BSA 1.5 % Saponin 1 % Triton®-X 100 Dissolved in PBS
Nuclear fast red	0.1 % Nuclear fast red 2.5 % Aluminium sulfate
Sirius Red Staining solution	0.5 g Sirius Red Picric acid
Sirius Red Washing solution	0.5 % acetic acid
Sodium chloride pH 2.0	1 % NaCl Adjust pH by use of HCl
Toluidine Blue stock solution	1 % Toluidine 70 % Ethanol
Toluidine staining solution	10 % Toluidine Blue stock solution 90 % Sodium chloride pH 2.0

3 METHODS

3.1 MOUSE EXPERIMENTS

All animal studies were performed meeting the requirements of the European guidelines for the care and the use of laboratory animals and were approved by local authorities.

3.1.1 MOUSE STRAINS AND BREEDING

For tissue specific expression of targeted mutations the conditional Cre/loxP (Orban et al., 1992) and the Flp/frt systems (Zhu et al., 1995) were used. For time and site specific expression or inactivation of genes an inducible dual-recombination Flp/frt;CreER^{T2}/loxP system was used (Feil et al., 1997; Schonhuber et al., 2014). Analysis of stroma cell types was performed combining the Flp/frt system (oncogenic Kras$^{G12D/+}$ expression directed to the pancreas) with the Cre/loxP system (targeting different cell types).

All animals were on a mixed *C57BL/6;129S6/SvEv* genetic background unless stated otherwise.

Pdx1-Flp (Schonhuber et al., 2014): This transgene mouse line was generated in Prof. Dr. Saur´s laboratories (Klinikum rechts der Isar, Technical University of Munich). The Flp recombinase is under the control of the *Pdx1* promoter resulting in expression in pancreatic progenitor cells and in adult pancreatic islets.

FSF-Kras^{G12D} (Schonhuber et al., 2014): This knock-in mouse line was generated in Prof. Dr. Saur´s laboratories (Klinikum rechts der Isar, Technical University of Munich). An oncogenic point mutation was introduced in the second exon of the *Kras* gene. The expression of the oncogene is blocked by a STOP cassette flanked by frt sites.

p53^{frt} (Lee et al., 2012): Exon two to six of the murine *Trp53* gene are flanked by frt-sites which are recognized by the Flp recombinase. Upon Flp recombination these flanked exons are excised and the p53 gene is disrupted and therefore inactivated.

FSF-R26$^{CAG-CreERT2}$ (Schonhuber et al., 2014): This knock-in mouse was designed and generated in Prof. Dr. Saur´s group (Klinikum rechts der Isar, Technical University of Munich). The expression of the inducible Cre recombinase is blocked by a frt-flanked STOP cassette.

After excision of the STOP cassette by the Flp recombinase the CreER^{T2} is expressed in cells of the *Flp* lineage. By administration of tamoxifen the Cre recombinase gets activated.

R26$^{CAG\text{-}CreERT2}$ (Schonhuber et al., 2014): This knock-in mouse strain was generated in Prof. Dr. Saur´s laboratories. For expression of the R26$^{CAG\text{-}CreERT2}$ in the whole mouse the *FSF-R26$^{CAG\text{-}CreERT2}$* mouse line was crossed with *R26^{Flp}* deleter-mouse line to remove the frt-flanked STOP cassette allowing CreER^{T2} expression in all organs and cells of the mouse.

R26$^{mT\text{-}mG}$ (Muzumdar et al., 2007): By the use of this mouse line Cre activity can be monitored. Membrane-bound tdTomato, flanked by loxP-sites, is expressed under the *CAG* promoter. Upon Cre-mediated excision of the tdTomato cassette EFGP is expressed, which is also targeted to the membrane. The whole construct was targeted to the *R26* locus as a knock-in.

p53^{LSL} (Ventura et al., 2007): A STOP cassette flanked by loxP sites was introduced in the first intron of the p53 gene. Expression of wildtype p53 is inhibited until Cre-mediated recombination and excision of the STOP cassette. This line allows reconstitution of the p53 protein upon Cre recombination. The mouse line was obtained from Jackson Laboratories (# 008361).

Fsp1-Cre (Bhowmick et al., 2004): The *Fsp1-Cre* line was obtained from Jackson Laboratories (# 012641). The expression of the Cre recombinase is directed to mesenchymal cells expressing the fibroblast specific protein 1 (Fsp1; S100a4, S100 calcium binding protein A4). This transgenic Cre line allows lineage tracing of cells expressing the Fsp1.

Sm22^{Cre} (Zhang et al., 2006): This knock-in mouse line was obtained from Jackson Laboratories (# 006878). Cre recombinase was inserted in-frame of the transgelin (Sm22alpha) initiation site.

Activity of Cre recombinase was detected in adult smooth muscle cells like in arteries, veins and in cardiac myocytes. With this line cells expressing the smooth muscle protein 22 alpha can be analyzed.

Sm22-Cre (Holtwick et al., 2002): The transgenic *Sm22-Cre* mouse line was obtained by Jackson Laboratories (# 004746). The expression of Cre is under control of the smooth muscle

protein 22 alpha promoter (Sm22; transgelin). Expression of Cre could be observed in aorta, uterus and intestine and any other cell which expresses the Sm22 protein.

mGFAP-Cre (Garcia et al., 2004): This transgenic mouse line was obtained from Jackson Laboratories (# 012886). With the help of this line the function of astrocytes and cells expressing GFAP (glial fibrillary acidic protein) can be studied. The Cre recombinase is under the control of the murine GFAP promoter.

hGFAP-Cre (Zhuo et al., 2001): The transgenic *hGFAP-Cre* mouse line was obtained from Jackson Laboratories (# 004600). Cre recombinase is under the control of the human glial fibrillary acidic protein in contrast to the *mGFAP-Cre* mouse line where the recombinase is under the control of the murine protein. Recombination can be detected in the central nervous system, astrocytes, oligodendroglia, ependyma and some neurons.

Cpa3^{Cre} (Feyerabend et al., 2011): This mouse line was kindly provided by Feyerabend et al. The expression of the Cre under the control of the mast cell specific promoter Cpa3 (mast cell protease carboxypeptidase A) leads to a depletion of all mast cells in transgenic mice through a genotoxic mechanism.

R26$^{CAG\text{-}FSF\text{-}LSL\text{-}Ai65tdTom}$ (Madisen et al., 2015): This dual reporter mouse line for Flp and Cre recombinases was obtained from Jackson Laboratories (# 021875). tdTomato expression is blocked by an frt-flanked STOP cassette and by an STOP cassette flanked by loxP sites. The whole construct was introduced as a knock-in into the *R26* locus.

3.1.2 MOUSE GENOTYPING

Mice were genotyped at an age of 2 - 3 weeks. Each mouse got an explicit earmarking which represented the mouse number. DNA for genotyping was extracted from the earmarks as described in 3.4.1.1.

3.1.3 MOUSE DISSECTION

Prior sacrification mice were intraperitoneally injected with 5 mg/kg 5-bromo-2'-deoxyuridine (BrdU), dissolved in sterile PBS, allowing proliferation assays. Instruments and general conditions were kept as sterile as possible. Mice were euthanized with Forene®

isoflurane, fixed and disinfected with 70 % ethanol. After opening the abdomen of the mice 2 mm pieces of the pancreatic tissue were taken for following RNA and protein isolation (3.4.2.1) as well as DNA extraction (3.4.1.1). Samples were stored at -80 °C until further use. In case of PDAC formation a piece of the tumor tissue was taken for tumor cell line isolation (3.3.1) and measurements were taken (weight and size of the tumor). In the following macroscopic pictures were done using the Zeiss Stemi 11 fluorescence stereomicroscope and all necessary organs were fixed overnight in 4 % Roti® Histofix for histological analysis (3.2.1). Samples for cryo sections were only fixed for 1.5 - 2 hours depending on tissue size for further histological analysis.

3.1.4 TAMOXIFEN TREATMENT OF MICE

Mice were fed tamoxifen-containing chow (400 mg tamoxifen citrate per kilogram chow; CreActive TAM400) for 2 - 4 weeks. Control animals were fed Pancrex-Vet food respectively.

3.1.5 ORTHOTOPIC IMPLANTATION OF PANCREATIC DUCTAL ADENOCARCINOMA (PDAC) CELLS IN MICE

For orthotopic implantation only mice on a *C57BL/6* background (F13) were used. Conditions and instruments for implantation were kept as sterile as possible. Mice were anesthetized with MMF (Midazolam, Medetomidine, Fentanyl) intraperitoneally injection. For orthotopic implantation of murine PDAC cells into the pancreas only a small incision in the skin of the abdomen was done. After opening the peritoneum pancreatic tissue was fetched carefully and 2500 cells in serum-free D-MEM medium were orthotopically injected directly into the pancreas (preparation of cells 3.3.7). Peritoneum was sewed with sterile EthilonII fiber with at least 4 - 5 knots. Subsequently the skin of the abdomen was closed using wound clips. Mice were given analgesic (Novalgin, Metacam) and woken up with AFN (atipamezole-flumazenil-naloxone) injection.

3.1.6 HIGH-RESOLUTION SONOGRAPHY

To allow monitoring of the tumor growth high-resolution sonography of implanted mice was performed regularly starting two weeks after implantation. Conditions for sonography were kept as sterile as possible. Mice were narcotized using Forene® isoflurane, fixed and sonography of the abdomen was done. Pictures of the tumor, perfusion of the tumor as well as

tumor volume (automated three-dimensional B-mode imaging) were acquired using Vevo 2100, VisualSonics system. Mice were woken up by withdrawal of Florene® isoflurane. Analysis of sonography was carried out using the integrated Vevo 2100 software package (VisualSonics).

3.2 HISTOLOGICAL ANALYSIS

3.2.1 TISSUE FIXATION AND TISSUE SECTION

For paraffin sections tissue was fixed overnight in 4 % Roti® Histofix. After dehydration by use of tissue processor ASP300 tissues were embedded in paraffin and stored at RT until further use. For staining analysis, series of 2.5 µm sections were prepared of the tissue using the microtome Microm HM355S.

Tissue samples for cryo sections were fixed for 1.5 - 2 h in 4 % Roti® Histofix and afterwards transferred to 15 % sucrose for dehydration and incubated for at least 4 h at 4 °C. For further dehydration tissue was transferred to 30 % sucrose overnight at 4 °C. Prior sectioning tissue was embedded in Tissue-Tek® O.C.T.™ and stored for long term at -80 °C. Series of 8 µm or 20 µm sections were prepared using the cryostat Microm HM 560. Sections were stored at -20 °C until further use.

3.2.2 HEMATOXYLIN AND EOSIN (H&E) STAINING OF TISSUE SECTIONS

Paraffin-embedded tissue sections were dewaxed in Roti® Histol for 2 x 5 min and rehydrated in a decreasing ethanol series (twice 99.8 %, twice 96 % and twice 80 %; each for 2 min). Sections were stained with hematoxylin for 10 sec followed by a 10 min washing step with H_2O. Subsequent staining with eosin was done for 15 sec followed by 3 washing steps with ddH_2O. After dehydration using an increasing ethanol series (twice 80 %, twice 96 % and twice 99.8 %, each 30 sec) sections were incubated 2 x 5 min in Roti® Histol and then mounted with Pertex mounting medium.

3.2.2.1 Quantification and counting of ADM and PanIN lesions

At least three animals per genotype were used for analysis of ADM formation and PanIN lesion formation. For counting, three H&E stained sections (at intervals of 100 µm) of the pancreas were used per mouse and the whole section was counted. Identification of ADM and

PanIN lesions was performed according to established grading for PanIN lesions in mice (Hruban et al., 2006).

3.2.2.2 Quantification of metastases

For the endogenous model 20 animals of each genotype were used for the metastases screen of liver and lung. In case of transplantation all animals were analyzed. 10 sections at intervals of 100 µm were stained for H&E and examined for metastases.

3.2.3 ALCIAN BLUE STAINING

Paraffin-embedded tissue was dewaxed and rehydrated as mentioned in 3.2.2. Slides were stained in alcian blue solution for 5 min, washed in water and counterstained with nuclear fast red staining. Slides were incubated in nuclear fast red staining solution for 5 min and washed in ddH2O. After dehydration and incubation in Roti® Histol as mentioned in 3.2.2 slides were mounted with Pertex mounting medium.

3.2.4 SIRIUS RED STAINING

Paraffin of paraffin-embedded tissue sections was removed as mentioned in 3.2.2. After rehydration of tissue samples using a decreasing ethanol series slides were stained for one hour in Sirius red staining solution. In the following slides were washed at least three times in 0.5 % acetic acid. After dehydration in 100 % ethanol for three times stained tissue samples were incubated for 3 minutes in Roti® Histol and subsequently mounted with Pertex mounting medium.

3.2.5 TOLUIDINE STAINING

Paraffin-embedded tissue was dewaxed and rehydrated as written in 3.2.2. Sections were stained in freshly prepared toluidine staining solution for 2 - 3 min and in the following washed three times with distilled water. Dehydration was done quickly through 96 % and 99.8 % ethanol (each 2 changes). After 2 x 3 min incubation in Rot® Histol sections were mounted with Pertex mounting medium.

3.2.6 IMMUNOHISTOCHEMISTRY

Dewaxing and rehydration of paraffin-embedded tissue sections was done as mentioned in 3.2.2. Sections were cooked in citric acid based unmasking solution for antigen retrieval for 10 min in a microwave and washed after cooling. To block endogenous peroxidase activity slides were incubated with 3 % H_2O_2 for 10 min at RT. Subsequently to avoid unspecific antibody binding sections were washed three times (1 x water, 2 x PBS) and blocked with 5 % serum in PBS for 1 h at RT. For additional blocking the Avidin/Biotin blocking kit (Vector laboratories) was used according to manufactory's protocol. Primary antibody (diluted 1:100) was incubated on sections overnight in 5 % serum in PBS at 4 °C. After three washing steps with PBS secondary antibody (1:500, conjugated to horse reddish peroxidase) was incubated for 1 h at RT in 5 % serum in PBS. For detection the Vectastain® elite ABC kit and the DAB peroxidase substrate kit were used according to manufactory´s protocol. After counterstaining the sections with hematoxylin for 2 - 3 seconds, slides were dehydrated, incubated in Roti® Histol and mounted with Pertex mounting medium as described in 3.2.2.

3.2.7 IMMUNOFLUORESCENCE

3.2.7.1 ToPro3 staining

Cryo sections were thawed and dried at RT. After fixing the sections in 4 % Roti® Histofix for one minute slides were washed with PBS before blocking was done for 1 h at RT using solution C. Cryo sections were incubated with ToPro3 diluted 1:1000 in solution C for 2 h. After washing twice with solution C and once with PBS sections were mounted with Vectashield® mounting medium and stored at 4 °C until they were analyzed by laser scanning microscope Zeiss LSM 510 with a 40x oil objective.

3.2.7.2 Immunofluorescence antibody staining

As mentioned in 3.2.7.1 cryo sections were thawed and dried. For CK19 staining sections were permeabilized with ice-cold methanol for 10 min at 4 °C. For all other antibody staining cryo sections were fixed with 4 % Roti® Histofix for one minute at RT. Subsequently slides were washed with PBS and incubated for 1 h in solution C. Antibodies were diluted 1:100 in solution C applied onto cryo sections. To avoid drying of the sections slides were covered with parafilm and incubated in humid chambers. First antibodies were incubated for 48h at 4 °C and in the following washed with solution C for three times. Secondary antibodies were diluted 1:100

in solution C and incubated overnight at 4 °C. In case of phalloidin staining, slides were additionally counterstained with Alexa Fluor 594–labeled phalloidin (1:250). Three washing steps were followed by mounting cryo sections with Vectashield® mounting medium and slides were stored at 4 °C until analysis was performed using Zeiss LSM 510 with a 40x oil objective.

3.2.7.3 Skin mast cell staining and counting

Ears of respective mice were separated into dorsal and ventral part. For staining, ears were fixed overnight in 1 % Roti® Histofix at 4 °C. After washing with PBS twice and incubation in 1 % BSA in PBS for 1 h at RT, mast cells were stained with avidin-Texas Red (1:500) (Klein et al., 2013). Nuclei were counterstained with ToPro3 as described in 3.2.7.1. At least three mice per genotype and 10 – 15 fields of view of each animal were analyzed by LSM for mast cell counting using the Zeiss LSM 510 microscope with a 20/0.5x air objective.

3.3 CELL CULTURE

All cells were kept under sterile conditions in a laminar flow bench. Cells were cultured in appropriate medium (Table 10) at 37 °C and 5 % CO_2.

3.3.1 ISOLATION, CULTIVATION AND CRYOPRESERVATION OF PANCREATIC TUMOR CELLS

To isolate primary murine pancreatic tumor cells a 3 - 5 mm piece of tumor tissue was taken, transferred into sterile PBS and cut with the help of scalpels into small pieces. Tissue was incubated 24 - 48 h at 37 °C in tumor cell medium containing 200 U/ml of collagenase type II allowing digesting. Subsequently, cells were centrifuged at 150 g and cultured in tumor cell medium.

For isolation of ascites or circulating tumor cells, bloody ascites or blood was collected and sterile EDTA was added to prevent coagulation. In case of non-bloody ascites, liquid was collected and transferred into a cell culture flask for cultivation. Blood or bloody ascites complemented with EDTA was centrifuged for 5 min at 150 g. Supernatant was discarded and cells were taken up in tumor cell medium for culturing.

Isolated primary pancreatic tumor cells and established murine pancreatic tumor cells were regularly supplied with fresh pre-warmed tumor cell medium. Upon reaching a confluence of 80 - 90 % cells were passaged by washing them with sterile PBS and subsequently adding

1 x Trypsin/EDTA to allow detaching of the cells. Small fraction of cell suspension was transferred into a new cell culture flask.

For long-term storage cells were frozen in liquid nitrogen. Therefore, cells were trypsinized and centrifuged for 5 min at 150 g. Supernatant was discarded and cell pellet was resuspended in ice-cold freezing medium and immediately stored at -80 °C for 24 h and then transferred to liquid nitrogen.

3.3.2 TAMOXIFEN TREATMENT OF ISOLATED PRIMARY PANCREATIC TUMOR CELLS

For tamoxifen treatment, cells were trypsinized and counted using Neubauer hemocytometer. 200.000 cells were seeded in 10 cm dishes and treated for 6 days with 500 nM 4-hydroxytamoxifen (4-OHT) or with ethanol as control respectively. Tamoxifen or ethanol medium was replaced every day. After tamoxifen treatment cells were seeded for functional assays.

3.3.3 CELL VIABILITY ASSAY OF PANCREATIC TUMOR CELLS

To measure cell viability of either tamoxifen-treated or ethanol-treated cells, 1000 cells were seeded per well in a 96-well plate. For the next four following days cell viability was measured using a colorimetric assay based on the chemical reduction of MTT (3-(4,5-Dimethylthiazol-2-yl)-2,5-diphenyltetrazolium bromide) to formazan which has a purple color. The reduction is mediated by NAD(P)H-dependent oxidoreductase assessing the cellular metabolic activity. 10 µL of MTT reagent (5 mg/mL MTT dissolved in PBS) were added to each well and incubated for 4 h at 37 °C. Afterwards, medium was discarded and cells were lysed in 300 µL ethanol/DMSO solution (mixed 1:1). Before OD determination plate was incubated on a shaker for about 10 minutes at RT. OD measurement was performed at 600 nm wavelengths. Technical triplicates in three independent experiments were carried out.

3.3.4 CLONOGENIC ASSAY

Cells treated with tamoxifen for 6 following days were counted and in the following 1000 cells were seeded per well of a six-well plate. After allowing growth of cell colonies for 10 to 14 days medium was discarded and cells washed with PBS twice. For fixation 99% ice-cold methanol was added to cells and incubated for 30 min at RT while shaking. Methanol was aspired and Giemsa staining solution (diluted 1:20 in distilled water) was used for staining of

cells. Colonies were stained for two hours shaking at RT and afterwards washed with distilled water until staining was even spread. Plates were scanned with the help of Epson scanner advice after air-drying of plates.

3.3.5 IMMUNOFLUORESCENCE OF PANCREATIC CANCER CELLS

Cells were counted using Neubauer hemocytometer and seeded on sterile coverslips. Upon confluence of 70 - 80% cells were washed with PBS and fixed with 4 % Roti® Histofix for 2 h. Coverslips were washed three times with PBS and afterwards mounted with Vectashield® mounting medium to allow analysis with Zeiss LSM 510 laser scanning microscope.

3.3.6 FACS ANALYSIS OF ISOLATED PRIMARY TUMOR CELLS

Isolated primary cancer cells of PDAC bearing animals were analyzed by FACSCalibur™. After trypsinization cells were centrifuged for 5 minutes at 150 g at RT and subsequently resuspended in PBS. FACS analysis was performed for cell size (forward and sideward scatter) and for tdTomato and EGFP fluorescence (FL2 and FL1). For each examined cell line 50000 cells were used. Analysis was performed with the help of FlowJo software.

3.3.7 PREPARATION OF CELLS FOR IMPLANTATION

Pancreatic tumor cells isolated from backcrossed mice were cultured in tumor cell medium. For implantation cells were trypsinized and cell number was determined with the Neubauer hemocytometer. Cells were centrifuged for 5 min at 150 g and cell pellet was resuspended in D-MEM medium without FCS and penicillin/streptomycin. For implantation 2500 cells were taken up in a small volume of D-MEM as possible.

3.4 MOLECULAR TECHNIQUES

3.4.1 DNA ANALYSIS

3.4.1.1 Genomic DNA isolation

For genotyping of mice DNA was isolated from earmarks of genotyping of mice (3.1.2). To analyze activity of recombinase a small piece of tissue was used for DNA isolation. Cells were centrifuged at 150 g for 5 min and cell pellet was used to isolate genomic DNA. Earmarks,

cell pellet or tissue were incubated in PCR lysis buffer (Soriano, with freshly added proteinase K, Table 6) for 90 minutes at 55 °C. To inactivate proteinase K samples were incubated at 95 °C for 15 minutes. Afterwards, samples were mixed thoroughly and centrifuged for 10 minutes at 16000 g. Supernatant containing DNA was carefully transferred into a new tube and PCR analysis was performed.

3.4.1.2 Polymerase chain reaction (PCR)

To determine the exact genotype of each mouse PCR analysis was performed. Reaction was done using a master pre-mix. Composition of pre-mix is shown in Table 13. General conditions of PCR are depicted in Table 14. For each reaction 1 µL of isolated DNA was used and amplification was done for 40 cycles. PCR products were visualized directly performing agarose gel electrophoresis (3.4.1.4) or stored at 4 °C until usage.

Table 13 Composition of pre-mix for PCR

Buffer/solution	Volume for one reaction
ddH_2O	4.375 µL
10 x buffer S	2.5 µL
30 % sucrose	2.5 µL
SucRot	2.5 µL
PeqTaq	0.125 µL
dNTPs (10 µM each)	0.5 µL

Table 14 Reaction mix and conditions of PCR

Reaction mix		PCR conditions		
12.5 µL	pre-mix	94 °C	3 min	
0.25 – 2 µL	forward primer (10 µM)	94 °C	30 sec	40 x
0.25 – 2 µL	reverse primer (10 µM)	55-65 °C	45 sec	
1 µL	isolated DNA	72 °C	90 sec	
ad 25 µL	ddH_2O	25 °C	∞	

3.4.1.3 Genotyping PCRs

Isolated genomic DNA (3.4.1.1) was used to distinguish different genotypes of mice. Specific primers were designed for each allele. Primer pairs, annealing temperature and specific PCR products are listed in Table 15. Annealing temperatures were adjusted according to used primers. Recombination-PCRs were designed to analyze activity of recombinase. PCRs and their products are depicted in Table 16.

Table 15 Genotyping-PCRs, annealing temperature and products

bp = base pairs; mut = mutated; WT = wild type

Genotyping-PCR	Annealing temperature	PCR products
Pdx1-Flp	55 °C	620 bp (mut)/290 bp (internal control)
FSF-Kras$^{G12D/+}$	56 °C	351 bp (mut)/270 bp (WT)
Cpa3^{Cre}	62 °C	450 bp (mut)/320 bp (WT)
p53^{frt}	57 °C	292 bp (mut)/258 bp (WT)
CreER^{T2}	55 °C	190 bp (mut)
FSF-STOP	60 °C	600 bp (mut)
R26-CAG	62 °C	450 bp (mut)/650 bp (WT)
R26^{mT-mG}	62 °C	450 bp (mut)/650 bp (WT)
General Cre	58 °C	390 bp (mut)/290 bp (internal control)
p53^{LSL}	65 °C	278 bp (mut)/365 bp (WT)
hGFAP-Cre	55 °C	190 bp (mut)/700 bp (WT)
R26	62 °C	310 bp (mut)/600 bp (WT)

Table 16 Recombination PCRs

Recombination-PCR	Annealing temperature	PCR products
FSF-Kras del	60 °C	196 bp
FSF-STOP del	60 °C	490 bp
p53-frt recombined	55 °C	352 bp

3.4.1.4 Agarose gel electrophoresis

To visualize PCR products agarose gel electrophoresis was performed. 1.5 – 2 % agarose gels (in 1 x TAE) containing ethidium bromide were loaded with 12.5 µL of each PCR sample and run for 1.5 h at 120 V. Separated bands were detected by the help of the Gel DocTM XR+ system.

3.4.2 PROTEIN ANALYSIS

3.4.2.1 Isolation of whole cell protein extract

For protein analysis of tissue samples were homogenized in protein lysis buffer supplemented with protease and phosphatase inhibitors (Table 6). Homogenized samples were immediately shock frozen in liquid nitrogen. For preparation of lysate from established cell lines, cells were washed with ice cold PBS, lysed in protein lysis buffer with added protease and phosphatase inhibitors and frozen in liquid nitrogen. Tissue lysates as well as cell line lysates were stored at -80 °C until further use. For whole cell protein extraction samples were thawed on ice and centrifuged at full speed for 20 min at 4 °C. Supernatant containing protein extract was transferred into new tube and protein concentration was determined as mentioned in 3.4.2.2.

3.4.2.2 Determination of protein concentration

Allowing same protein load for protein analysis the protein concentration was determined by performing Bradford assay (Bradford, 1976). Therefore, Bradford reagent was diluted 1:5 in water and to 300 µL reagent 1 µL of prepared protein sample (3.4.2.1) was added and mixed. OD values at 600 nm were measured and protein concentration calculated with the help of a BSA standard curve. Triplicates of each sample were performed. Subsequently, protein concentration was adjusted by adding protein loading buffer (Laemmli, 1970). For denaturation protein samples were incubated for 5 minutes at 95 °C and afterwards stored at -20 °C until further use.

3.4.2.3 SDS polyacrylamide gel electrophoresis

To separate proteins by size standard sodium dodecyl sulfate polyacrylamide gel electrophoresis (SDS-PAGE) was performed (Laemmli, 1970). Therefore, a 10 % or 12 % separation gel was prepared according to Table 17. TEMED was added last and separation gel mix was poured into gel caster. Gel was covered with 2-propanol and allowed to polymerize.

Stacking gel was pipetted according to Table 17 and poured onto separation gel. After polymerization 80 µg of protein samples were loaded onto the gel. Electrophoresis was performed for 1 to 2 hours in running buffer at 80 to 120 V depending on molecular weight of protein of interest. To estimate approximate molecular weight of separated proteins Prestained protein ladder PageRuler^{TM} was loaded onto the gel.

Table 17 SDS gel for electrophoresis of proteins

Stacking gel		10 % separating gel		12 % separating gel	
1500 µL	H_2O	2050 µL	H_2O	1700 µL	H2O
650 µL	Stacking gel buffer	1300 µL	Separating gel buffer	1300 µL	Separating gel buffer
375 µL	Rotiphorese® gel 30	1650 µL	Rotiphorese® gel 30	2000 µL	Rotiphorese® gel 30
25 µL	10 % SDS	50 µL	10 % SDS	50 µL	10 % SDS
12.5 µL	10 % APS	25 µL	10 % APS	25 µL	APS
7.5 µL	TEMED	5 µL	TEMED	5 µL	TEMED

3.4.2.4 Immunoblotting

Separated proteins were transferred onto PVDF membrane, which was activated before by incubation in methanol (immobilon-P). Wet blot was carried out at 360 mA for 2 hours in transfer buffer (Towbin et al., 1979). To block unspecific antibody binding membrane was incubated in blocking solution (PBS containing 0.1 % Tween® 20 and 5 % non-fat dry milk or BSA) for at least 30 min at RT shaking. After three washing steps in PBS with 0.1 % Tween® 20, membrane was incubated with first antibody (dilutions as mentioned in 0) overnight at 4 °C while gentle shaking. Next, membrane was washed with PBS containing 0.1 % Tween® 20 three times and incubated with secondary antibody, diluted 1:10000, for at least one hour at RT while shaking. Subsequently, after additional washing steps membrane was scanned at 700 nm and 800 nm wave length using Odyssey® infrared imaging system. Loading control was performed using α-tubulin.

4 RESULTS

Genetically engineered mouse models have been a useful tool for recapitulating the human disease in many aspects but the well-established *Ptf1a*$^{Cre/+}$*;LSL-Kras*$^{G12D/+}$ (*KC*) model does not allow sequential or secondary manipulation of the tumor. Therefore, a new dual-recombination mouse model has been generated combining the Cre/loxP and the Flp/frt recombination systems (Schonhuber et al., 2014).

4.1 ONCOGENIC KRAS^{G12D} EXPRESSION IN THE *PDX1-FLP* LINEAGE LEADS TO PDAC DEVELOPMENT

In this present study, the Flp recombinase driven by the *Pdx1* promoter leads to expression of oncogenic Kras^{G12D}, which is silenced by an frt-flanked STOP cassette. Schonhuber et al. have shown that *Pdx1-Flp;FSF-Kras*$^{G12D/+}$ (*KF*) mice develop PanIN lesions and PDAC similar to the most-commonly used murine model of PDAC *Pdx1-Cre;LSL-Kras*$^{G12D/+}$ (*KC*) (Schonhuber et al., 2014). *KF* mice show a similar overall survival compared to *KC* mice (401 days vs. 383 days, respectively). The tumor suppressor p53 is known to be inactivated in many different tumor types. Its inactivation leads to an acceleration of tumor progression (Feldmann and Maitra, 2008). Therefore, the *p53*^{frt} mouse line was bred with *Pdx1-Flp;FSF-Kras*$^{G12D/+}$ (*KF*) mice (genetic scheme in Fig.4 A). Obtained *Pdx1-Flp;FSF-Kras*$^{G12D/+}$*;p53*^{frt} mice (*KPF*) were compared to *Pdx1-Cre;LSL-Kras*$^{G12D/+}$*;LSL-p53*$^{R172H/+}$ (*KPC*) animals. *Pdx1-Flp;FSF-Kras*$^{G12D/+}$*;p53*$^{frt/+}$ (*KPF*) and *Pdx1-Flp;FSF-Kras*$^{G12D/+}$*;p53*$^{frt/frt}$ mice developed solid pancreatic ductal adenocarcinomas, which were well-to-moderately differentiated as well as undifferentiated (Fig.4 B).

Heterozygous as well as homozygous *p53* inactivation accelerated tumor progression resulting in a shortened survival (Fig.4 C). Animals with heterozygous p53 inactivation showed a median survival of 181 days. In comparison, *KPC* mice with a heterozygous p53 gain of function mutation (R172H) lived 160 days (Schonhuber et al., 2014). Homozygous inactivation of p53 in *Pdx1-Flp;FSF-Kras*$^{G12D/+}$ mice shortened the survival to 83 days (Fig.4 C), which was similar to the median survival time of the classical mouse model *KPC* with homozygous p53 gain-of-function mutation (60 days).

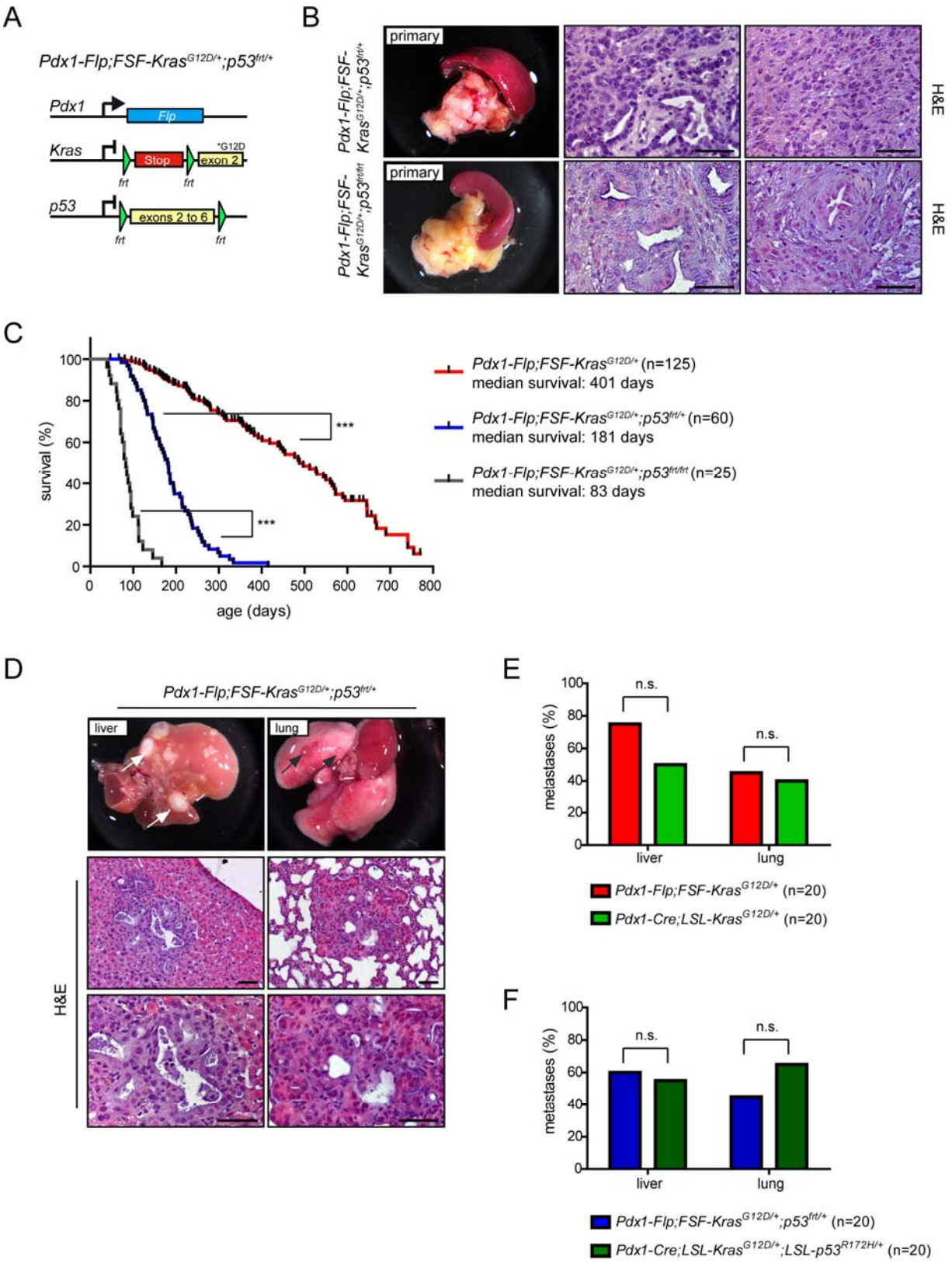

Fig.4 ***Pdx1-Flp*-activated expression of oncogenic Kras^{G12D} leads to pancreatic adenocarcinoma and metastases.** (Figure legend continued on next page)

(**A**) Genetic scheme of *Pdx1-Flp;FSF-Kras*$^{G12D/+}$*;p53*^{frt} mouse model. Expression of oncogenic Kras^{G12D} is blocked by a STOP cassette flanked by frt-sites. *Pdx1-Flp*-induced p53 deletion by excision of exons 2 to 6. (**B**) Left panel: representative macroscopic pictures of primary pancreatic tumors of *Pdx1-Flp;FSF-Kras*$^{G12D/+}$*;p53*$^{frt/+}$ as well as *Pdx1-Flp;FSF-Kras*$^{G12D/+}$*;p53*$^{frt/frt}$. Right panel: Corresponding Hematoxylin and Eosin (H&E) staining of primary well-to-moderately differentiated and undifferentiated PDAC. (**C**) Kaplan-Meier survival curves of indicated genotypes. $^{+}$ denotes the wild type allele, *p53*^{frt} denotes the conditional frt-flanked p53 allele. Log rank test was performed, ($p<0.0001$); *** means p-value below 0.0001. (*KF* mice n=125; heterozygous *KPF* mice n=60; homozygous *KPF* mice n=25) (**D**) Upper panel: representative macroscopic pictures of liver and lung metastases of *Pdx1-Flp;FSF-Kras*$^{G12D/+}$*;p53*$^{frt/+}$ mice; lower panel: H&E staining of PDAC-associated liver and lung metastases of *Pdx1-Flp;FSF-Kras*$^{G12D/+}$*;p53*$^{frt/+}$ mice (liver metastases indicated by white arrows; lung metastases indicated by black arrows). (**E+F**) Quantification of PDAC-bearing mice with microscopic liver and lung metastases of indicated genotypes (n=20 mice per genotype). Bar graphs show percentage of mice with microscopic liver and lung metastases (n.s.; not significant by Fisher´s exact test). (**E)** Mice with p53 wild type status; (**F)** Mice carrying either heterozygous p53 deletion or heterozygous p53 activating mutation *R172H*. Scale bars 50 µm.

Tumor-bearing *KF* mice with either wild type p53 or inactivated p53 gene developed liver and lung metastases (Fig.4 D-F) as do *KC* and *KPC* animals. 75 % of the *KF* mice showed liver metastases whereas only half of the analyzed *KC* mice developed liver metastases (Fig.4 E). In case of observed lung metastases, the rates of their occurrence was similar between the *KF* (45 % developed lung metastases) and the *KC* mice (40 % showing lung metastases, Fig.4 E). 60 % of the analyzed mice of the *KPF* cohort developed liver metastases compared to 55 % of the *KPC* mice. In 45 % of the *KPF* animals and in 65 % of the *KPC* lung metastases were detected (Fig.4 F). The *KF* as well as the *KPF* mouse models are comparable to the well-established *KC* and *KPC* models (Schonhuber et al., 2014).

4.2 DUAL-RECOMBINATION SYSTEM FOR PANCREATIC DUCTAL ADENOCARCINOMA (PDAC)

4.2.1 SEQUENTIAL MANIPULATION OF THE PANCREAS

Using the newly generated *KF* mouse model, it is possible to phenocopy a multi-step carcinogenesis process similar to the human disease. The combination of the Flp/frt recombination system with the Cre/loxP recombination system allows the sequentially and time-specifically manipulation of tumor development and its progression. The *KF* mice were bred with a tamoxifen-inducible *CreER*^{T2} mouse line (Feil et al., 1997) directed to the *Pdx1-Flp* lineage (Fig.5 A). A STOP cassette flanked by frt sites blocks the expression of *CreER*^{T2}. Upon Flp expression the STOP cassette is excised and CreER^{T2} is expressed from the *Rosa 26* locus (under the control of the CAG promoter; *FSF-R26*$^{CAG\text{-}CreERT2}$) (Schonhuber et al., 2014). By treatment of mice with tamoxifen, CreER^{T2} gets activated and floxed genes can get activated or

inactivated. PCR analysis of different tissues isolated from *Pdx1-Flp;FSF-R26*$^{CAG\text{-}CreERT2}$ animal showed deletion of the frt-STOP-frt (FSF) cassette in Pdx1 expressing tissues only (Fig.5 B). Excision of the FSF cassette was detected in the pancreas, duodenum and common bile duct whereas tissues negative for Pdx1 expression showed no deletion of the STOP cassette like heart, lung or liver. To analyze the *CreER*^{T2} activity in the *Flp* lineage, the *R26*$^{mT\text{-}mG}$ reporter line was used (Muzumdar et al., 2007). This reporter switches from membrane-bound tdTomato to membrane-tagged EGFP upon Cre activity (Fig.5 C). Tamoxifen treatment of *Pdx1-Flp;FSF-R26*$^{CAG\text{-}CreERT2}$*;R26*$^{mT\text{-}mG}$ animals resulted in change from tdTomato signal to EGFP expression (Fig.5 D). To prove that all compartments of the pancreatic tissue are targeted by the *Pdx1-Flp*-dependent CreER^{T2} activity, pancreata of vehicle-treated and tamoxifen-treated animals were stained for insulin, CK19 and α-amylase (Fig.5 E-G). Upon tamoxifen treatment pancreatic islets (stained by insulin, Fig.5 E), pancreatic acini (shown by α-amylase staining, Fig.5 F) as well as pancreatic ducts (here shown by CK19 staining, Fig.5 G) get recombined by Cre recombinase.

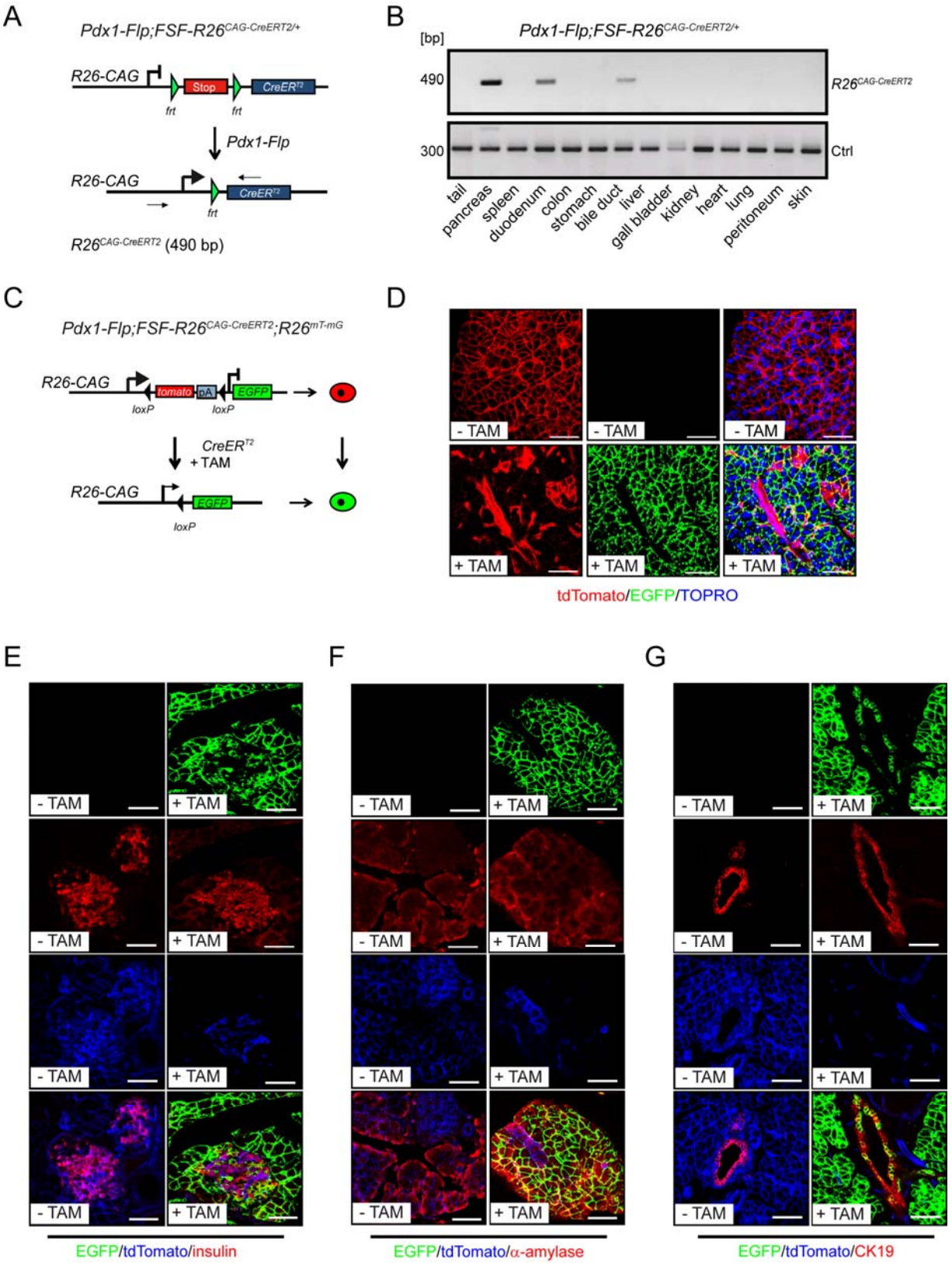

Fig.5 Sequential targeting of the pancreas using a dual-recombination system. (Figure legend continued on next page)

(**A**) Genetic scheme of *Pdx1-Flp* activated expression of $CreER^{T2}$ from the *Rosa26* locus. (**B**) PCR analyses of *Pdx1-Flp*-induced excision of the STOP cassette flanked by frt-sites in the *Rosa26* locus in indicated tissues. (**C**) Genetic strategy to induce *Pdx1-Flp* dependent Cre activation upon tamoxifen treatment. Monitoring of Cre activity in the *Flp* lineage by using a double fluorescent floxed tdTomato-EGFP reporter line ($R26^{mT\text{-}mG}$). Upon tamoxifen treatment Cre recombinase is activated leading to a switch from membrane-tagged tdTomato to membrane-tagged EGFP expression. (**D**) Representative confocal microscopy pictures of pancreatic tissue of $Pdx1\text{-}Flp;FSF\text{-}R26^{CAG\text{-}CreERT2};R26^{mT\text{-}mG}$ mice either vehicle-treated (-TAM) or tamoxifen-treated (+TAM). Cre activity in the *Flp* lineage after tamoxifen treatment is depicted in green whereas red color shows expression of tdTomato of vehicle-treated cells and cells independent of Flp. Nuclei were counterstained with TOPRO-3 (blue). (**E-G**) Pancreas of $Pdx1\text{-}Flp;FSF\text{-}R26^{CAG\text{-}CreERT2};R26^{mT\text{-}mG}$. Cells depicted in blue express tdTomato; cells depicted in green show Cre activity upon tamoxifen treatment. (**E**) Staining of pancreatic islets for insulin (red) of either vehicle or tamoxifen-treated mice. (**F**) α-amylase staining (red) of acini of pancreas of vehicle or tamoxifen-treated mice. (**G**) CK19 staining of pancreatic ducts (red) of mice treated with vehicle or tamoxifen. Scale bars 50 μm.

Besides pancreatic tissue various other organs of vehicle-treated and tamoxifen-treated animals were analyzed for Cre activity. Vehicle-treated animals showed no recombination excluding leaky Cre activity (Fig.6 A). Sporadic extrapancreatic Cre-mediated recombination after tamoxifen treatment was observed in stomach and duodenum. No recombination was detected in liver, heart, lung and spleen (Fig.6 B).

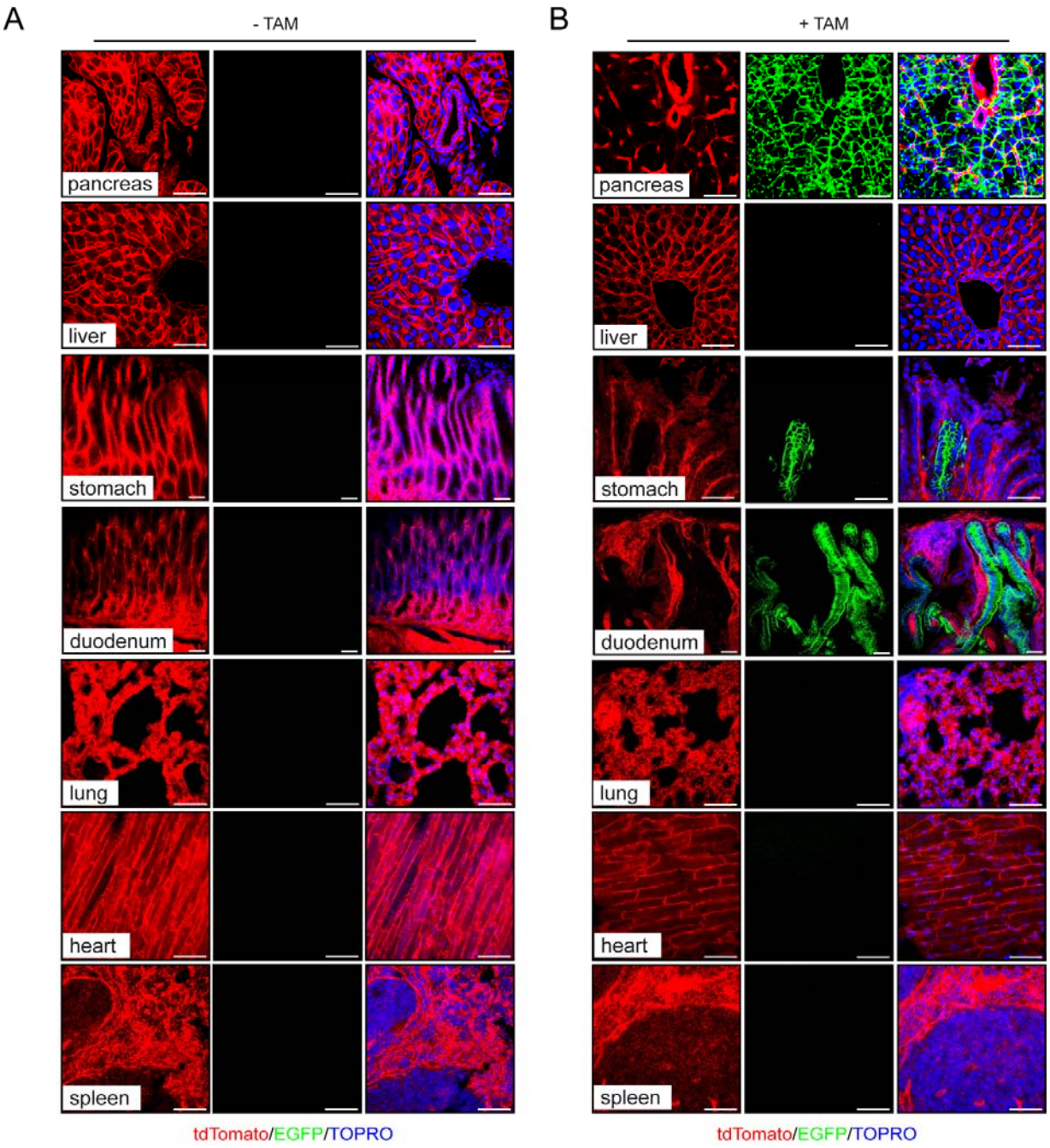

Fig.6 Cre recombination in the *Pdx1* lineage.
(**A**) Representative confocal microscopy pictures of indicated tissues of vehicle-treated (-TAM) *Pdx1-Flp;FSF-R26*$^{CAG\text{-}CreERT2}$*;R26*$^{mT\text{-}mG}$ mouse. Left panel: tdTomato expressing cells, middle panel; EGFP positive cells, right panel: merged picture. (**B**) Representative confocal microscopy pictures of tamoxifen-treated (+TAM) *Pdx1-Flp;FSF-R26*$^{CAG\text{-}CreERT2}$*;R26*$^{mT\text{-}m}$ animals. Left panel: tdTomato positive cells, middle panel: EGFP positive cells which are recombined by Cre, right panel: merged picture. Red cells are non-recombined and express tdTomato. (**A+B**) Nuclei were stained with TOPRO-3 (blue). Scale bars 50µm.

4.2.2 TAMOXIFEN-INDUCIBLE GENETIC MANIPULATION OF THE WHOLE ANIMAL

To allow analysis of possible consequences of inactivation/activation of therapeutic targets or their pathways of the whole organism, a *R26*$^{CAG\text{-}CreERT2}$ mouse line was used. The FSF cassette of the *FSF-R26*$^{CAG\text{-}CreERT2}$ construct was deleted using a *R26*^{Flp} mouse line. Upon removal of the FSF cassette the *CreER*^{T2} was expressed ubiquitously from the *Rosa 26* locus under the control of the CAG promoter. Upon high dose tamoxifen treatment, Cre-mediated recombination was identified in various tissues (Fig.7). Stereomicroscopic pictures visualize no switch from tdTomato to EGFP in vehicle-treated animals (Fig.7 A), whereas recombination of the *R26*$^{mT\text{-}mG}$ reporter from membrane-tagged tdTomato to membrane-bound EGFP was observed after tamoxifen treatment (Fig.7 B). Confocal microscopic images of different organs show efficient Cre recombination of the *R26*$^{mT\text{-}mG}$ reporter (Fig.7 C).

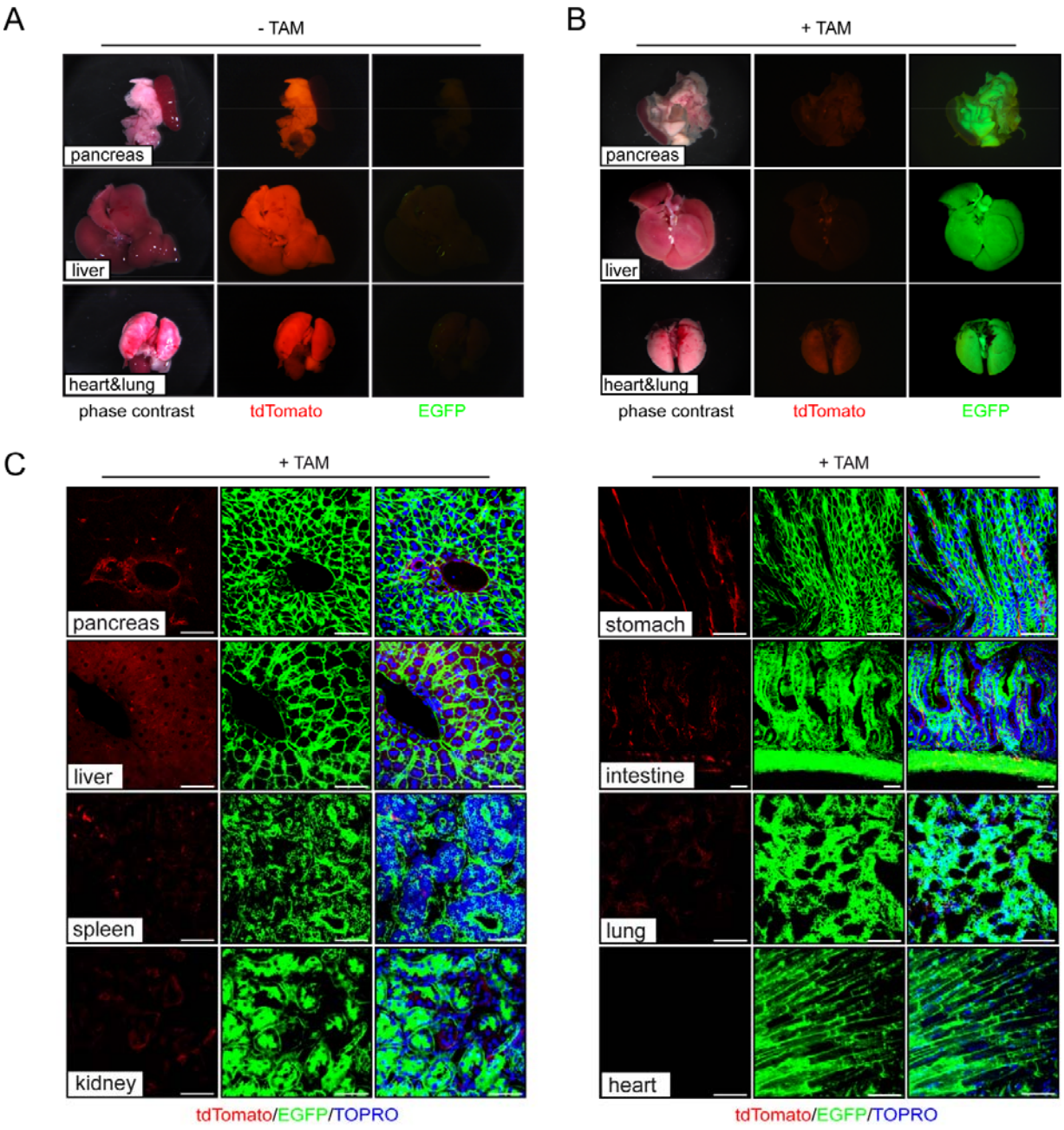

Fig.7 Inducible Cre-mediated gene targeting in the whole organism.
(**A**) Representative macroscopic pictures of spleen and pancreas, liver, heart and lung of vehicle-treated (-TAM). (**B**) Representative macroscopic images of tamoxifen-treated (+TAM) animals. (**A+B**) Left: white-light pictures and corresponding fluorescent pictures. tdTomato (red color, non Cre-recombined cells, middle panel) and EGFP (green color, Cre-recombined cells, right panel) expression was visualized by fluorescence stereomicroscopy. (**C**) Confocal microscopy pictures of indicated organs after tamoxifen treatment. Red color shows membrane-tagged tdTomato of non-Cre recombined cells; green color shows EGFP expression of Cre recombined cells. Nuclei were counterstained with TOPRO-3 (blue). Scale bars 50 µm.

Vehicle-treated animals showed no recombination of the *R26*$^{mT\text{-}mG}$ reporter (Fig.8 A), whereas a low dose tamoxifen treatment resulted in sporadic recombination of the *R26*$^{mT\text{-}mG}$ reporter by Cre (Fig.8 B).

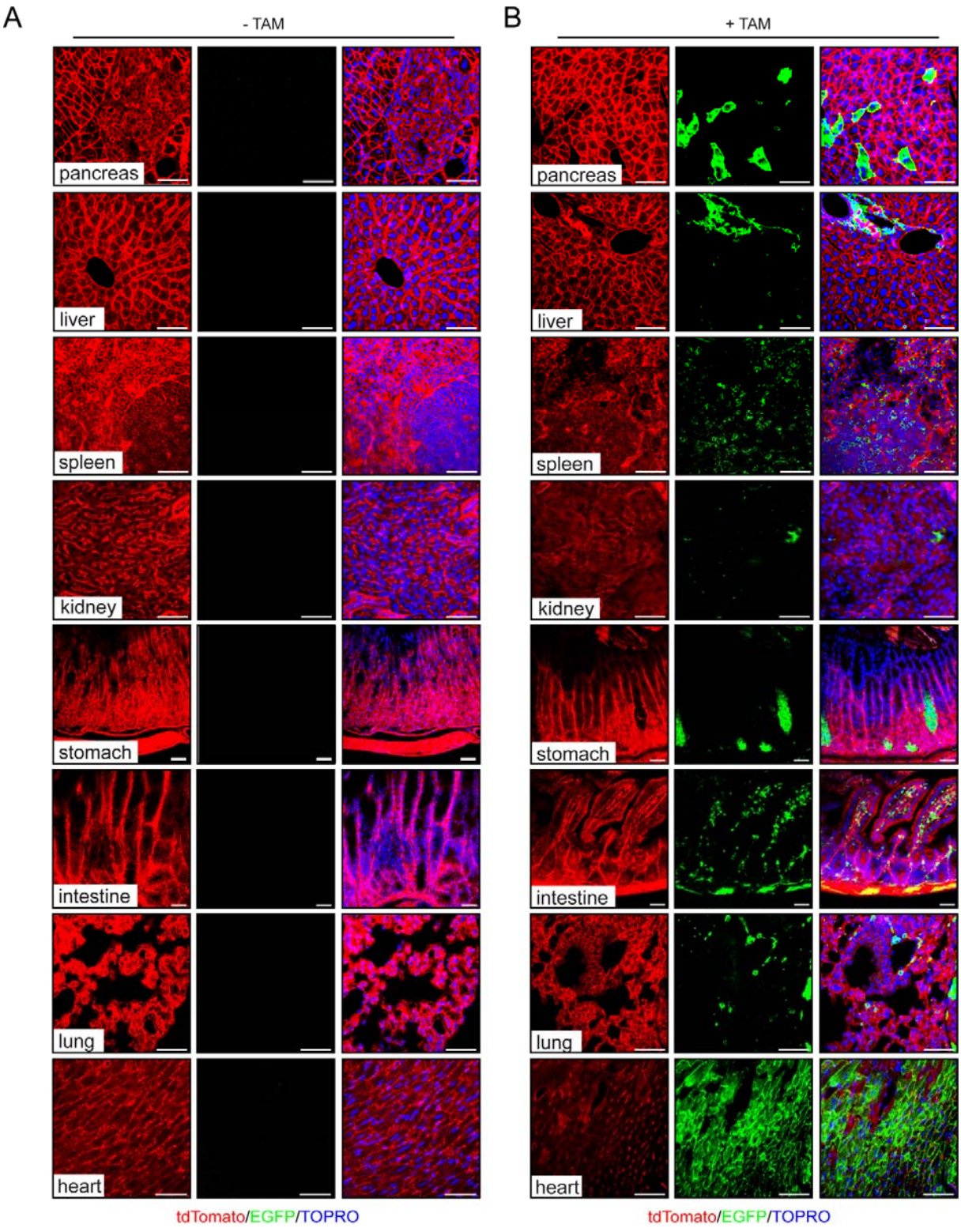

Fig.8 Dose dependency of tamoxifen-induced recombination in whole body.
Representative images of $R26^{CAG\text{-}CreERT2}$;$R26^{mT\text{-}mG}$ animals. (**A**) Confocal microscopy pictures of indicated organs of a vehicle-treated mice (-TAM). (Figure legend continued on next page)

(**B**) Representative confocal microscopy pictures of indicated organs after low dose of tamoxifen treatment (+TAM). Red color depicts tdTomato expressing cells, green depicts EGFP expressing cells. Nuclei were stained with TOPRO-3 (blue). Scale bars 50 μm.

4.2.3 SECONDARY MANIPULATION OF PANIN LESIONS

For secondary manipulation of PanIN lesions and PDAC, *FSF-R26*$^{CAG\text{-}CreERT2}$ mice were bred with *KF* mice (Fig.9). To monitor tamoxifen-induced Cre activity, the *R26*$^{mT\text{-}mG}$ reporter line was used (genetic scheme is given in Fig.9 A). In Fig.9 B the switch from tdTomato to EGFP in PanIN lesions of *Pdx1-Flp;FSF-Kras*$^{G12D/+}$*;FSF-R26*$^{CAG\text{-}CreERT2}$*;R26*$^{mT\text{-}mG}$ mice is depicted. Cells of PanIN lesions were recombined after tamoxifen treatment (as visualized by EGFP expression, green color; PanIN lesions with highest observed grade are indicated by arrow heads) whereas stromal cells remained red (tdTomato expression, indicated by arrows) (Fig. 9B, right panel). There was no evidence of Cre-mediated recombination in the vehicle-treated animals (Fig.9 B, left panel) excluding leaky Cre activity. Recombined PanIN lesions also express the ductal marker CK19 as depicted in Fig.9 C.

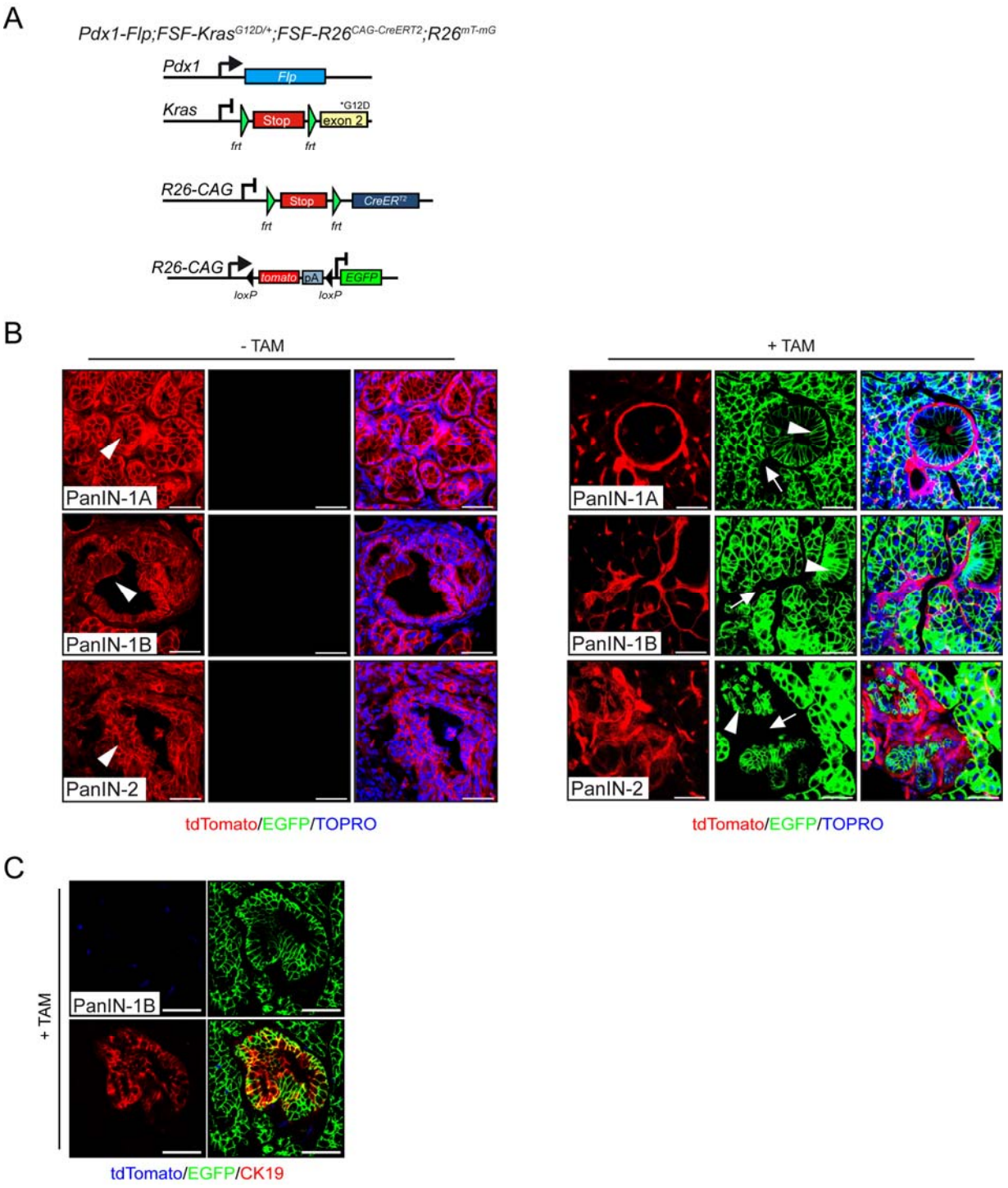

Fig.9 Secondary genetic manipulation of established Kras^{G12D}-induced PanIN lesions in the *Pdx1-Flp* lineage.

(**A**) Genetic strategy of *Pdx1-Flp* activated expression of oncogenic Kras^{G12D} and CreERT2 from the *Rosa26* locus. Tamoxifen treatment leads to activation of Cre recombinase and switch of membrane-tagged tdTomato to membrane-tagged EGFP. (**B**) Confocal microscopy pictures of PanINs of different grades (PanIN-1A to PanIN-2) of *Pdx1-Flp;FSF-Kras$^{G12D/+}$;FSF-R26$^{CAG-CreERT2}$;R26^{mT-mG}* mice. Left panel: Different PanIN stages of vehicle-treated mice. Arrowheads indicate highest-grade PanIN lesions. Right panel: PanINs of different grades of tamoxifen-treated mice (Figure legend continued on next page).

Red color shows non Cre recombined cells, green color shows Cre recombined cells. Arrowheads indicate highest-grade PanIN lesions. Arrows show non Cre recombined stromal cells. Nuclei were counterstained with TOPRO-3 (blue). (**C**) CK19 staining (red) of PanIN-1B of tamoxifen-treated mouse. Membrane-tagged tdTomato is shown in blue, membrane-tagged EGFP is shown in green. Scale bars 50 µm.

4.2.4 RESTORATION OF P53 WILD TYPE IN ESTABLISHED PDAC

Schonhuber et al. could show that time-specific modulation of the pancreas is possible using the dual-recombination system and this system provides the chance to recapitulate the human multistep carcinogenesis (Schonhuber et al., 2014). Tumor development and progression often require oncogene activation and inactivation of tumor suppressor genes like p53. Loss of p53 is not only necessary for tumor development but also important for continued cell proliferation or for survival of established tumor (Ventura et al., 2007). To analyze the influence of p53 loss as well as p53 restoration on tumor progression, a mouse line carrying a floxed STOP cassette between exon 1 and exon 2 of the p53 gene was used ($p53^{LSL}$, (Ventura et al., 2007)). Upon Cre-mediated recombination, the STOP cassette was excised and p53 wild type is expressed. Bred with the *Pdx1-Flp;FSF-Kras*$^{G12D/+}$*;FSF-R26*$^{CAG\text{-}CreERT2}$ mouse line the impact of p53 restoration in established tumor can be analyzed after tamoxifen treatment (Fig.10 A). Vehicle-treated *Pdx1-Flp;FSF-Kras*$^{G12D/+}$*;FSF-R26*$^{CAG\text{-}CreERT2}$*;p53*$^{LSL/LSL}$ mice displayed a dramatically shortened median survival of 41 days due to the lack of p53 expression, which is blocked by the LSL element (Fig.10 B). Heterozygous mutant mice with LSL mediated blockade of one p53 allele (*Pdx1-Flp;FSF-Kras*$^{G12D/+}$*;FSF-R26*$^{CAG\text{-}CreERT2}$*;p53*$^{LSL/+}$) had an overall median survival of 127 days. *KPF* mice, with an heterozygous loss of p53 due to recombination of frt-sites, displayed an overall survival of 181 days of (Fig.4 C) and lived around 50 days longer (which is significantly longer; $p<0.0001\%$) than vehicle-treated *Pdx1-Flp;FSF-Kras*$^{G12D/+}$*;FSF-R26*$^{CAG\text{-}CreERT2}$*;p53*$^{LSL/+}$ animals. This might be due to the global inactivation of one *p53* allele in the *p53*^{LSL} model, compared to the pancreas specific deletion of *p53* in the *p53*^{frt} model. Analysis of PDAC in animals with a heterozygous p53 inactivation showed well-to-moderately differentiated as well as undifferentiated tumors (Fig.10 C). Expression of p53 was detectable in few tumor cells of mice carrying a heterozygous p53 inactivation (Fig.10 C), indicating that loss of heterozygousity of the p53 WT allele occurs in some, but not in all tumour cells.

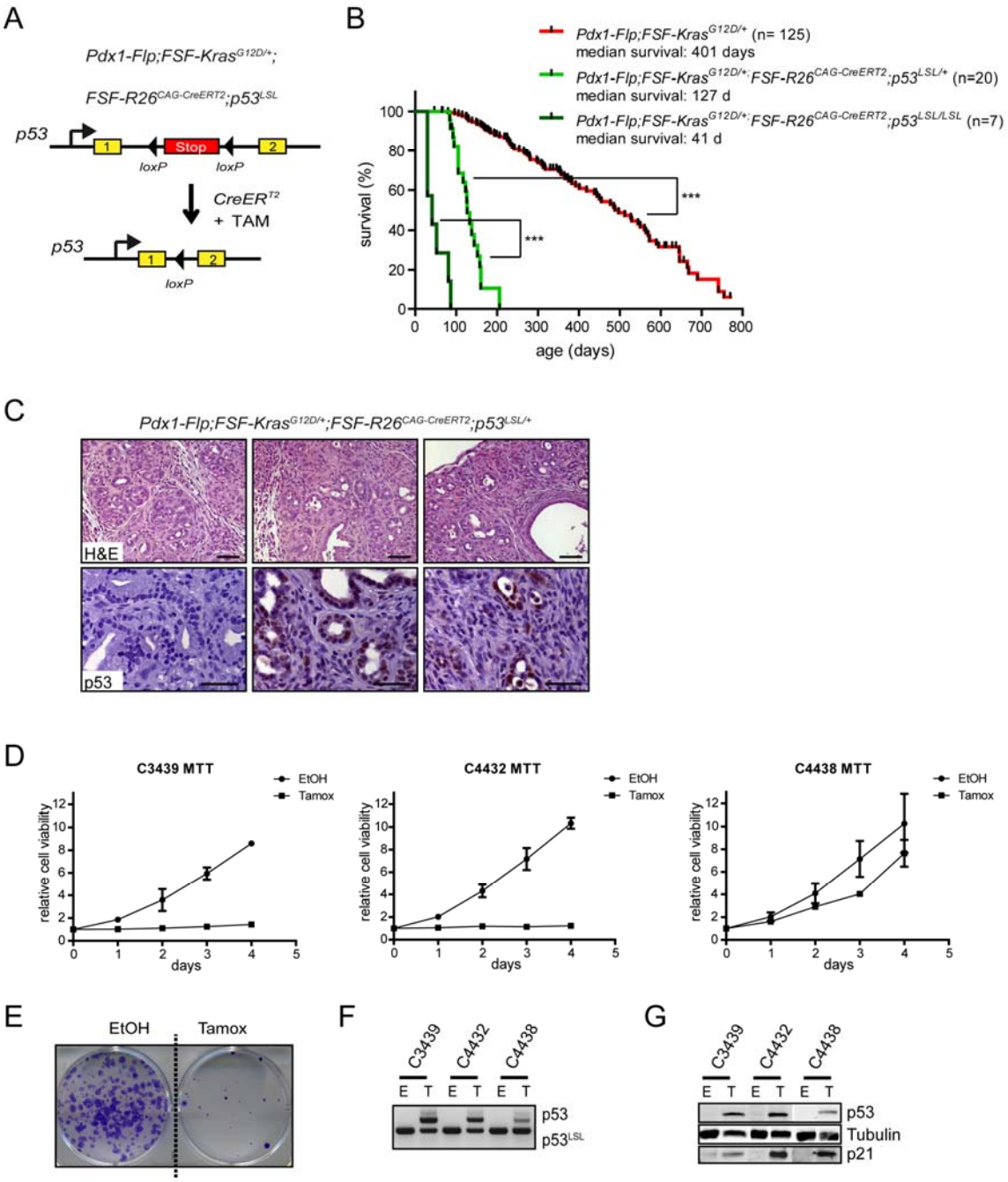

Fig.10 Restoration of p53 wild type *in vitro* inhibited cell proliferation.
(**A**) Genetic strategy of restoration of p53 wild type after tamoxifen treatment using dual-recombination system of *Pdx1-Flp;FSF-Kras^{G12D};FSF-R26$^{CAG-CreERT2}$;p53^{LSL}*. Upon Cre recombination, STOP cassette flanked by loxP sites between exon 1 and exon 2 of p53 gene is excised and wild type p53 is re-expressed. (**B**) Kaplan-Meier survival curve of indicated genotypes; all animals were vehicle-treated. $^{+}$ denotes the wild type allele;*p53^{LSL}* denotes the p53 allele containing the floxed STOP cassette. Log rank test was performed, ($p<0.0001$); *** means p-value below 0.0001. (*KF*: n=125; *KF;FSF-R26$^{CAG-CreERT2}$;p53$^{LSL/+}$*: n=20; *KF;FSF-R26$^{CAG-CreERT2}$;p53$^{LSL/LSL}$*: n=7). (**C**) Upper panel: representative H&E staining of PDAC of indicated genotype. Lower panel: corresponding immunohistological staining of p53 in PDAC. (Figure legend continued on next page)

(**D**) Relative cell viability of three isolated primary tumor cell lines of untreated *Pdx1-Flp;FSF-Kras^{G12D};FSF-R26$^{CAG-CreERT2}$;p53$^{LSL/+}$* mice. Cells were either vehicle-treated (EtOH) or treated with 0.5 µM 4-hydoxitamoxifen (Tamox). Triplicates are shown. (**E**) Representative pictures of clonogenic assay of ethanol-treated and tamoxifen-treated cell line corresponding to cell viability assay. (**E**) PCR analysis of isolated tumor cell lines used for cell viability assay and clonogenic assay after vehicle treatment (EtOH) or tamoxifen treatment (Tamox). (**F**) Protein analysis of cell lines used for cell viability assay. Cells were either vehicle-treated (EtOH) or 0.5 µM 4-hydroxitamoxifen (Tamox)-treated. Immunoblotting analysis for p53 restoration, p21 and tubulin. Scale bars 50 µm.

Primary tumor cells were isolated from *Pdx1-Flp;FSF-Kras$^{G12D/+}$;FSF-R26$^{CAG-CreERT2}$;p53$^{LSL/+}$* mice. Since these mice were not treated with tamoxifen, p53 was inactivated in the isolated cell lines. To restore wild type p53, cells were treated with 0.5 µM 4-hydroxitamoxifen (4-OHT) for 6 days, ethanol was used as control. In the following, cell viability was determined by colorimetric MTT cell viability assay. 2 out of 3 cell lines displayed decreased cell viability after tamoxifen treatment whereas one cell line showed almost no difference in cell viability (Fig.10 D). The decreased cell viability was confirmed by clonogenic assay, representative pictures are shown in Fig.10 E. In ethanol-treated samples more cells were able to form colonies compared to tamoxifen-treated samples (Fig.10 E). PCR analysis of those samples proved restoration of p53 expression in tamoxifen-treated samples as well as loss of the second allele of p53 in the heterozygous cell lines (Fig.10 F). Loss of heterozygosity is well known for p53 with increasing grade of PanIN lesions and it is often detected in PDAC (Luttges et al., 2001). Restoration of p53 in 4-OHT-treated cell lines could be demonstrated by western blot analysis (Fig.10 G). Furthermore, a downstream target of p53, p21, was upregulated after p53 restoration in tamoxifen-treated samples. These results indicated that restoration of functional p53 as evidenced by activated p21 expression, leads to a cytostatic effect in some, but not all PDAC cell lines. The underlying mechanisms for this cell specific effect are currently under investigation.

4.3 THE MICROENVIRONMENT OF PANCREATIC DUCTAL ADENOCARCINOMA

PDAC is known to be a stroma-rich tumor with infiltrating immune cells and a desmoplastic reaction called fibrosis. With an advanced tumor stage more stromal cells infiltrate the tumor and make up more mass of the cancer. New therapy strategies focus not only on the cancer cells themselves but also on the stromal compartment. There is a need to understand the composition of the tumor microenvironment and how the interaction between stromal and cancer cells influence the progression of the tumor or the resistance towards therapy. With the help of

the new developed dual-recombination system, it is not only possible to sequentially manipulate the cancer cells but also to analyze and target stroma thereby allowing genetic manipulation of stromal cells. Using cell-type specific Cre driver lines enables the investigation and characterization of the microenvironment. Identification of infiltrating and recruited cells, to which extend they are present, and subsequently also the analysis how stromal cells possibly influence cancer progression is possible.

4.3.1 Role of mast cells in PDAC development and maintenance

Mast cells are part of the innate and adaptive immune system and have been reported playing a role in tumor initiation, progression, and metastasis of various tumors. Mast cells infiltrate human PDAC as well as PDAC of *KC* mice (Schonhuber et al., 2014). However, the role of mast cells during tumorigenesis remains controversial as tumor-promoting and anti-tumor effects have been reported (Galinsky and Nechushtan, 2008). The dual-recombination system allows analysis of mast cells during tumor development. To investigate the impact of the depletion of mast cells in PDAC, the *Cpa3*$^{Cre/+}$ mouse line was used since it was shown to be mast-cell deficient (Feyerabend et al., 2011). Cre recombinase is expressed under the control of the mast-cell specific promoter *carboxypeptidase A3* (*Cpa3*). This Cre expression results in eradication of the entire mast-cell lineage due to Cre overexpression which led to genomic deletions and pseudotrisomy supporting genotoxic mechanism of mast-cell ablation. Cpa3 is also weakly expressed in hematopoietic progenitor cells and in splenic basophils (Feyerabend et al., 2011). Depletion of mast cells using the *Cpa3*$^{Cre/+}$ mouse line is independent of Kit hypomorphism which is most commonly used to deplete mast cells (Berrozpe et al., 1999; Kitamura et al., 1978).

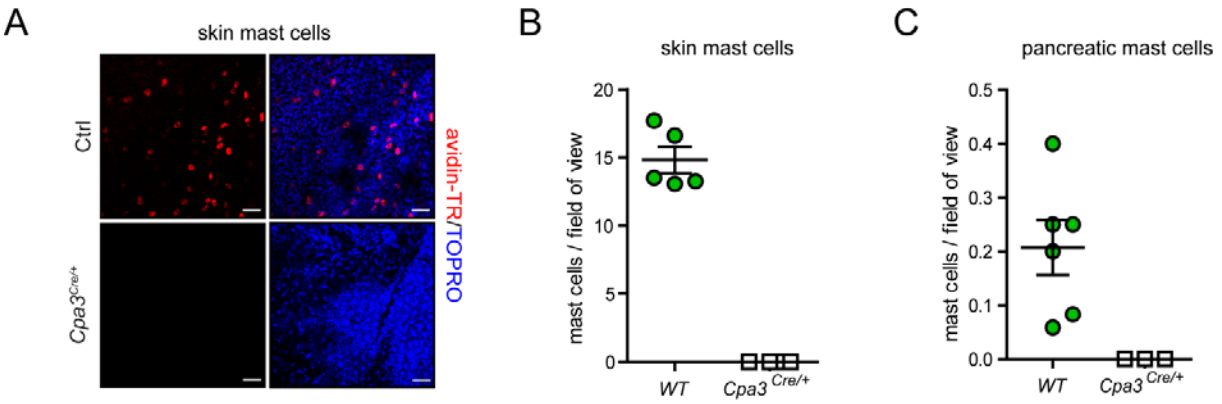

Fig.11 **Mast cells depletion in *Cpa3*$^{Cre/+}$ animals.** (Figure legend continued on next page)

(**A**) Representative confocal microscopy pictures of skin whole-mounts of *Cpa3*$^{Cre/+}$ (lower panel) and littermate control (upper panel, Ctrl) animals on a *C57BL/6* genetic background. Staining of mast cells was done using avidin-TexasRed (red color). Nuclei were stained with TOPRO-3 (blue). (**B**) Quantification of skin mast cells of *Cpa3*$^{Cre/+}$ and control mice (*WT*) (mean ± S.E.M.; 10-15 fields of view per animal; each dot represents one mouse). (**C**) Quantification of pancreatic mast cells of *Cpa3*$^{Cre/+}$ and control animals (*WT*) (mean ± S.E.M.; 10-15 fields of view per mouse; each dot represents one animal). Scale bars 50µm.

Mast cell deficiency was confirmed by staining for skin mast cells as well as for pancreatic mast cells in *Cpa3*$^{Cre/+}$ and wild type (*WT*) littermate control animals. Skin whole mounts of wild type mice showed mast cells stained by avidin-TexasRed (Fig.11 A) whereas in littermate control *Cpa3*$^{Cre/+}$ mice no mast cells were detectable. Quantification of skin mast cells in both cohorts revealed around 15 mast cells per field of view in wild type animals and no mast cells in *Cpa3*$^{Cre/+}$ mice (Fig.11 B). Determination of mast cells in pancreas of wild type and *Cpa3*$^{Cre/+}$ mice resulted in 0.2 mast cells per field of view for wild type animals and no mast cells in *Cpa3*$^{Cre/+}$ animals (Fig.11 C).

As a next step, mast cell infiltration was analyzed in *KF* mice without or with *Cpa3*$^{Cre/+}$ (Fig.12 A+B). Toluidine blue staining of pancreata of *KF* mice depict mast cell infiltration during PanIN lesion development (Fig.12 A). In comparison, mast-cell deficient *KF* mice (*Pdx1-Flp;FSF-Kras*$^{G12D/+}$*;Cpa3*$^{Cre/+}$) showed no mast cells at analyzed time points (Fig.12 B). *KF* mice with and without *Cpa3*$^{Cre/+}$ were analyzed at an age of nine months for mast cell infiltration and PanIN lesion formation (Fig.12 C+D). There was no difference detected in precursor lesions between *KF* mice and *KF;Cpa3*$^{Cre/+}$ mice. The number of formed acinar-to-ductal-metaplasia (ADM) and developed PanIN1 to PanIN3 were the same in both groups (Fig.12 D). Fibrosis is one of the features of PDAC beginning with PanIN lesion formation. Therefore, the fibrotic area in 9 months old *KF* and *KF;Cpa3*$^{Cre/+}$ mice was determined by Sirius Red staining (Fig.12 E). In all mice analyzed no difference of fibrotic area could be observed. Mast-cell deficiency seems to have no effect on fibrosis occurring during PanIN development. Besides mast cells, macrophages are often detected in tumor tissue. Thus, macrophage infiltration was investigated and revealed no difference between mast-cell deficient mice and control animals at the age of nine months. In both cohorts almost the same amounts of macrophages were detected (Fig.12 F). This data suggests that macrophage infiltration is independent of mast cells.

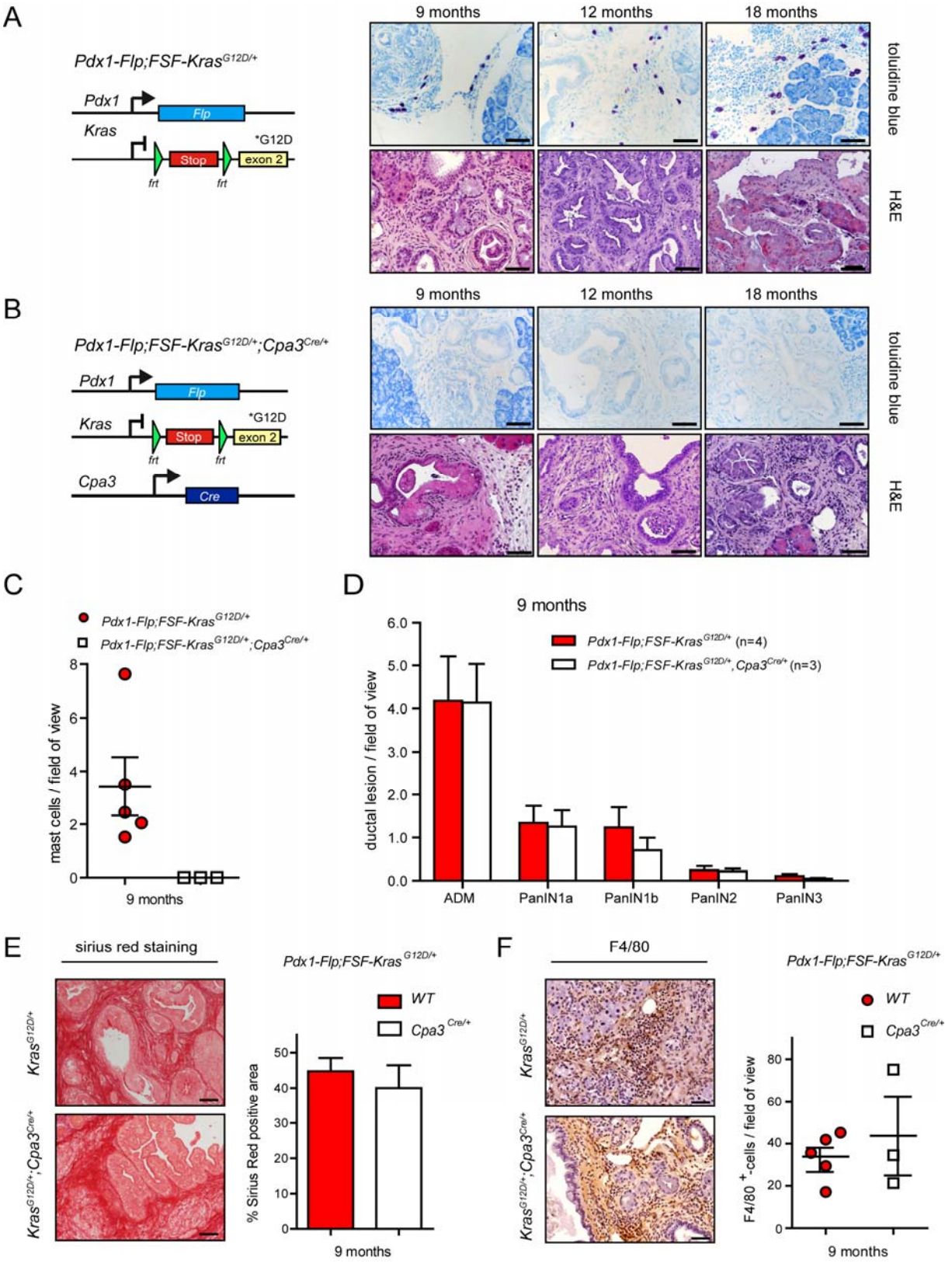

Fig.12 **Mast cells are dispensable for PDAC initiation.** (Figure legend continued on next page)

(**A**) Genetic strategy of oncogenic $Kras^{G12D}$ expression in the *Pdx1-Flp* lineage (left panel). Representative microscopy images of toluidine blue-stained metachromatic mast cells (purple, upper panel) in PanIN-bearing pancreata and corresponding H&E staining (lower panel) of *Pdx1-Flp;FSF-Kras*$^{G12D/+}$ animals analyzed at indicated time points. (**B**) Genetic scheme of mast cell depletion in the *Pdx1-Flp;FSF-Kras*$^{G12D/+}$ mouse model by Cre recombinase expression using *Cpa3*$^{Cre/+}$ mice (left panel). Representative microscopy images of toluidine blue-staining (upper panel) of PanIN-bearing pancreata and corresponding H&E staining (lower panel) of *Pdx1-Flp;FSF-Kras*$^{G12D/+}$*;Cpa3*$^{Cre/+}$ mice analyzed at indicated time points. (**C**) Quantification of tumor-infiltrating mast cells of PanIN-bearing animals with indicated genotypes at an age of 9 months (mean ± S.E.M.; 16-20 fields of view per animal/slide, three slides per animal). (**D**) Quantification of ADM and PanIN lesions of different grades in 9-month-old *Pdx1-Flp;FSF-Kras*$^{G12D/+}$ (n=4) and *Pdx1-Flp;FSF-Kras*$^{G12D/+}$*;Cpa3*$^{Cre/+}$ (n=3) animals (mean and S.E.M.; three representative slides per mouse). (**E**) Left panel: representative microscopic pictures of pancreatic tissue of 9-month-old mice with indicated genotypes stained with Sirius red. Right panel: Quantification of Sirius red positive areas of 9-month-old mice (mean ± S.E.M.). 3 mice per genotype and at least 5 pictures were used for quantification (p=0.5117). (**F**) Left panel: Representative images of F4/80 staining of macrophages of pancreata of 9-month-old mice of indicated genotypes. Right panel: Quantification of F4/80 staining (mean ± S.E.M.). At least three animals of each genotype were considered for analysis (*KF*: n=5; *KF;Cpa3*$^{Cre/+}$: n=3) and per mouse at least 12 pictures were counted (p=0.1141). Scale bars 50µm.

To investigate the influence of mast-cell deficiency on tumor development, survival of *KPF* mice and *KPF;Cpa3*$^{Cre/+}$ mice was analyzed. There was no shortened or prolonged survival of mast-cell deficient mice observed compared to *KPF* mice. *KPF* mice lacking mast cells had an overall survival of 203 days compared to 181 days of *KPF* animals (Fig.13 A). Furthermore, *KF* animals either proficient or deficient for mast cells were analyzed at the age of 12 months. Tumor formation was observed sporadically in 12-month-old *KF* mice as well as in *KF;Cpa3*$^{Cre/+}$ mice (Fig.13 B). Immunofluorescence staining of high-affinity IgE receptor FcεRI detected mast-cell infiltration in PDAC of 12-month-old *KF* mice and their absence in tumor of *KF;Cpa3*$^{Cre/+}$ mice at the age of 12 months (Fig.13 C).

So far, other studies analyzing the role of mast cells in tumor development and progression used Kit hypomorphic mice which lack mast cells, but display also other abnormalities, such as haematopoetic defects as well as impaired c-Kit expression. As c-Kit was already known to be expressed by cancer cells (Micke et al., 2003; Yasuda et al., 2006), pancreatic tissue of PanIN- and tumor-bearing mice was analyzed for expression of c-Kit. Cells of PanIN lesions and PDAC expressed c-Kit as depicted in Fig.13 D. Immunofluorescence staining of c-Kit in tumor samples revealed also c-Kit expression in cancer cells (Fig.13 E). Both stainings suggest that c-Kit is not only expressed by mast cells but by pancreatic cancer cells as well. Furthermore, *KF* mice lacking mast cells were analyzed for extrapancreatic tumors as those are occurring in *KF* animals as shown by Schonhuber and colleagues (Schonhuber et al., 2014). In mice deficient for mast cells, bile duct dilations and papilloma of the skin could be observed in around 9 % of analyzed animals whereas intestinal alterations could be detected in almost 81 % of the animals (Fig.13 F). The rates of occurring skin or bile duct papillomas in mast cell-deficient mice were similar to the occurrence of those extrapancreatic alterations of *KF* mice

(Schonhuber et al., 2014). There were less intestinal alterations detected in *KF;Cpa3*$^{Cre/+}$ compared to *KF* mice (81 % instead of 100 %). Taken together, these data suggest that the formation of PDAC and extrapancreatic tumors is independent of mast cells.

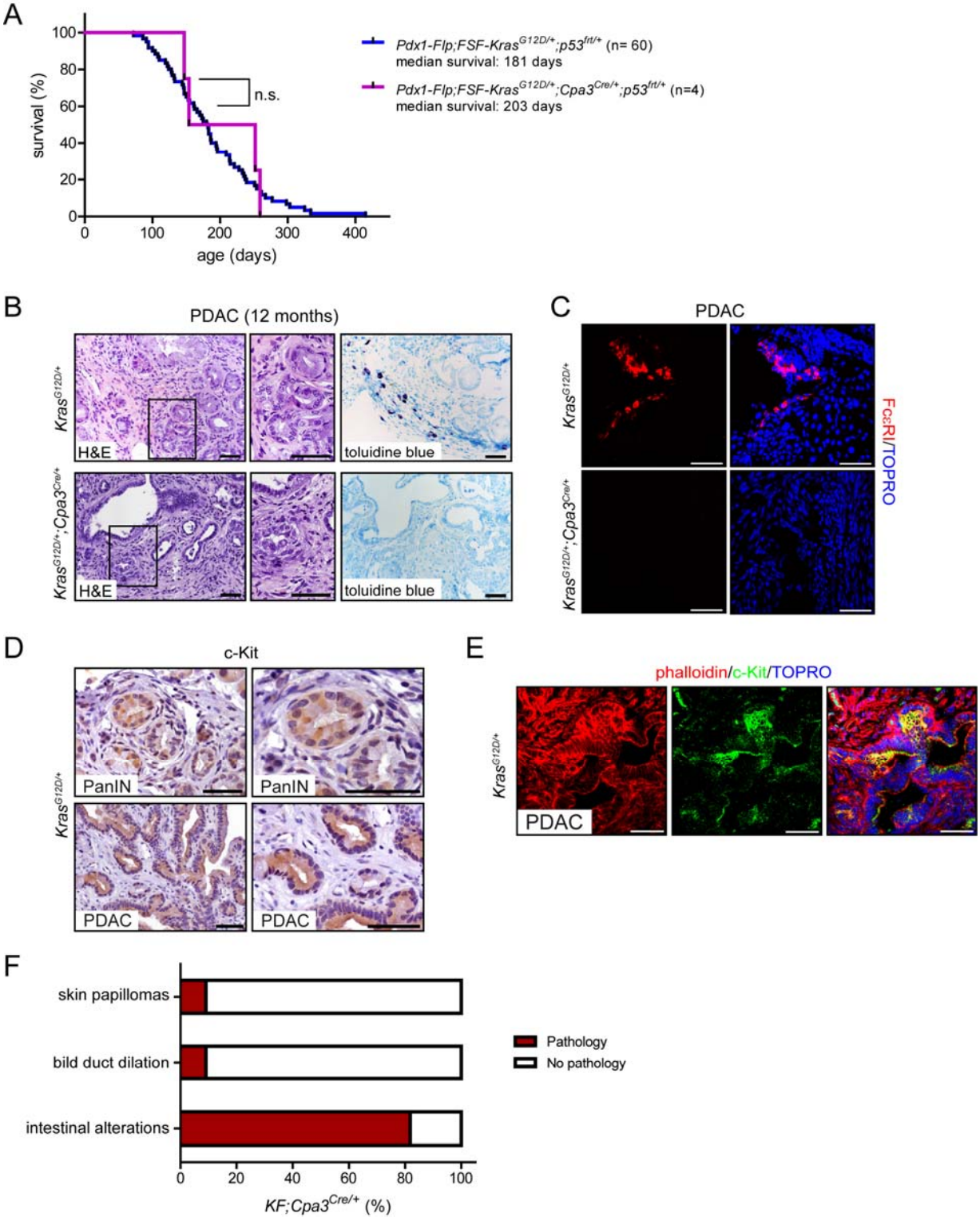

Fig.13 Tumor development is independent of mast cells.
(**A**) Kaplan-Meier survival curve of indicated genotypes. $^{+}$ denotes the wild type allele; *p53f^{rt}* denotes the p53 allele containing frt-sites. Log rank test was performed. (p=0.5596; n.s.: not significant) (*KPF*: n=60; *KPF;Cpa3$^{Cre/+}$*: n=4) (Figure legend continued on next page)

(**B**) Representative microscopy images of H&E (left and middle panel) and toluidine staining (right panel) of 12-month-old *Pdx1-Flp;FSF-Kras*$^{G12D/+}$ (upper panel) and *Pdx1-Flp;FSF-Kras*$^{G12D/+}$*;Cpa3*$^{Cre/+}$ mice (lower panel) with established PDAC (3 representative slides per mouse; since few animals develop PDAC at the age of 12 months, only one mouse per genotype was analyzed). Black outlines indicate image sections shown at higher magnification in the middle panel. (**C**) Representative confocal microscopy pictures of FcεR1-stained mast cells (red) in PDAC-bearing *KF* (upper panel) and *KF;Cpa3*$^{Cre/+}$ (lower panel) mice. Nuclei were counterstained with TOPRO-3 (blue). (**D**) Representative immunohistochemical c-Kit staining in PanIN lesions and tumor of *KF* animals. (**E**) Immunofluorescent staining of c-Kit (green) of PDAC-bearing *KF* mouse. Cells were stained with phalloidin (red) and nuclei were counterstained with TOPRO-3 (blue). (**F**) Quantification of extrapancreatic tumors occurring in mast cell-deficient mice (mice with PanIN lesions and tumors were included into analysis; n=11). Scale bars 50 μm.

To examine the role of mast cells in PDAC maintenance, wild type and mast cell-deficient mice on a C57BL6/J background were orthotopically transplanted with syngenic pancreatic tumor cells. In both groups tumors engrafted and were imaged by high resolution ultrasound over time (Fig.14 A). No difference in tumor histology was observed in PDAC of mice proficient for mast cells compared to PDAC of mast-cell depleted animals (Fig.14 A). Vascularization of primary tumors was comparable between the two different cohorts (Fig.14 A, shown by Doppler mode). Whereas mast cell-proficient animals display mast-cell infiltration into the tumor, no infiltration was detected in mast cell-deficient animals (Fig.14 A, purple stained cells mark mast cells). The overall survival was similar in the two models (Fig.14 B). Sonography of orthotopically transplanted wild type mice as well as mice lacking mast cells (*Cpa3*$^{Cre/+}$) revealed similar tumor growth over time starting 14 days after transplantation (Fig.14 C). Furthermore, the weight of the primary pancreatic tumor displayed no difference between the two groups (Fig.14 D). Metastases of liver, lung, lymph nodes, and diaphragm were discovered in both groups as shown in Fig.14 E. Investigation of tumor-infiltrating macrophages revealed no statistically significant difference between wild type littermate controls and *Cpa3*$^{Cre/+}$ mice. In both cohorts the same number of macrophages was detected by F4/80 staining (Fig.14 F). Furthermore, fibrotic area was analyzed by Sirius Red staining (Fig.14 G), showing no significant difference between the cohorts. Taken together, these results indicate that tumor maintenance is independent of mast cells.

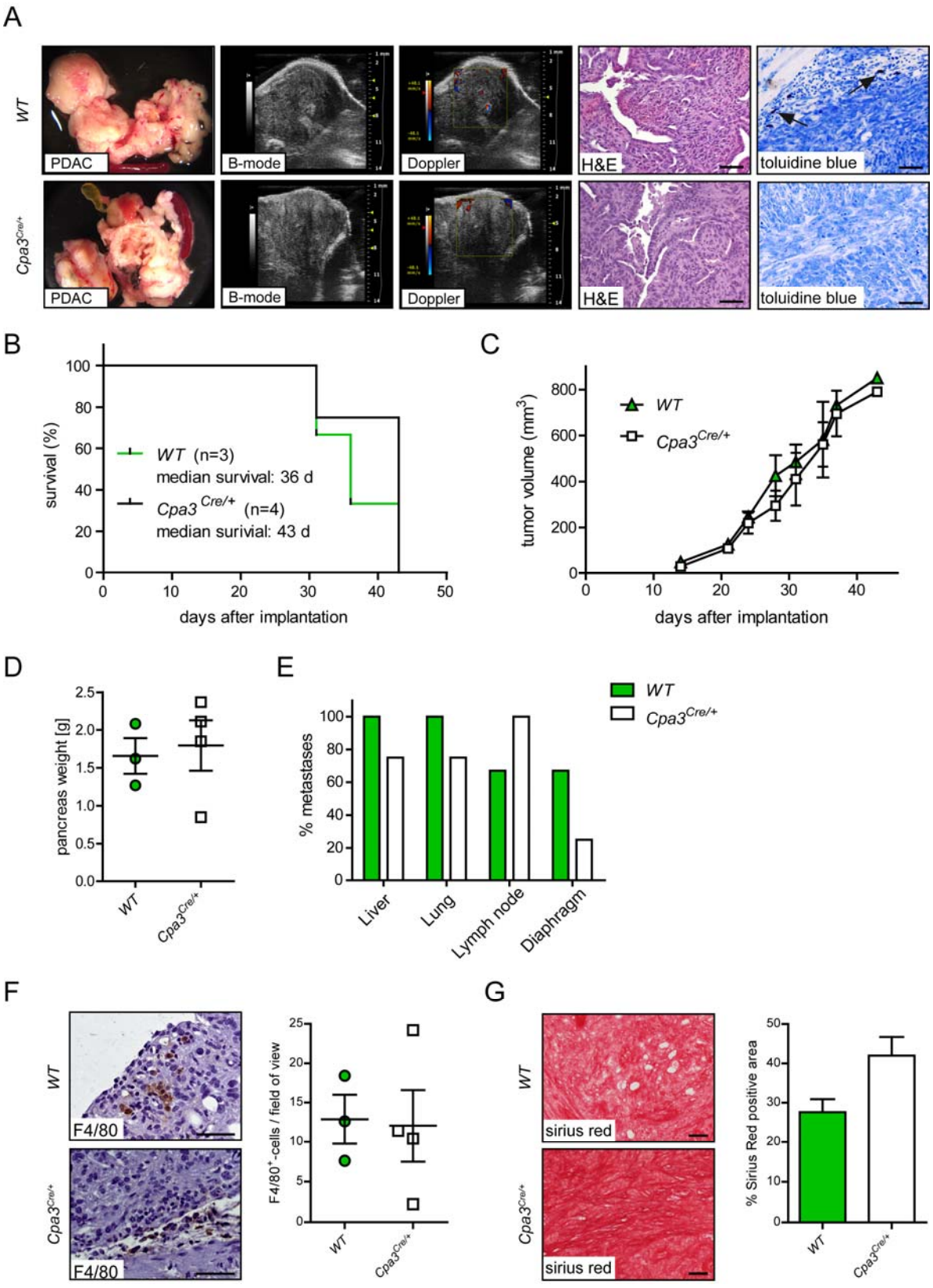

Fig.14 Progression and maintenance of PDAC is independent of mast cells. (Figure legend continued on next page)

Mast cell-deficient (*Cpa3*$^{Cre/+}$) and wild type littermate control mice (*WT*) were orthotopically transplanted with murine pancreatic tumor cells isolated from *Ptf11*$^{Cre/+}$*;LSL-Kras*$^{G12D/+}$ (*KC*) mice on a *C57BL/6* background. Tumors, their progression, and metastasis formation were analyzed. (**A**) Upper panel: *WT* mice, lower panel: *Cpa3*$^{Cre/+}$ mice. From left to right: representative macroscopic images of developed tumors; sonography images (left panel: B-mode; right panel: Doppler effect to visualize vascularization); corresponding microscopic pictures of H&E stained pancreatic tumors; tumor-infiltrating mast cells (purple, indicated by arrows) were stained with toluidine blue. (**B**) Kaplan Meier survival curve of orthotopically transplanted animals of indicated genotypes. Log rank test was performed. (p=0.3562) (**C**) Quantification of tumor volume of transplanted mice of both genotypes, mast cell-deficient mice (*Cpa3*$^{Cre/+}$; n=4) and littermate control wild type mice (*WT*; n=3) (mean ± S.E.M.). (**D**) Weight of primary pancreatic tumors of transplanted animals (n=3 for wild type mice; n=4 for *Cpa3*$^{Cre/+}$ mice) (p=0.7657). (**E**) Quantification of macroscopic and microscopic metastases in transplanted animals either mast cell-proficient (*WT*; n=3) or mast cell-deficient (*Cpa3*$^{Cre/+}$; n=4). Appearance of lymph node, diaphragm and liver and lung metastases was documented (means are depicted). (**F**) Left panel: representative pictures of immunohistochemically stained macrophages (F4/80-positive cells) in PDAC of transplanted *WT* and *Cpa3*$^{Cre/+}$ mice. Right: Quantification of F4/80-positive cells (mean ± S.E.M.; *WT*: n=3; *Cpa3*$^{Cre/+}$: n=4; per mouse 5 pictures of one section were analyzed) (p=0.8967) (**G**) Analysis of fibrotic area in primary tumors of *WT* and *Cpa3*$^{Cre/+}$ mice. Left panel: representative images of Sirius Red staining. Fibrotic area, dark red; tumor cells, lighter red. Right: Quantification of fibrosis occurring in tumors. (mean ± S.E.M., *WT*: n=3; *Cpa3*$^{Cre/+}$: n=4; for each mouse 5 pictures of one section were analyzed) (p=0.0705). Scale bars 50 µm.

4.3.2 PANCREATIC STELLATE CELLS

In normal pancreatic tissue, pancreatic stellate cells (PSCs) are quiescent whereas upon tissue damage or tumor development they get activated. Once in their active state, these cells are known to produce high amount of extracellular matrix (ECM) components. Transplantation experiments of mixture of pancreatic cancer cells and PSCs demonstrated accelerated tumor growth and increased metastasis formation (Apte and Wilson, 2012). To address and characterize the influence of pancreatic stellate cells in PDAC, *KPF* mice were crossed with mice containing Cre recombinase under control of glial fibrillary acidic protein (GFAP) promoter. It is known that GFAP is expressed not only in astrocytes but is also a marker for pancreatic stellate cells (Omary et al., 2007). Two transgenic *GFAP-Cre* mouse lines were analyzed for Cre recombination in the stromal compartment of developed PDAC for their specificity to target PSCs.

The first mouse line analyzed has a Cre recombinase under control of the human GFAP promoter (*hGFAP-Cre*) (Zhuo et al., 2001). Cre expression was monitored with the help of the *R26*$^{mT-mG}$ Cre reporter mouse line where Cre positive cells switch from tomato fluorescence to green fluorescence. PDAC samples of *KPF;hGFAP-Cre;R26*$^{mT-mG}$ mice were analyzed for EGFP-positive cells present in primary tumor tissue. Although macroscopic images of PDAC revealed only tomato expression and no EFGP expression, confocal microscopy pictures depicted recombination of cells (Fig.15 A+B). It could be observed that not only stromal cells showed Cre activity and subsequently EFGP expression but also some ductal and tumor cells expressed EFGP indicating Cre activity (Fig.15 B). First analysis of tumor samples of three

different mice revealed huge variance in Cre-recombined cells (Fig.15 C). Depending on the field of view between 0 and above 250 EGFP-expressing cells were detected. To determine the specificity of this *hGFAP-Cre* mouse line, immunofluorescent staining of GFAP was performed (Fig.15 D). Co-localization of GFAP staining and EGFP expression was observed in few mesenchymal cells. It is known that activated pancreatic stellate cells are positive for αSMA, desmin and nestin (Omary et al., 2007). Staining of αSMA resulted in mostly distinct localization of Cre-recombined cells (EGFP expressing cells) and αSMA-positive cells (in Fig.15 E shown in red). Some EGFP-positive cells have a ductal like morphology and therefore an immunofluorescence staining for the ductal marker CK19 was done. As depicted in Fig.15 F, double positive cells were observed indicating that hGFAP-Cre is also active in ductal tumor cells.

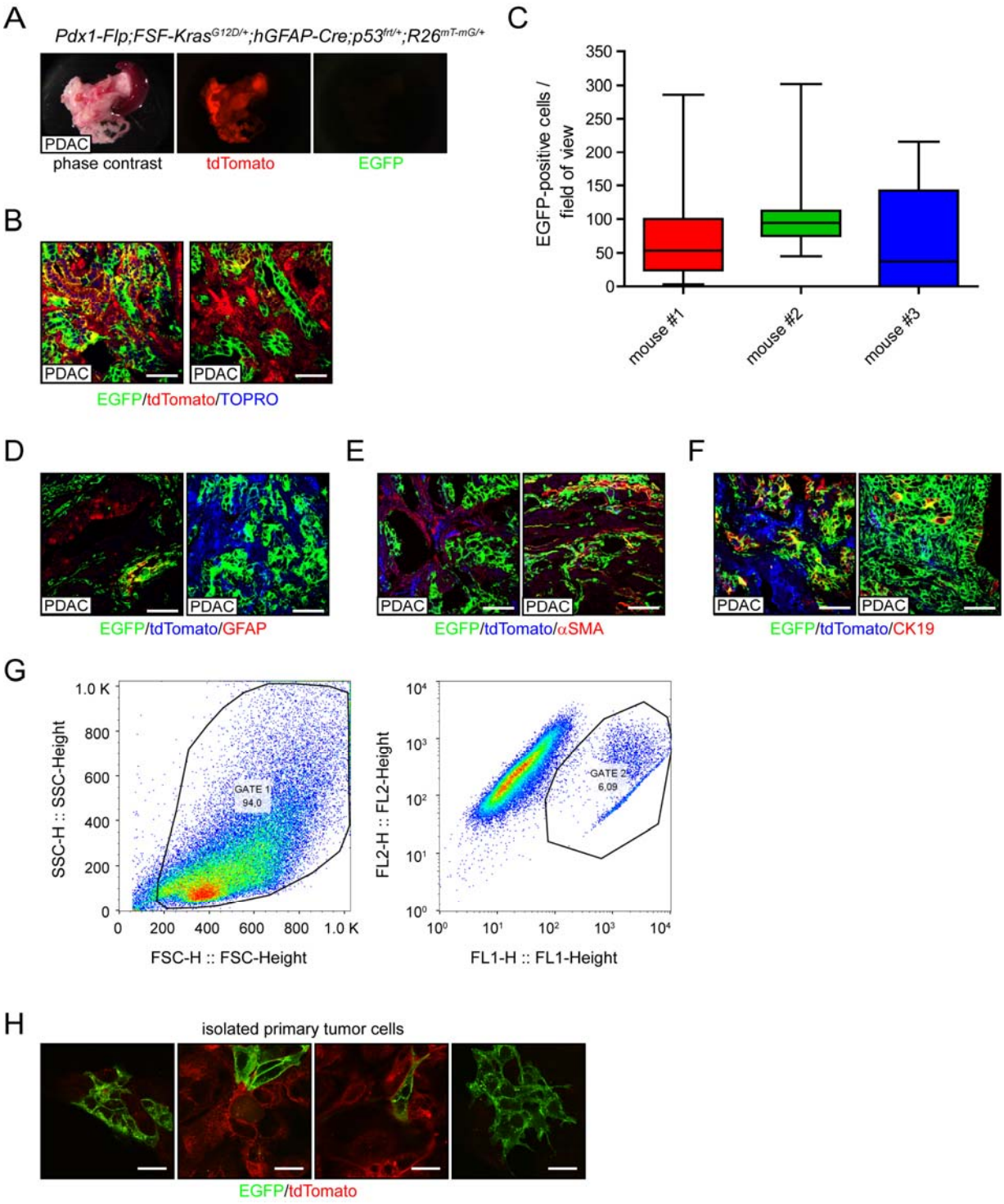

Fig.15 Analysis of hGFAP-Cre in pancreatic ductal adenocarcinoma.
(**A**) Macroscopic pictures of PDAC of a *Pdx1-Flp;FSF-Kras$^{G12D/+}$;hGFAP-Cre;p53$^{frt/+}$;R26^{mT-mG}* mouse. From left to right: bright field, tdTomato and EGFP. (**B**) Representative confocal microscopy images of PDAC tissue. Cre-recombined cells are depicted in green (EGFP expression) and non-recombined cells are shown in red (tdTomato expression). Nuclei were stained with TOPRO-3 (blue). (Figure legend continued on next page)

(**C**) Quantification of EGFP-positive cells (Cre-recombined) of tumor-bearing mice. Per mouse 30 fields of view were counted (n=3). Minimun to maximum counts are represented. (**D-F**) Immunofluorescence images of PDAC samples of *KPF;hGFAP-Cre;R26*$^{mT\text{-}mG}$ mice. TdTomato-expressing cells are indicated by blue color, Cre-recombined cells are depicted in green (EFGP expression). (**D**) Staining of αSMA in PDAC (red). (**E**) GFAP-immunofluorescence staining of tumor tissue (red color). (**F**) Immunofluorescence staining of CK19 shown in red. (**G**) FACS analysis of isolated primary tumor cells of *KPF;hGFAP-Cre;R26*$^{mT\text{-}mG}$ mouse. Left panel: gating for living cells according to size (forward and side scatter); Right panel: gated cell population analyzed for tdTomato (FL2 on y-axis) and EGFP expression (FL1 on x-axis). (**H**) Representative confocal microscopy images of isolated primary cancer cell line. Scale bars 50 μm.

Primary isolated tumor cells were tested for EGFP expression by FACS, revealing that these isolated cells express partly EGFP (Fig.15 G). Around 6 % of the gated cells showed not only tdTomato expression but also EGFP expression (right panel of Fig.15 G). These results indicate that the *hGFAP-Cre* mouse line is not suitable to target pancreatic stellate cells since this Cre line seems to target cancer cells as well to some extent.

Therefore, a second transgenic mouse line *mGFAP-Cre* was analyzed for specificity to target pancreatic stellate cells. The difference between the two *GFAP-Cre* lines is the promoter controlling Cre activity. In this line the recombinase is under the control of the murine GFAP promoter (Garcia et al., 2004). For determination of targeted cell type, *mGFAP-Cre* animals were bred with *KPF* mice allowing tumor formation. Developed PDAC was examined for Cre recombined cells with the help of the Cre reporter *R26*$^{mT\text{-}mG}$. In macroscopic images of primary tumors of *KPF;mGFAP-Cre;R26*$^{mT\text{-}mG/+}$ no EGFP expression was detected Fig.16 A. Four different PDAC samples were investigated and few Cre-recombined cells could be observed (Fig.16 B+C). Similar to the *KPF;hGFAP-Cre;R26*$^{mT\text{-}mG}$ mice, the *KPF;mGFAP-Cre;R26*$^{mT\text{-}mG}$ mice were analyzed for co-localizing with GFAP, αSMA and nestin. Efficiency was determined by dividing stained Cre-recombined cells by all stained cells (for all tested Cre lines). About 40 % of EGFP-expressing cells were stained for GFAP (Fig.16 D). There were variances in the amount of double positive cells between the investigated tumor samples from 20 % up to 60 %. In case of αSMA in none of the tested tumor sample any EGFP- and αSMA double-positive cell could be observed (Fig.16 E). Immunofluorescent staining of nestin showed co-localization of EGFP-positive cells for less than 1 % in all tested tumor samples (Fig.16 F). Not only tumor tissue was analyzed for recombination but isolated primary cancer cells as well. Confocal microscopy pictures showed no EGFP-expressing cells for *KPF;mGFAP-Cre;R26*$^{mT\text{-}mG}$ mice (Fig.16 G). tdTomato and EGFP expression of isolated cancer cells was investigated using FACS (Fig.16 H). Only a very low fraction of EGFP-positive cells (<1%) was detected in all analyzed cell lines (Fig.16 I). The EGFP positive cells are most likely stroma cells contaminating the PDAC cell culture. This possibility is currently under investigation with FACS using stromal

markers. Taken all these results together, the *mGFAP-Cre* line could be used to target stromal cells although further characterization of recombined cells is necessary to identify the cell population which is targeted by this Cre line.

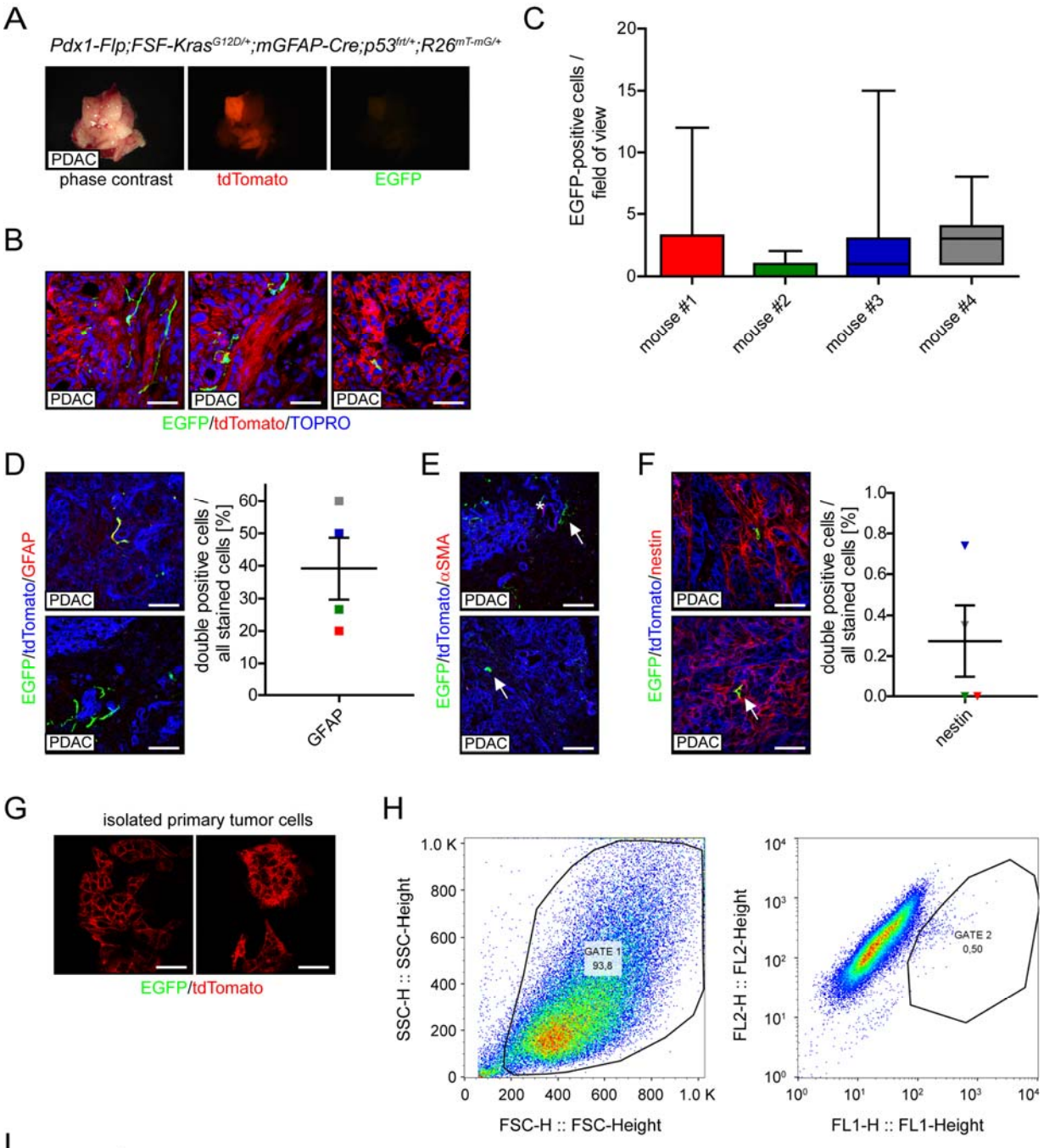

I

	mGFAP-Cre recombined cells [%]
cell line 1	0
cell line 2	0,035
cell line 3	0,5
cell line 4	0,15
cell line 5	0

Fig.16 Characterization of mGFAP-Cre-recombined cells in murine primary PDAC.
(**A**) Macroscopic pictures of primary PDAC of *KPF;mGFAP-Cre;R26$^{mT-mG/+}$* mouse. From left to right: bright field, tdTomato and EGFP. (Figure legend continued on next page)

(**B**) Representative confocal microscopy images of pancreatic tumor tissue. Cre-recombined cells are depicted in green (EGFP expression) and Cre non-recombined cells are shown in red (tdTomato). Nuclei are counterstained with TOPRO-3 (blue). (**C**) Counting of Cre-recombined cells per field of view. At least 20 images per animal were analyzed (n=4). Minimun to maximum counts are represented. (**D-F**) Immunofluorescence staining for GFAP, αSMA and nestin of tumor samples of *KF;mGFAP-Cre;R26*$^{mT\text{-}mG/+}$. (**D**) Left panel: Representative confocal microscopy pictures of PDAC samples stained for GFAP. Blue are the Cre non-recombined cells, Cre recombined cells are depicted in green and GFAP-stained cells are shown in red. Right panel: Quantification of Cre-recombined cells which were positive in GFAP staining. 10 pictures per animal were analyzed (n=4). Double positive cells were compared to all GFAP-stained cells. (**E**) Microscopy images of αSMA-staining of PDAC. Cre-recombined cell: green, Cre-negative cells: blue, in red αSMA-positive are depicted. (**F**) Right panel: Confocal microscopy pictures of nestin staining of PDAC. Green cells are recombined by mGFAP-Cre, blue cells are not recombined. Nestin-positive cells are shown in red. Left panel: Quantification of nestin staining. Cells which are Cre-recombined and nestin-positive were normalized to all cells stained for nestin. For each animal 10 images were analyzed (n=4). (**G**) Primary cancer cells isolated from PDAC were analyzed for Cre-recombined cells by confocal microscopy. Non-recombined cells are expressing tdTomato (red) and Cre-recombined cells express EGFP (green). (**H**) FACS analysis of isolated primary tumor cells. Left panel: cells gated for forward and sideward scatter. Right panel: Gated cells were analyzed for tdTomato expression (FL1 on y-axis) and for EGFP expression (FL2 on x-axis). (**I**) Summary of *KPF;mGFAP-Cre;R26*$^{mT\text{-}mG}$ cell lines analyzed by FACS. Scale bars 50 µm.

4.3.3 FIBROBLASTS IN PDAC

One major feature of pancreatic ductal adenocarcinoma is the abundant stroma. Myofibroblasts or activated fibroblasts make up a huge amount of stromal compartment and are therefore one cell type of interest for new therapy options (Provenzano et al., 2012; Sclafani et al., 2015).

In the present study, different transgenic Cre mouse lines were analyzed for their specificity and efficiency to target fibroblasts in PDAC. Various studies have shown before that collagen is one the components which gets produced and secreted in huge amounts during PDAC development. Two different transgenic mouse lines were studied expressing the Cre recombinase under the control of the *Col1a2* gene; the constitutive active *C-Cre* and the tamoxifen-inducible *Col1a2-Cre*^{ER} (Zheng et al., 2002). Both Cre lines should be active in connective tissues of spleen, skin, lung, and blood vessels (Zheng et al., 2002). In case of the *C-Cre* mouse line, no Cre recombination could be detected in any analyzed tissues (data not shown) and was subsequently excluded from any further study. The *Col1a2-Cre*^{ER} was induced by tamoxifen administration and afterwards analyzed for recombination. All tissues examined for Cre activity displayed no recombination (data not shown). These two Cre lines were not suitable to target and investigate the tumor stroma.

Besides collagen production, activated fibroblasts are identified by different markers like expression of αSMA, fibroblast specific protein 1 (FSP1), vimentin, desmin or FAP (Kalluri and Zeisberg, 2006; Shiga et al., 2015). To target fibroblasts, Cre recombinases under control of the

smooth muscle protein 22alpha (*Sm22-Cre*/*Sm22*$^{Cre/+}$) or FSP1 (*Fsp1-Cre*) promoter were used in the *KF/KPF* mouse model.

Two different *Sm22-Cre* mouse lines were analyzed for their specificity to target fibroblasts in pancreatic tumor development. First, a transgenic *Sm22-Cre* line was investigated. This mouse line was used for studying vascular smooth muscle cells (Holtwick et al., 2002). The line was crossed with *KF* or *KPF* mice to identify Cre-recombined cells in the tumor stroma of PDAC. Tumors were analyzed for Cre recombination with the help of the *R26*$^{mT-mG}$ Cre reporter mouse line. Macroscopic pictures of primary tumors revealed not only tdTomato expression but EGFP expression as well (Fig.17 A). Cre recombination was observed not only in cells having a stromal morphology but also in cells of PanIN lesions and subsequently in tumor cells (Fig.17 B). Five different primary tumors were analyzed for Cre recombination and number of EGFP-positive cells was counted. As depicted in Fig.17 C, the amount of Cre-recombined cells varied from just 10 cells per field of view up to almost 200 cells. Even within the same tumor there seems to be a huge variance in Cre-recombined cells. For characterization of targeted cells immunofluorescence staining for αSMA and vimentin were performed (Fig.17 D and Fig.17 E). Quantification of these staining resulted in a small percentage of Cre-targeted cells which were also positive for expression of αSMA or vimentin (Fig.17 F). In one tumor sample about 30 % of all αSMA-stained cells showed also Cre recombination. All other tested samples had even lower percentages of double-positive cells. Of all vimentin-stained cells about 2.5 % in average were also recombined by Cre.

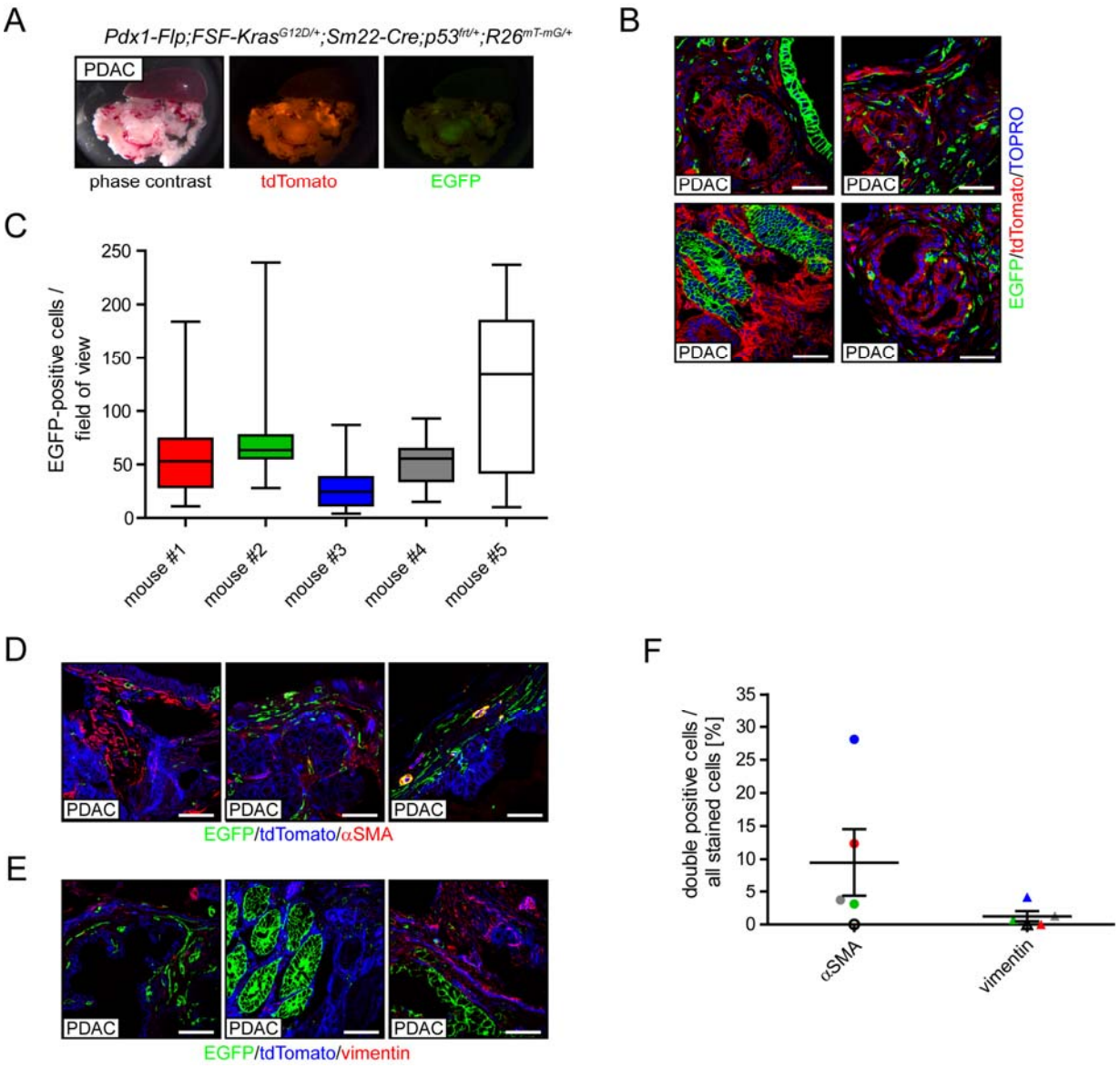

Fig.17 Targeting fibroblasts in PDAC using the *Sm22-Cre* line.
(**A**) Representative macroscopic images of PDAC of *Pdx1-Flp;FSF-Kras$^{G12D/+}$;Sm22-Cre;p53$^{frt/+}$;R26^{mT-mG}* mouse. (**B**) Confocal microscopy pictures of tumor samples. Cre-recombined cells are green (EGFP expression), Cre-non-recombined cells are red (tdTomato expression). Nuclei were stained with TOPR-3 (blue). (**C**) Overview of number of Cre-recombined cells in five different tumor-bearing mice. At least 15 pictures per animal were analyzed (n=5). Minimun to maximum counts are represented. (**D**) αSMA-immunofluorescence staining of PDAC samples. tdTomato-expressing cells are shown in blue; Cre-recombined cells are in green and αSMA-stained cells are red. (**E**) Confocal microscopy images of vimentin staining of tumors of *KPF;Sm22-Cre;R26^{mT-mG}* mice. In red vimentin staining is shown; Cre-negative cells express tdTomato depicted in blue; Cre-recombined cells are expressing EGFP (green). (F) Quantification of αSMA and vimentin staining of *KPF;Sm22-Cre;R26^{mT-mG}* mice. Double positive cells (for Cre-recombination and staining) were normalized to all stained cells. 10 images per animal (n=5) were used for analysis. Scale bars 50 µm.

Staining for CK19 was performed since EGFP-expression was detected in cells of PanIN lesions (Fig.18 A). CK19 staining was negative for EGFP-positive cells when displaying a fibroblast-like morphology but there was a co-localization in ductal-like Cre-recombined cells. Therefore, isolated primary tumor cells were analyzed for Cre recombination. Cre-recombined cells express EGFP and Cre-negative cells express tdTomato. Confocal microscopy images of cell lines revealed EGFP expression (Fig.18 B). FACS analysis of different isolated cancer cell lines *of KPF;Sm22-Cre;R26*$^{mT\text{-}mG}$ mice detected EGFP expression in tumor cells (Fig.18 C) and not only in fibroblasts. The amount of EGFP-expressing cells differed from 0 % to 95 % of all cells (Fig.18 D). Those results indicate that Sm22-Cre-targeted cells are not only activated fibroblasts or stromal cells. This Cre line seems to target also PDAC cells and is therefore not suitable to analyze the stroma of pancreatic cancer.

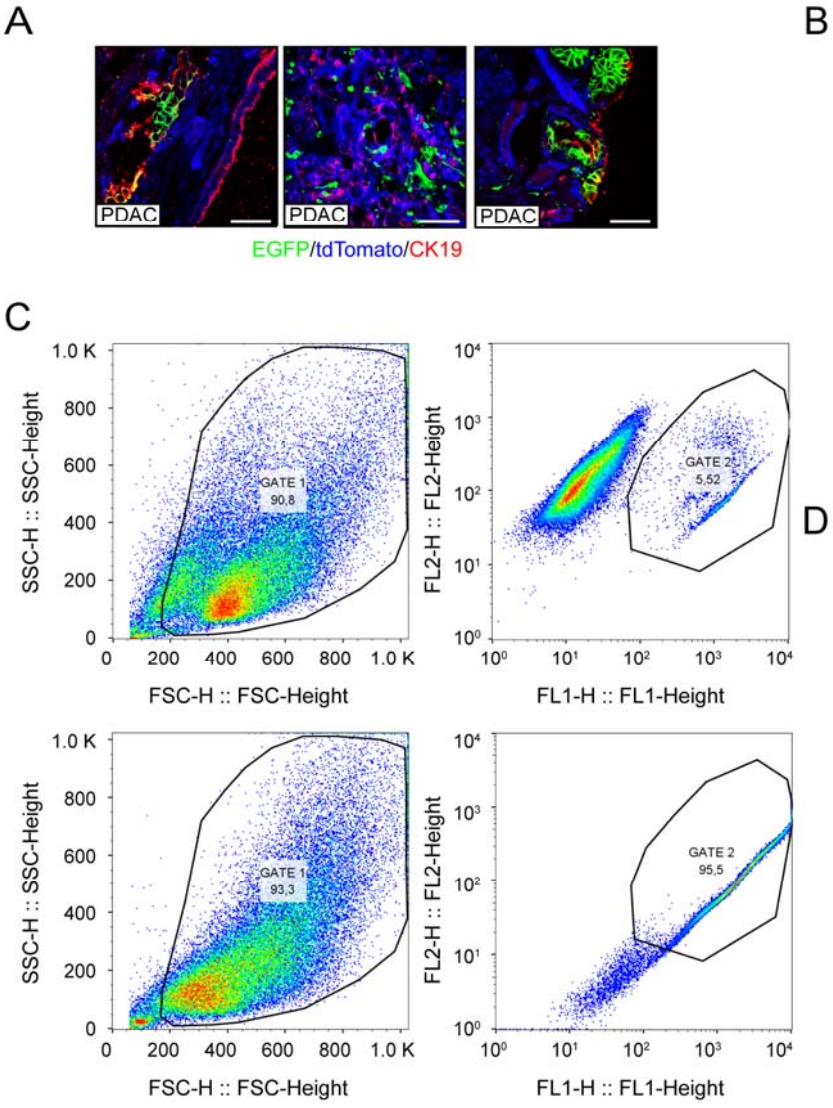

D

	Sm22-Cre recombined cells [%]
cell line 1	5,52
cell line 2	95,5
cell line 3	6,83E-03
cell line 4	0,062

Fig.18 Sm22-Cre is expressed in tumor cells. (Figure legend continued on next page)

(**A**) Confocal microscopy images of *KPF;Sm22-Cre;R26*$^{mT\text{-}mG}$ tumors stained for CK19 expression. Cre-recombined cells expressing EGFP (green); Cre-non-recombined cells express tdTomato (blue). CK19 staining is depicted in red. (Figure legend continued on next page)
(**B**) Isolated primary tumor cell lines were investigated for tdTomato- and EGFP-expression. Confocal microscopy images of cell lines. ((**C**) FACS analysis of two different cell lines for EGFP- and tdTomato-expression. Upper panel: Cell line 1 isolated from PDAC of *KPF;Sm22-Cre;R26*$^{mT\text{-}mG}$ mouse displaying partly EGFP expression (FL1 on x-axis). Most cells express tdTomato only (FL2 on y-axis). Lower panel: Cell line 2 showing only EGFP expression (right panel). (**D**) Summary of analyzed cell lines of *KPF;Sm22-Cre;R26*$^{mT\text{-}mG}$ tumors. Scale bars 50 µm.

The transgenic *Sm22-Cre* mouse line is active in tumor cells and thus another mouse line was characterized for its specificity to target fibroblasts. Here, the Cre recombinase was inserted as a knock-in into the *transgelin* locus (smooth-muscle protein alpha; Sm22) (Zhang et al., 2006). Similar to the transgenic line other research groups used this line to investigate smooth muscle cells. This Cre line was bred with *KF* and *KPF* mice allowing PDAC development. Cre-recombined cells of the *Sm22*$^{Cre/+}$ line were identified and characterized in the same manner as the transgenic line with the help of the Cre reporter line *R26*$^{mT\text{-}mG}$. Primary pancreatic tumors were macroscopically examined for EGFP and tdTomato expression (Fig.19 A) which revealed expression of both proteins. Confocal microscopy pictures of tumor samples showed EGFP expression and Cre activity was not only detected in stromal cells but in cancer cells and cells of PanIN lesions as well (Fig.19 B). The amount of Cre-recombined cells varied between the mice and between the field of view of analyzed pancreatic tissue (Fig.19 C). As already shown for the transgenic *Sm22-Cre* mouse line, the knock-in Cre line seems also to target cancer cells. Therefore, pancreatic tumors were stained for the ductal marker CK19. Interestingly, although cells of PanIN lesions are recombined by the Cre, these cells were negative for CK19 whereas non-recombined cells showed CK19 expression (Fig.19 D). Isolated primary cancer cells were analyzed for EGFP and tdTomato expression by confocal microscopy (Fig.19 E) and FACS analysis (Fig.19 F). Both examinations revealed EGFP expression in tumor cells to different extent. 3 different cell lines were analyzed for EGFP and tdTomato expression by FACS (Fig.19 G). Up to 11 % of cancer cells were recombined by *Sm22*$^{Cre/+}$. Evidently, this knock-in mouse line seems to not only target stromal cells and is consequently not adequate for targeting fibroblast-like cells of the tumor microenvironment of PDAC.

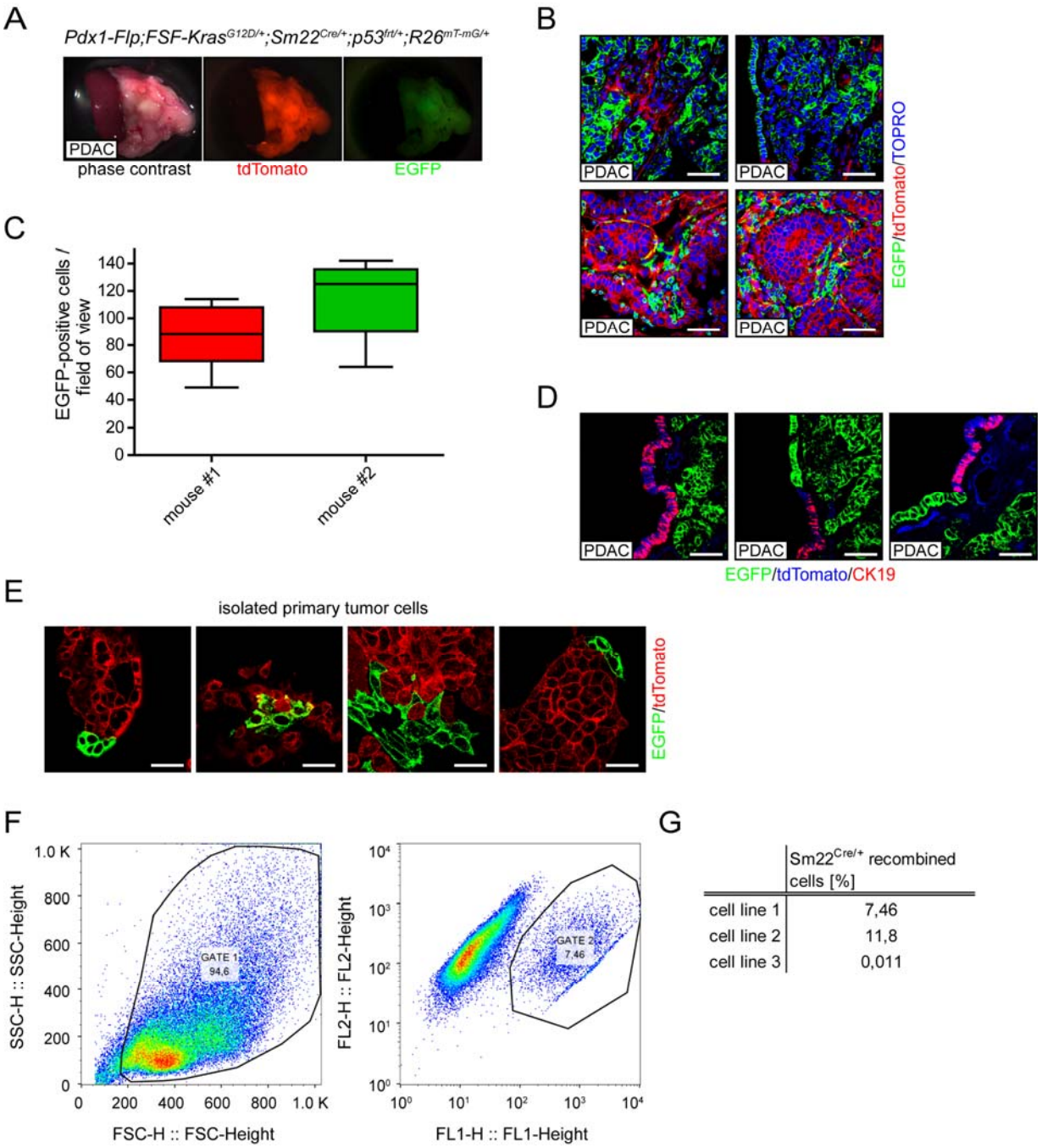

Fig.19 Characterization of Sm22$^{Cre/+}$ in PDAC of *KPF* mice.
(**A**) Macroscopical pictures of tumors of *KPF;Sm22$^{Cre/+}$;R26^{mT-mG}* mouse. (**B**) Representative confocal microscopy images of PDAC. Cells targeted by Sm22$^{Cre/+}$ express membrane-tagged EGFP (green), all other cells express membrane-bound tdTomato (red). Nuclei were counterstained with TOPRO-3 (blue). (**C**) Quantification of Cre-recombined cells in tumor samples. At least 12 pictures of each animal were examined (n=2). Minimun to maximum counts are represented. (**D**) CK19 staining of tumor samples of *KPF;Sm22$^{Cre/+}$;R26^{mT-mG}* mice. Cre-recombined cells depicted in green (EGFP expression), Cre-non-recombined cells express tdTomato (blue). Staining of CK19 is shown in red. (**E**) Confocal microscopy images of isolated primary cancer cells. EGFP-expressing cells are shown in green, tdTomato-expressing cells are red. (Figure legend continued on next page)

(**F**) FACS analysis of tumor cell line isolated from *KPF;Sm22$^{Cre/+}$;R26^{mT-mG}* mouse. Cells were gated according to size (forward and sideward scatter, left panel). Right panel: Gated cells were examined for EGFP and tdTomato expression (EGFP on x-axis: FL1; tdTomato on y-axis: FL2). (**G**) Overview of all investigated cell lines for EGFP and tdTomato expression. Scale bars 50 μm.

To target specifically fibroblasts in the tumor microenvironment, another transgenic mouse line was characterized. As mentioned before, Fsp1 is a marker for fibroblasts and in various studies the *Fsp1-Cre* was used to target fibroblasts (Bhowmick et al., 2004; Cheng et al., 2005; Li et al., 2012; Tsutsumi et al., 2009). Hence, in this present study the transgenic mouse line *Fsp1-Cre* was examined for efficiency and specificity to target activated fibroblasts in the stroma of PDAC. *KF* or *KPF* mice were bred with *Fsp1-Cre* animals and upon tumor development the pancreas was analyzed. Macroscopic examination of primary tumor showed expression of EGFP and tdTomato (Fig.20 A). Metastases in the liver and in the lung were also analyzed for EGFP and tdTomato expression. As shown in Fig.20 A the liver metastasis was expressing EGFP in contrast to the metastasis in the lung which was only expressing tdTomato (indicated by arrows). Investigation of *Fsp1-Cre* recombination in PDAC by confocal microscopy revealed Cre recombination in cells which morphologically resemble stromal cells (Fig.20 B). The number of Fsp1-Cre-targeted cells was determined by counting EGFP-positive cells. The amount of Cre-recombined cells varied between the analyzed animals as well as between the different fields of view. The mean number of Cre-recombined cells of all examined mice was around 80 cells per field of view (Fig.20 C). Further characterization of Fsp1-Cre-recombined cells by immunofluorescence staining was performed. Activated fibroblast-specific markers like αSMA, vimentin, and FAP were used to identify possible co-localization. As shown in Fig.20 D, localization of αSMA-positive cells was distinct from those being recombined by Fsp1-Cre. Similar results could be observed in case of vimentin staining (Fig.20 F). For both stainings hardly any double positive cell could be detected in all analyzed tumor samples (Fig.20 I). In contrast to the most commonly used markers for activated fibroblasts, staining of fibroblast-activating protein (FAP) resulted in more double positive cells (Fig.20 G). The average of FAP- and EGFP-double positive cells was around 60% for all analyzed tumor samples compared to 1 % for vimentin and 1.5 % for αSMA. Furthermore, immunofluorescence staining for nestin was done (Fig.20 H). Around 15 % of all nestin-stained cells displayed expression of Fsp1 (Fig.20 I). As in the injured liver Fsp1-Cre-targeted cells were identified as a subpopulation of macrophages (Osterreicher et al., 2011), pancreatic cancer samples were analyzed for co-expression of EGFP (Cre-recombined cells) and the macrophage marker F4/80. A small EGFP- and F4/80 double-positive population could be observed (Fig.20 E). Quantification analysis

revealed that in some tumors about 30 % of Fsp1-Cre-recombined cells expressed F4/80 (Fig.20 I).

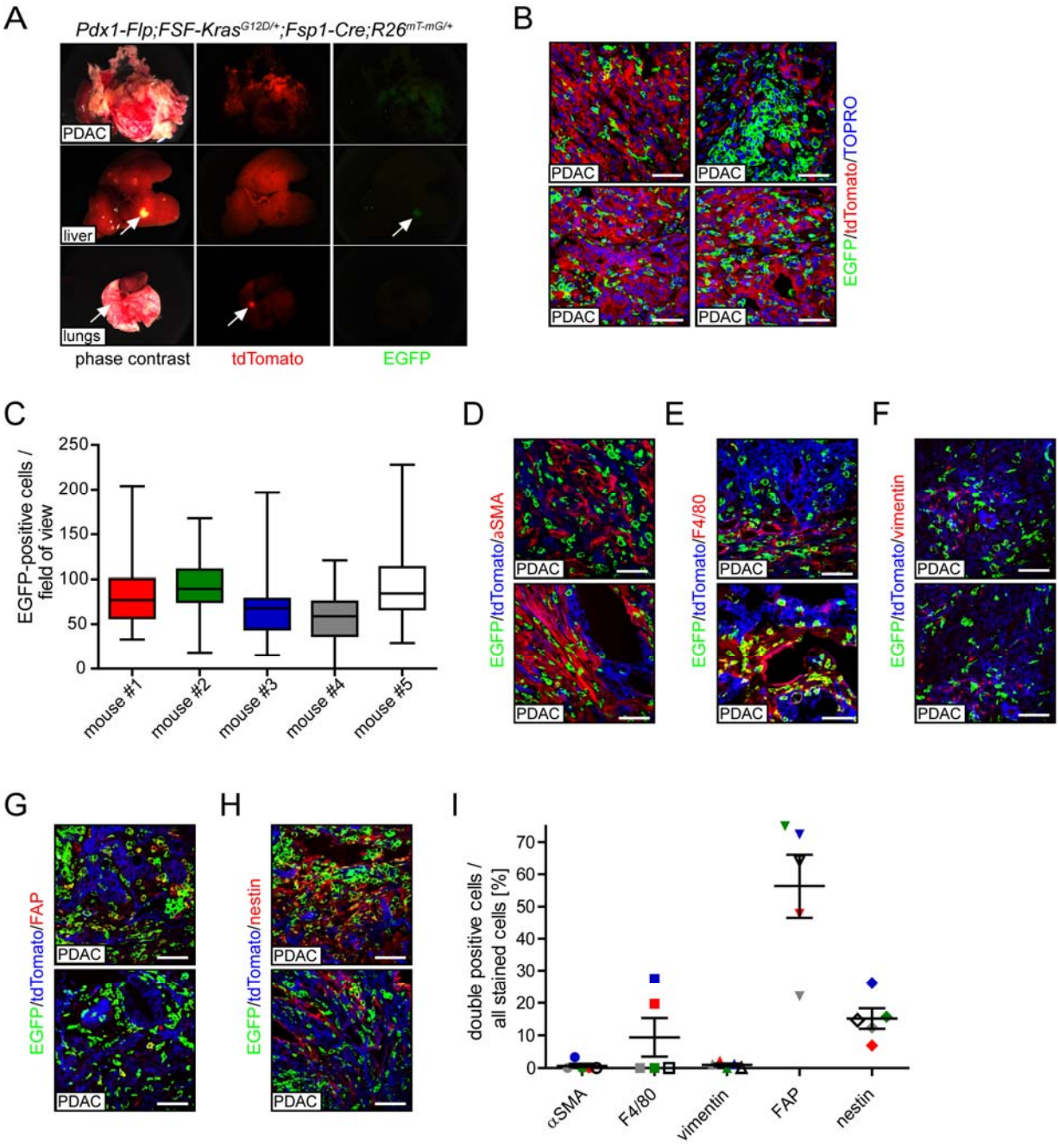

Fig.20 Fsp1-Cre-targeted cells in stroma of PDAC.
(**A**) Macroscopic pictures of primary tumor, liver and lung of *Pdx1-Flp;FSF-Kras$^{G12D/+}$;Fsp1-Cre;R26^{mT-mG}* mouse. Liver and lung metastases are indicated by arrows. (**B**) Confocal microscopic images of PDAC of *KF;Fsp1-Cre;R26^{mT-mG}* mice. Cre-recombined cells express EGFP (green), Cre-negative cells express membrane-bound tdTomato (red). Nuclei are stained by TOPRO-3 (blue). (Figure legend continued on next page)

(**C**) Quantification of Cre-recombined cell expressing EGFP in five different animals. At least 50 pictures per animal were counted (n=5). Minimum to maximum numbers are displayed. (**D-H**) Representative confocal pictures of immunofluorescence staining for fibroblast markers like αSMA, vimentin, FAP, nestin and F4/80. Fsp1-Cre-recombined cells are shown in green; Non-recombined cells are depicted in blue. (**D**) αSMA staining of PDAC samples. In red αSMA-staining is given. (**E**) Tumor tissue of *KF;Fsp1-Cre;R26*$^{mT\text{-}mG}$ stained for macrophage marker F4/80. Positive-stained cells are red. (**F**) Immunofluorescence staining for vimentin of pancreatic cancer tissue. Vimentin staining is shown in red. (**G**) Staining for FAP in PDAC samples. FAP-positive cells are depicted in red. (**H**) Nestin staining of PDAC. Stained cells are shown in red. (**I**) Quantification of staining. Double-positive cells (stained for corresponding marker and imaged for EGFP expression which indicates Fsp1-Cre mediated recombination) are normalized to all stained cells. For each tumor sample 10 images were analyzed (n=5). Scale bars 50 µm.

For further characterization of Fsp1-targeted cells, tumor cell lines were generated of *KF/KPF;Fsp1-Cre;R26*$^{mT\text{-}mG}$ mice. Those cancer cell lines were investigated for tdTomato and EGFP expression by confocal microscopy (Fig.21 A) and FACS (Fig.21 B). EGFP expression of cancer cells could be observed by both methods. The amount of Fsp1-expressing cancer cells varied between 0 % and almost 6 % as summarized in Fig.21 C.

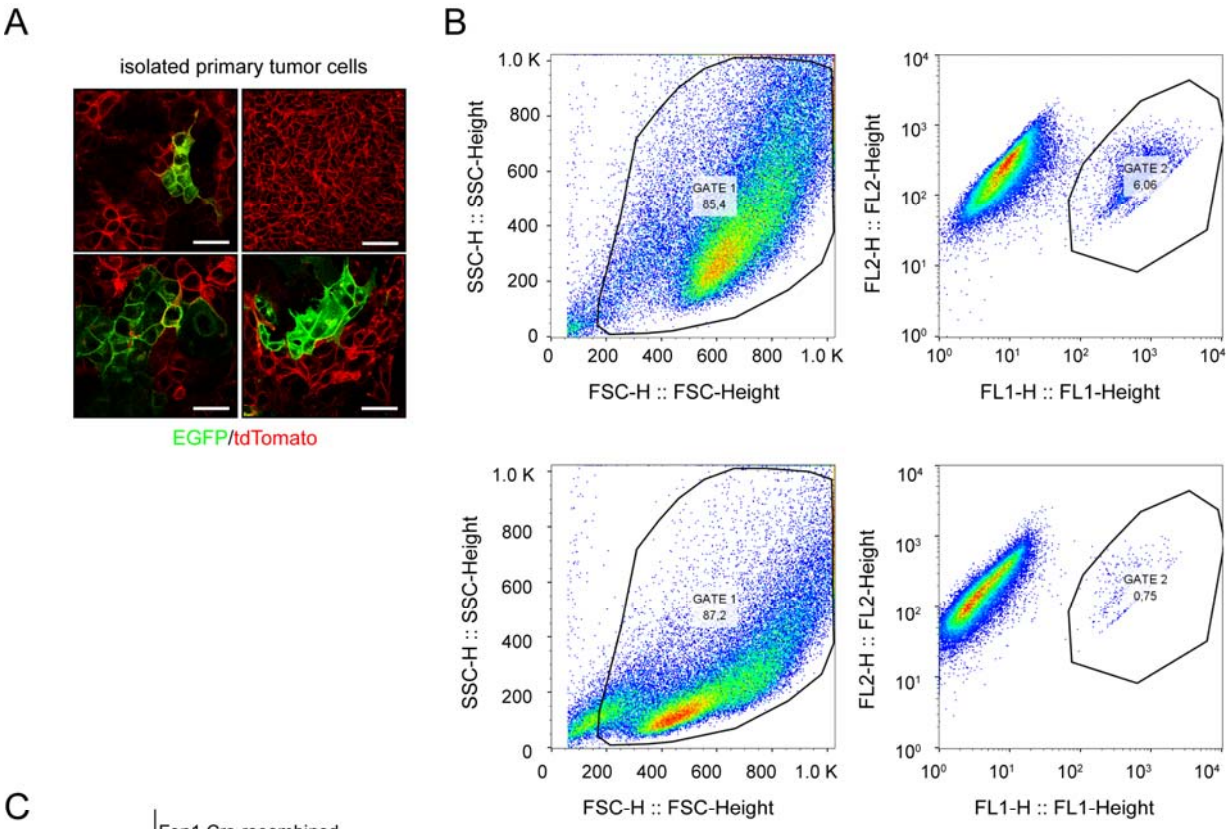

C

	Fsp1-Cre recombined cells [%]
cell line 1	6,06
cell line 2	0,75
cell line 3	0,036
cell line 4	0,026
cell line 5	2,79

Fig.21 Analysis of primary cancer cell lines isolated of *KF/KPF;Fsp1-Cre;R26^{mT-mG}*.
(**A**) Representative confocal microscopy pictures of isolated tumor cells. Cre-con-recombined cells are red; Cre-recombined cells are green. (**B**) FACS analysis of tumor cell lines. Left panels: Cells were gated according to size (forward and sideward scatter); right panels: gated cells were separated by tdTomato and EGFP-expression (on y-axis: tdTomato, FL2; on x-axis: EGFP; FL1). Exemplary two different cell lines were shown. (**C**) Table of all analyzed tumor cell lines of *KF/KPF;Fsp1-Cre;R26^{mT-mG}* cancers for tdTomato and EGFP expression. Scale bars 50 µm.

Taken into account that Fsp1 was already described as a marker for tumor cells undergoing epithelial-to mesenchymal transition (EMT) (Nishitani et al., 2005; Smith and Bhowmick, 2016) additional experiments were performed, using EMT marker genes, such as vimentin. The present amount of vimentin- and Fsp1-double positive cells in analyzed tumor samples was 1 % as shown in Fig.20 I. To identify whether Fsp1 positive cancer cells undergo indeed EMT *in vivo*, a dual reporter line for Flp and Cre activity was bred into the *KPF;Fsp1-Cre* line to track EMT events. The *R26$^{CAG-FSF-LSL-Ai65-tdTom}$* reporter indicates cells which express both

recombinases. Upon Flp- and Cre-recombination those cells express tdTomato (Madisen et al., 2015).

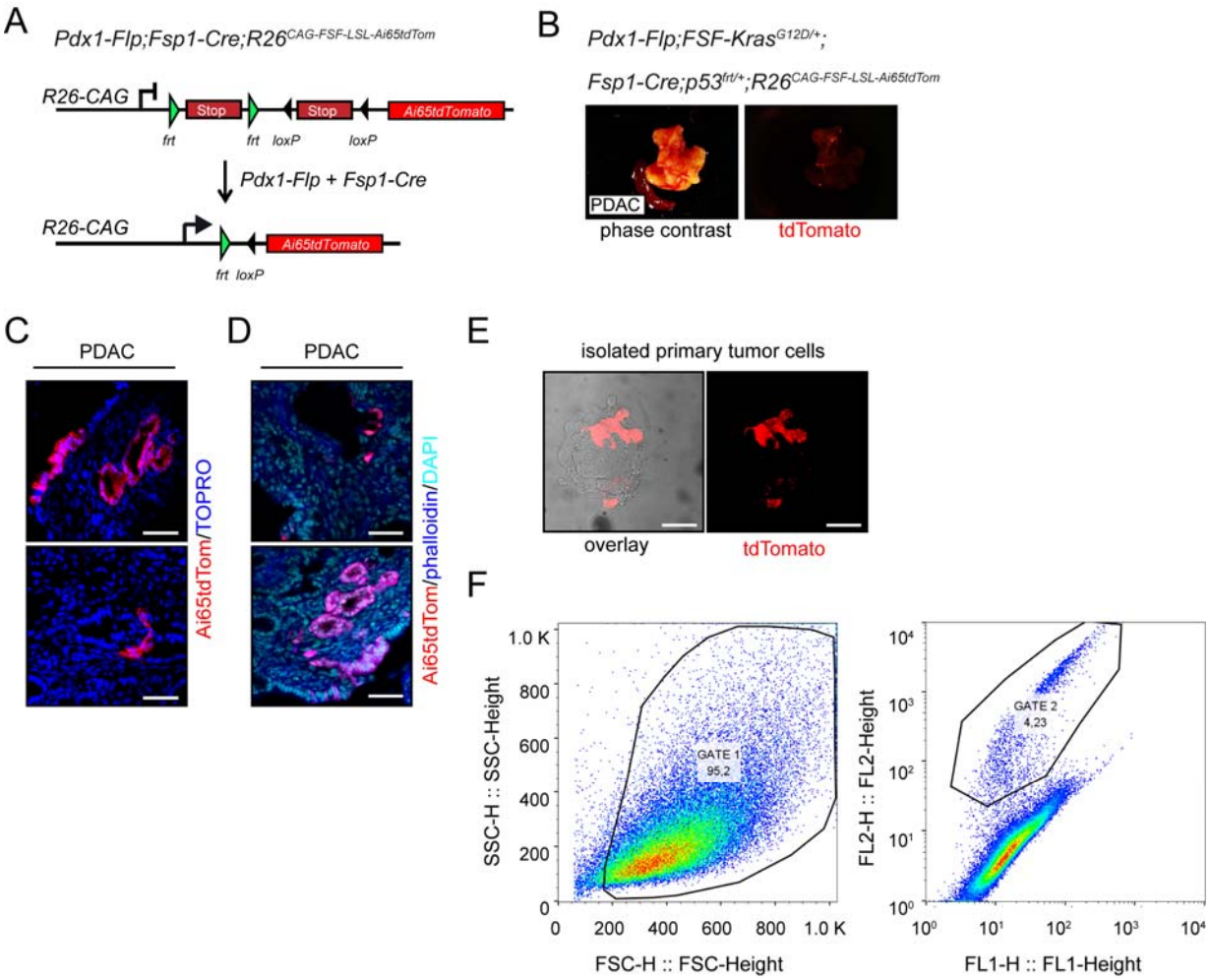

Fig.22 Fsp1 is expressed by *Pdx1-Flp;FSF-Kras$^{G12D/+}$* tumor cells.
(**A**) Scheme of the dual Flp and Cre reporter *R26$^{CAG-FSF-LSL-Ai65-tdTom}$*. tdTomato is only expressed after Flp and Cre recombination by excision of the two STOP cassettes, one flanked by frt sites and the other one flanked by loxP sites. (**B**) Representative macroscopic pictures of primary tumor of *KPF;Fsp1-Cre; R26$^{CAG-FSF-LSL-Ai65-tdTom}$*.animal. (**C**) Confocal microscopy images of pancreatic cancer tissue of *Pdx1-Flp;FSF-Kras$^{G12D/+}$;Fsp1-Cre;p53$^{frt/+}$;R26$^{CAG-FSF-LSL-Ai65-tdTom}$* mice. Cells which express Flp and Cre are expressing tdTomato (red). All other cells are without color. Nuclei were counterstained with TORPO-3 (blue). (**D**) PDAC samples of *KPF;Fsp1-Cre;R26$^{CAG-FSF-LSL-Ai65-tdTom}$*. Pancreatic cancer tissue was stained with phalloidin (blue) to visualize cells and DAPI staining the nuclei (turquoise). Cells expressing Flp and Cre recombinase are expressing tdTomato (red). (**E**) Confocal microscopy pictures of isolated primary cancer cells. Cells double positive for Flp and Cre activity express tdTomato whereas all other cells display no tdTomato expression. (**F**) FACS analysis of tumor cell line of *KPF;Fsp1-Cre;R26$^{CAG-FSF-LSL-Ai65-tdTom}$* mouse. Left panel: Cells were analyzed according to size (forward and sideward scatter). Right panel: Gated cells examined for tdTomato expression (FL2 on y-axis).

In Fig.22 A the genetic scheme of the dual reporter for Flp and Cre recombination is given. Primary pancreatic tumors of *KPF;Fsp1-Cre;R26*$^{CAG\text{-}FSF\text{-}LSL\text{-}Ai65\text{-}tdTom}$ mice showed tdTomato expression in some parts of the tumor (Fig.22 B). Not the whole tumor was positive for tdTomato expression indicating that few cells were expressing Pdx1-Flp and Fsp1-Cre. Confocal microscopy analysis of cancer tissue revealed tdTomato expression in some PDAC cells of *KPF;Fsp1-Cre; R26*$^{CAG\text{-}FSF\text{-}LSL\text{-}Ai65\text{-}tdTom}$ mice (Fig.22 C and D), indicating Flp and Cre activity in those cells. Isolated primary tumor cells were investigated for tdTomato expression as well. First results revealed tdTomato positive cells in the cancer cell line (Fig.22 E). FACS analysis of this cell line discovered that about 6 % of the tumor cells express tdTomato (Fig.22 F). Therefore, this Cre-driver line might be indeed capable of traking EMT and thereby helpful to clarify the role of EMT for metastasis formation. Because some metastases remained unrecombined in the Fsp1-Cre model, these results might indicate that EMT is dispensable for metastasis formation.

In sum, the *Fsp1-Cre* mouse line is not only targeting fibroblasts in the pancreatic tumor microenvironment but also F4/80 positive macrophages, and could be useful as an *in vivo* EMT tracker.

4.3.4 Overview of analyzed Cre lines for targeting fibroblasts and stellate cells in PDAC

Table 18 gives a summary of analyzed Cre lines targeting either pancreatic stellate cells or fibroblasts. As depicted in Table 18 not all characterized Cre lines are specifically targeting one type of stromal cells but possibly different subpopulations.

Table 18 Summary of analyzed Cre lines and their specificity
Displayed are percentages of all stained cells which were positive for Cre recombination (EGFP expression).

cell type	Cre line	marker	% of stained cells
pancreatic stellate cells	hGFAP-Cre	αSMA	0.0 – 29.1
		GFAP	11.4 – 22.3
		CK19	7.3 – 32.5
	mGFAP-Cre	αSMA	0.0
		GFAP	20.0 – 60.0
		nestin	0.0 – 0.7
fibroblasts	Sm22-Cre	αSMA	0.0 – 28.1
		vimentin	0.0 – 4.2
	Fsp1-Cre	αSMA	0.0 – 3.3
		vimentin	0.0 – 2.2
		F4/80	0.0 – 27.5
		nestin	6.9 – 26.2
		FAP	22.0 – 75.0

5 DISCUSSION

Although intensively studied, pancreatic ductal adenocarcinoma still accounts for many cancer-related deaths. Over the last years the survival prognosis did not improve and diagnosis still occurs at an already advanced stage of disease. As PDAC is characterized by a dense desmoplastic tumor microenvironment, which makes up most of the tumor volume, the identification of different cells which infiltrate the tumor and which are involved in the excessive production of stroma is gaining importance. With the help of genetically engineered mouse models (GEMM) many aspects of the disease were already deciphered. The well-established murine model of pancreatic cancer using the Cre/LoxP system is limited, as the initiation and progression of cancer can be simulated but the sequential and multi-step process of cancerogenesis cannot be recapitulated. Furthermore, the investigation of cell types, which infiltrate the tumor stroma and interact with cancer cells, is not possible. Here, the novel dual-recombination system was characterized for time- and host-specific manipulation of pancreatic cancer.

5.1 CHARACTERIZATION OF THE DUAL-RECOMBINATION SYSTEM COMBINING FLP/FRT AND CRE/LOXP

To analyze the tumorigenesis as a multi-step process, two recombination systems – Cre/loxP and Flp/frt – were combined in this work. Endogenous pancreatic cancer development was induced by the Flp/frt system, directing the oncogenic $Kras^{G12D}$ expression (carrying an activation mutation in the second exon) to the *Pdx1* lineage introducing an frt-flanked STOP cassette upstream of *Kras* (*FSF-*$Kras^{G12D}$). With the help of a Flp-dependent, tamoxifen-inducible Cre line (*FSF-*$R26^{CAG\text{-}CreERT2}$) additional target genes can be time-specifically activated/inactivated (Schonhuber et al., 2014). Furthermore, other cell types were targeted using Cre lines under control of cell type specific promoter.

Examination of *Pdx1-Flp;FSF-*$Kras^{G12D/+}$ (*KF*) animals reveals that formation of precursor lesions of different grades similar to the well established *Pdx1-Cre;LSL-*$Kras^{G12D/+}$ (*KC*) mouse model for PDAC. Furthermore, the occurrence of PDAC and overall survival is comparable in both models (Schonhuber et al., 2014). The expression pattern of *Pdx1-Flp* (acitive in pancreas, parts of the duodenum, bile duct, skin, and some cells of the stomach) equals the one known of Pdx1 (Fukuda et al., 2006; Offield et al., 1996). In human cancer often p53 mutations accumulate over time (Feldmann and Maitra, 2008) thus a $p53^{frt}$ allele was introduced in the *KF*

mouse model. Formation of pancreatic tumors of *Pdx1-Flp;FSF-Kras$^{G12D/+}$;p53^{frt}* (*KPF*) mice occurred similar to the known *KPC* model (Schonhuber et al., 2014). Formation of metastases in liver and lung are often observed in patients with PDAC (Kim et al., 2015). Analysis of liver and lung tissue of PDAC-bearing mice of both models displays that metastases occur with roughly same frequency in examined organs. These data show that *KF* and the *KPF* mouse model mimic the human disease as it was reported for the *KC* and *KPC* (Hingorani et al., 2003; Schonhuber et al., 2014).

The established mouse models *KC* and *KPC* are limited in recapitulating the human situation of tumor development and progression as a multi-step and sequential process. In human cancerogenesis mutations accumulate over time (Hruban et al., 2000a). This multi-step process can be simulated with the novel dual-recombination system which allows sequential and time-specific manipulation of cancer cells. Secondary genetic targeting is possible as shown by the Cre reporter *R26^{mT-mG}*. After tamoxifen treatment all compartments of the pancreas (acini, ducts, and islets) show EGFP expression upon Cre recombination. The dual-recombination system allows genetic manipulation of already established tumors resembling the human situation of tumor progression. Recently, Schönhuber et al. has shown, that the tamoxifen-induced deletion of p53 resulted in accelerated PDAC formation in *Pdx1-Flp;FSF-Kras$^{G12D/+}$;FSF-R26$^{CAG-CreERT2}$;p53$^{lox/lox}$* (Schonhuber et al., 2014). In general, this dual-recombination system can be used to analyze any candidate gene for its influence on tumor formation and its progression as well as survival. Schonhuber et al. could demonstrate that tamoxifen-induced expression of diphtheria toxin A in cancer cells results in cell death *in vitro* and tumor shrinkage of tumor-bearing mice (Schonhuber et al., 2014). 3-phosphoinositide-dependent protein kinase 1 (Pdk1) is a protein kinase which activates PKB/AKT and is involved in various cellular processes like cell survival, proliferation, and growth. Embryonic inactivation of Pdk1 is shown to completely block ADM, PanIN and subsequently PDAC formation in *Ptf1a$^{Cre/+}$;LSL-Kras$^{G12D/+}$* mice (Eser et al., 2013). The importance of Pdk1 in tumor maintenance was examined with the help of the dual-recombination system. In PanIN-bearing animals tumor progression can be blocked upon depletion of Pdk1 by tamoxifen treatment of 3-month-old *KF;FSF-R26$^{CAG-CreERT2}$;Pdk1$^{fl/fl}$* mice (Schonhuber et al., 2014).

Here, the therapeutic options of p53 wild type restoration in tumor cells were investigated with the dual-recombination system. It could be demonstrated that upon restoration of p53 expression in isolated primary pancreatic tumor cells the cell viability and capability of colony formation is reduced. The diminished growth rate and colony formation indicate that wild type p53 restoration lead to decreased tumor growth *in vivo*. Ventura et al. demonstrated p53 restoration of a *p53^{LSL}* mouse line after application of Adeno-Cre in soft tissue sarcoma-bearing

mice and after tamoxifen-induced CreER^{T2} activation in lymphoma-bearing mice. They show decrease of tumor volume, growth suppression and induction of apoptosis in tumor-bearing p53 null mice after restoration of p53 wild type expression (Ventura et al., 2007). Others report tumor clearance upon p53 reactivation in murine liver carcinomas using an inducible RNAi system; suppression of viral E6 oncogene and decrease in tumor volume by treatment of squamous cell carcinoma with small molecule Minnelide^{TM} which lead to restoration of wild type p53 or p53 reactivation upon treatment of lymphomas or breat cancers with small inhibitors of MDM2 (Caicedo-Granados et al., 2014; Lu et al., 2016; Selivanova, 2014; Xue et al., 2007).Due to the fact that p53 is known to regulate various cellular processes like cell cycle arrest, senescence, apoptosis and differentiation (Evan and Vousden, 2001; Riley et al., 2008; Schmitt et al., 2002) it needs to be investigated how exactly restoration of p53 results in decreased cell viability in our model system. One out of the three tested cell lines seems to be resistant to restoration of the function of wild type p53 as only a slight decrease in cell viability was observed. How tumor cells are still able to proliferate is still under investigation. Incomplete recombination of the tumor cells or failure of restoration of wild type p53 in all tumor cells can be an explanation as in PCR and protein analysis this cell line showed less p53 restoration compared to the other tested cell lines. Furthermore, upregulated MDM2 levels could explain continued proliferation of cells with wild type p53 as it has been reported that elevated MDM2 levels can induce tumorigenesis independent of p53 (Jones et al., 1998). The growth arrest is achieved by p53-dependent p21 activiation. If p53 fails to induce p21^{BAX}, cells will not undergo apoptosis as it is reported for gliablastoma (Shu et al., 1998). Deregulation of other downstream pathways (induction of cell cycle arrest or senescence) of p53 can also lead to continued growth of tumor cells. To assess the function of p53 wild type restoration in established tumors, orthotopic implantation of isolated cell lines could be performed to analyze if survival of tamoxifen-treated animals is prolonged compared to vehicle-treated mice. Furthermore, possible tumor shrinkage *in vivo* upon restoration of p53 wild type could be analyzed as well as any effects on metastasis formation.

The dual-recombination system does not only allow examination of host-cell specific genes but furthermore enables the investigation of stromal compartment by targeting stromal cells with cell-type specific Cre driver lines as it was done in this present study for targeting mast cells, pancreatic stellate cells, and fibroblasts.

5.2 TARGETING THE TUMOR MICROENVIRONMENT OF PDAC

5.2.1 ROLE OF MAST CELLS IN PANCREATIC DUCTAL ADENOCARCINOMA

In the year 2000, six main hallmarks were described by Hanahan and Weinberg, like resisting cell death, sustaining proliferation signals, induction of angiogenesis, and initiation of invasion and metastasis (Hanahan and Weinberg, 2000). These originally identified hallmarks were complemented by the role of the tumor microenvironment and its stromal cells (Hanahan and Weinberg, 2011), like infiltrating immune cells, activated fibroblasts or myofibroblasts. In this present study, the role of mast cells was investigated in pancreatic cancer. It could be shown that mast cells are negligible during development and progression of PDAC, as well as for tumor maintenance.

In many different studies the role of mast cells in disease and cancer was investigated (Galinsky and Nechushtan, 2008; Hodges et al., 2012). Tumor-promoting role of mast cells was described for example by Chang et al., who used the $Kras^{G12V}$ oncogene for PDAC induction and the $Kit^{W\text{-}sh/W\text{-}sh}$ mouse model to achieve mast cell deficiency. They observed reduced tumor growth in mast-cell deficient mice with prolonged survival and associated the early influx of mast cells with the appearance of pancreatic cancer (Chang et al., 2011). The results fit to data already published in 2004 by Esposito et al., where human tissue samples were analyzed for mast cell count and outcome of PDAC patients. They reported that higher infiltration of mast cells and macrophages correlate to a shorter survival of PDAC patients (Esposito et al., 2004). Further, high mast cell infiltration in intratumoral border zone was correlated to tumor stage and lymph node metastases (Cai et al., 2011). Furthermore, the influence of cancer cells on mast cells could be shown *in vitro*. Pancreatic cancer cells secrete SCF, the ligand for the Kit receptor, which is expressed by mast cells. Conditioned medium of pancreatic cancer cells induced mast-cell migration whereas mast cells increased proliferation and invasion of cancer cells. However, in this study they could show that mast-cell infiltration induce an angiogenic phenotype whereas no correlation of mast-cell infiltration and survival or tumor grade could be drawn (Strouch et al., 2010). Other groups could demonstrate that pharmacological inhibition of mast cell activation by cromolyn led to decrease in tumor growth and suppression of tumor progression (Ma et al., 2013; Soucek et al., 2007). In myc-induced endocrine pancreatic cancers derived from pancreatic β-cells infiltration of mast cells was correlated to expansion of tumor which could be limited upon mast-cell inhibition by cromolyn. Further, smaller tumors developed upon implantation of pancreatic cancer cells in mast-cell deficient $Kit^{W\text{-}sh}$ mice compared to control group (Soucek et al., 2007). In a study published last year, another pharmacological

inhibitor of mast cells, ibrutinib, was used and resulted in less fibrosis, fewer F4/80+ and fewer Cd11b+ cells in a Kras-driven PDAC mouse model. In implanted animals the survival was prolonged after combined treatment of ibrutinib and gemcitabine compared to gemcitabine-alone treated animals (Masso-Valles et al., 2015). Mast cells may contribute to the progression of cancer by infiltrating the tumor and releasing chemokines, cytokines and growth factors and inducing angiogenesis (Ammendola et al., 2014; Chang et al., 2011; Ma et al., 2013; Masso-Valles et al., 2015; Soucek et al., 2007) thereby promoting tumor development and maintenance. By secreting MMPs, mast cell could also enhance metastasis formation. It was shown that e.g. inhibition of histamine release by mast cells reduces tumor growth (Johnson et al., 2016). As already mentioned, chronic pancreatitis is a known tumor risk factor (Lowenfels et al., 1993; McKay et al., 2008) and the role of mast cells in chronic pancreatitis is under investigation as well. In chronic pancreatitis patients an increase of degranulated mast cells was observed with increasing stage of fibrosis (Zimnoch et al., 2002). Recently, a comparative study of human tissue samples of PDAC and acute pancreatitis revealed an increased number of non-degranulated mast cells in PDAC, whereas in acute pancreatitis high number of degranulated mast cells was detected (Karamitopoulou et al., 2014).

As mast cells express c-Kit, this can be used as a mast cell marker. Most of the studies examined the role of mast cells using either hypomorphic mutations in the *Kit* locus which results in mast cell deficiency (Berrozpe et al., 1999; Kitamura et al., 1978) or pharmacological inhibitors of mast cell degranulation (Beppu et al., 2004; Masso-Valles et al., 2015; Soucek et al., 2007). Kit hypomorphisms are described as a useful model for mast-cell research (Grimbaldeston et al., 2005). Kit is known to be expressed not only by mast cells but by other cell types as well like interstitial cells of Cajal (Klein et al., 2013). Lineage tracing of Kit expression in the pancreas using a $Kit^{CreERT2}$ mouse line determined a cell population of pancreatic acinus cells which expresses Kit (Schonhuber et al., 2014). Analysis of Kit expression in pancreatic tumors and precursor lesions reveals Kit expression in cells of PanIN lesions and in PDAC. These results indicate that hypomorphic Kit mutations, which are expressed in pancreatic tumor cells as well, could contribute to an altered phenotype of tumor development and progression in mast-cell deficient models. Further, Kit-independent depletion of mast cells can lead to different results in same experimental settings (Rodewald and Feyerabend, 2012). In this present study, mast cell deficiency was achieved using a Kit-independent mouse model to avoid possible contribution of Kit mutations in pancreatic cells to PDAC development, progression, and maintenance. Mast-cell deficiency is achieved using the $Cpa3^{Cre/+}$, where the Cre recombinase is expressed from the *Cpa3* locus resulting in mast-cell depletion (Feyerabend et al., 2011). Here, it is shown that PDAC development and its progression is independent of mast cells. Furthermore, mast cells

are observed to be dispensable for PDAC maintenance and metastasis formation in an orthotopic transplantation model.

Consistent with the data of this present study, others could report that mast cells have no effect on survival or disease relapse. Tumor samples of esophageal cancer patients investigated the infiltration of mast cells. Analysis of mast cell counts and relapse displayed no correlation. The number of present mast cells did not associate with survival (Tinge et al., 2010). There are also reports suggesting an anti-tumor role of mast cells. A protective role for mast cells was described in intestinal tumorigenesis (Sinnamon et al., 2008). They used a model of early intestinal tumorigenesis, the *Min* mouse (multiple intestinal neoplasia, which is due to a germ line mutation in the *Adenomatous polyposis coli* (*Apc*) gene). Infiltration of mast cells in the tumor tissue could be observed and upon analysis of developed tumors in mast cell-proficient and mast cell-deficient mice (*c-kit*$^{W\text{-}sh/W\text{-}sh}$), it was revealed that more tumors (benign and malignant tumors) evolved in mice deficient for mast cells (Sinnamon et al., 2008). Epidemiological studies linked high number of mast cells with better prognosis for breast cancer. A clinical study of over 4000 invasive breast cancer samples revealed that patients with mast cells present in the tumor core have a favorable prognosis. Additionally, mean survival of patients displaying stromal mast cells was more than one year longer compared to those patients without stromal mast cells (Rajput et al., 2008). In diffuse large B-cell lymphomas high mast cell counts were correlated to better prognosis as well. Patients with many mast cells had a better event-free survival indicating a more favorable outcome (Hedstrom et al., 2007). Lampaisi et al. showed the influence of mast cells on the growth of HCC (hepatocellular carcinoma) tumor cells. *In vitro* they observed that mast-cell derived conditioned medium reduced cell viability and proliferation of HCC cells (Lampiasi et al., 2007). Further, mast cell heparin was described to be disadvantageous for cancer (Samoszuk et al., 2005) and mast cell-infiltration was correlated to favorable prognosis (Hedstrom et al., 2007; Rajput et al., 2008).

The research of the last years disclosed different roles of mast cells in cancer. As described above, mast cells were shown to be beneficial and detrimental for tumor development and progression. In this study it could be shown that mast cells are dispensable for PDAC development, progression, and maintenance by using a clean genetic mouse model independent of Kit.

5.2.2 TARGETING FIBROBLASTS AND STELLATE CELLS OF PDAC

The newly generated dual-recombination system was not only used to manipulate pancreatic cancer cells in a time-dependent manner but also to target stromal cells of the tumor

microenvironment of PDAC. The tumor microenvironment of PDAC is described to be rich in extracellular matrix, infiltrating immune cells (including mast cells), and activated fibroblasts as well as pancreatic stellate cells. Here, various Cre-driver lines were examined for their specificity and efficiency to target either pancreatic stellate cells or fibroblasts.

Various studies analyzed the influence of tumor stroma on pancreatic cancer progression assessing the amount and composition of the stroma. High stromal index; strong αSMA expression and low collagen deposition; was correlated to poor prognosis whereas high collagen deposition and weak stromal activation indicated better prognosis (Erkan et al., 2008). Others reported that increased expression of stromal serine protein acidic and rich in cysteine (SPARC) and periostin also correlate with poor prognosis (Erkan et al., 2007; Mantoni et al., 2008). Contrary, it was demonstrated that a high stromal index, based on collagen deposition related to tumor mass, is associated with longer survival (Bever et al., 2015). Furthermore, stromal activity assessed by high αSMA expression did not correlate with clinical outcome which indicated that αSMA cannot be used as a prognostic marker (Bever et al., 2015). One signaling pathway known to contribute to stromal desmoplasia is the hedgehog signaling which is absent in adult healthy pancreatic tissue but reactivated in neoplasia (Thayer et al., 2003). Deletion of the receptor Smoothened (Smo), part of the hedgehog signaling pathway, from epithelial cells had no influence on PDAC progression whereas it was demonstrated that the secretion of the ligand SHH by epithelium activates the Smo-dependent signaling in stromal cells and subsequently promoting desmoplasia (Bailey et al., 2008; Tian et al., 2009). Upon inhibition of SHH by IPI-926 and combined treatment with gemcitabine tumor growth was reduced slightly (Olive et al., 2009). Conversely, Rhim et al. observed accelerated tumor formation in a PDAC mouse model with conditionally inactivated SHH. Developed PDACs were undifferentiated, more aggressive and displayed higher vascularity and less stroma (Rhim et al., 2014). In line with these data Özedmir et al. reported that depletion of αSMA+ myofibroblasts in a PDAC mouse model (*Ptf1a*$^{Cre/+}$*;LSL-Kras*$^{G12D/+}$*;Tgfbr2*$^{flox/flox}$) results in more undifferentiated, increased invasive tumors compared to control cohorts. Similar to Bever and colleagues, high αSMA scoring of patients samples correlated with longer survival (Ozdemir et al., 2014). As depicted above, the inhibition of stromal cells or their depletion for PDAC therapy is still under debate and therefore more studies are necessary to decipher the role of various stromal cell types.

Pancreatic stellate cells are shown to be the main source of extracellular matrix proteins like collagen and fibronectin (Apte et al., 2004; Bachem et al., 2005). As described previously, pancreatic stellate cells are characterized by Vitamin A storage, GFAP, and vimentin expression (Omary et al., 2007). PSCs were targeted with the help of Cre lines under control of either

human or murine GFAP promoter. Tumor-bearing mice were analyzed for GFAP-positive cells as indicated by Cre recombination induced EGFP-expression. The human *GFAP-Cre* line was initially used for the characterization of neurons and glial cells. Co-localization of Cre protein and GFAP protein was observed in Bergmann glia, which are cells of the cerebellum. Furthermore, in tissue analysis using the LacZ reporter Cre activity was detected in the brain (Zhuo et al., 2001), which is found in this study as well (data not shown). Results of this present study show that the *hGFAP-Cre* line targets not only stellate cells but ductal PDAC cells as well. Furthermore, no expression of markers identifying activated pancreatic stellate cells like αSMA is observed. Already, Zhuo et al. reported hGFAP-Cre activity in some cells of the liver in the periportal region (Zhuo et al., 2001) which are probably not hepatic stellate cells expressing GFAP. Taken together, the *hGFAP-Cre* line is not suitable to target activated PSCs.

Another Cre line under the control of the murine GFAP promoter was investigated for its specificity to target PSCs. Garcia et al. established this Cre line to identify GFAP-expressing neuronal progenitor cells in adult mice. They observed cells with unipolar or bipolar morphology, with some cells expressing vimentin (Garcia et al., 2004), a marker used to identify PSCs as well (Omary et al., 2007). Results of this study show that some but not all GFAP-expressing cells can be targeted with the *mGFAP-Cre* line. In line with these findings, it was reported that about 90 % of all PSCs are positive for αSMA and 20 % are positive for desmin which suggests that not all PSCs express all identified markers (Moir et al., 2015). This argues for the existence of several different PSC subtypes.

Besides activated PSCs, cancer-associated fibroblasts are another important source of the stroma surrounding tumor cells. Cancer-associated fibroblasts (CAFs) are shown to secrete cytokines, chemokines, and several growth factors. Those fibroblasts and their secreted products have been observed to promote proliferation, migration, and invasion of cancer cells (Augsten, 2014). The origin of CAFs is still under debate. Sugimoto et al. was one of the first to describe different subpopulations of fibroblasts present in breast or pancreatic cancer (Sugimoto et al., 2006). Several studies determined the amount of resident fibroblasts in various diseases. In an inflammation-induced gastric cancer model it was observed that about 20 % of the myofibroblasts have been recruited from the bone marrow (Quante et al., 2011); in pancreatic cancer model the amount of myofibroblasts derived from the bone marrow was 40 % (Ishii et al., 2003). Furthermore, CAFs are reported to originate from resident fibroblasts (Hinz et al., 2007; Ronnov-Jessen and Petersen, 1993), pericytes, stellate cells, and endothelial cells (Polanska and Orimo, 2013; Zeisberg et al., 2007). Various markers have been described for CAFs in context with the heterogeneity of their origin like Fsp1, αSMA, NG2, PDGFRα/β, vimentin, and

FAP (Desmouliere et al., 2004; Kalluri and Zeisberg, 2006; Sugimoto et al., 2006). Some of those proteins were used as marker proteins to identify and target fibroblasts.

In this present study, fibroblasts surrounding PDAC were targeted with the help of Cre lines under control of specific promoters and Cre activity was again determined by the Cre reporter line *R26*$^{mT\text{-}mG}$ (Muzumdar et al., 2007). Sm22 is shown to be expressed in smooth muscle cells like vascular cells and cells of the intestine (Holtwick et al., 2002). It is reported that the smooth muscle protein 22alpha is expressed in myeloid cells as well (Shen et al., 2012). CAFs are described as myofibroblast-like cells which resemble in their morphology smooth-muscle cells (Kalluri and Zeisberg, 2006). Therefore, Cre recombinase under control of the Sm22 promoter was used to identify a fibroblasts population in the tumor microenvironment of PDAC. As shown in this study both Cre lines seem to target not only stromal cells but to some extent pancreatic cancer cells and also acinar cells as well. Therefore, targeting activated fibroblasts is not suitable by these lines. Although, in case of the *Sm22-knock-in Cre* line more experiments are necessary to clearly show whether Cre-recombined cells express fibroblast markers like vimentin or αSMA.

Fsp1 was described to be specifically expressed in fibroblasts (Strutz et al., 1995). In this study it is revealed that cells which were recombined by Fsp1-Cre express different marker proteins possibly indicating some subgroups of fibroblasts. In 2011 Österreicher et al. reported an inflammatory subpopulation of macrophages in the liver which expresses Fsp1 (Osterreicher et al., 2011). Upon liver injury they could not confirm αSMA expression in Fsp1-Cre-targeted cells but the expression of the macrophage marker F4/80. Similar results are shown in this present study. Fsp1-Cre seems to target to some extent macrophages and not only fibroblasts. Analysis of isolated primary cancer cell lines reveals Fsp1-Cre-recombined cells by EGFP expression in some tumor cells. To clarify whether Fsp1-Cre is expressed in Pdx1-Flp-targeted cells as well a reporter line was used which monitors cells expressing Flp and Cre recombinase. Cells which are positive for both recombinases express tdTomato (Madisen et al., 2015). tdTomato expression is observed in cells of PanIN lesions and in tumor cells. These results suggest that Fsp1 is expressed by tumor cells as well. It was already reported that epithelial cells express Fsp1 when undergoing EMT (Iwano et al., 2002; Nishitani et al., 2005; Rhim et al., 2012). To address this hypothesis, that Fsp1-Cre identifies a population of cancer cells undergoing EMT, further analysis of *KPF;Fsp1-Cre* tumors is necessary. Co-localization of tdTomato-expressing cells with mesenchymal markers like ZEB1, Twist or Snail needs to be proven.

As mentioned before, it is already reported that Sm22 is expressed in hepatic and pulmonary arteries (Holtwick et al., 2002) as well as in cardiomyocytes (Zhang et al., 2006). Similar results are observed in this study (data not shown) which argues that the *Sm22*-driven Cre lines are not suitable to target only fibroblasts but other cell types as well. The same effect of targeting more than one cell type is shown for *GFAP*-driven Cre lines which are also active in cells of the cerebellum and liver (Garcia et al., 2004; Zhuo et al., 2001). In case of the Fsp1-Cre it is known that it recombines a subpopulation of macrophages in the liver (Osterreicher et al., 2011). Although, those markers are described to be expressed in activated fibroblasts or pancreatic stellate cells, the analyzed Cre lines lines of this study are only partially suitable to target fibroblast and/or pancreatic stellate cells. This can be due to the fact that these Cre lines are not inducible and therefore, it is possible that different cell populations are targeted for example due to Cre activity in the embryogenesis. To target stromal cells which are characterized by expression of specific marker proteins, the use of inducible Cre lines is a more specific option. αSMA-CreER^{T2} has been described to be expressed in smooth muscle cells of various organs (Wendling et al., 2009) and could be used to target myofibroblasts in tumor stroma upon expression of αSMA. Others developed inducible CreER lines under control of e.g. *NG2* (*NG2-CreER^{TM}*) (Zhu et al., 2011) or smooth muscle protein 22 alpha (*Sm22-CreER^{T2}*) (Kuhbandner et al., 2000) which have been reported to be used as marker for fibroblasts. To clearly identify the targeted cell type of the investigated different Cre lines more analyses are necessary. As mentioned before, not all activated pancreatic stellate cells express GFAP, αSMA or vimentin. This also applies for cancer-associated fibroblasts which presumably originate from different cell types. Augsten proposed that more subtypes of CAFs exist although it remains unclear how many exists in one tumor type and whether those are different between tumor types (Augsten, 2014). Therefore, it is difficult to target all activated PSCs or CAFs in the microenvironment with the help of a Cre line under control of one marker protein.

In this study, a novel dual-recombination system was established which allows secondary targeting and manipulation of tumor cells and targeting of stromal cells as well. One has to take in account that studies describing cell-type specific effects relying on expression of markers could be inaccurate as other cell types share those markers (Augsten, 2014).

In general, the possibility to target stromal cells with specific Cre-driver lines allows manipulation of various stroma cells by inactivation or activation of additional target structures. Additionally, the depletion of stromal cells can be achieved and the effect of the ablation on tumor growth and its progression can be studied by the use of the dual-recombination system. However, as already mentioned before, new studies have reported that the depletion of the

stromal cells did not favor tumor regression but promote tumor progression and its aggressiveness (Gore and Korc, 2014; Lee et al., 2014; Ozdemir et al., 2014). Therefore, reprogramming of the tumor stroma might be a new and better therapy option for the treatment of PDAC instead of complete deletion of stromal cells. Sherman et al. detected expression of the vitamin D receptor in human PDAC tissue samples, especially in PSCs, and less fibrosis and inflammation in the stroma was observed upon treatment with the receptor ligand. Activated PSCs went back to their quiescent state, less collagen fibers were detected and intratumoral drug distribution was improved resulting in reduced tumor volume (Sherman et al., 2014). Similar results were achieved by treatment of gemcitabine in combination with inhibition of STAT3 in PDAC mouse model. In this study, they could show that STAT3 expression in PDAC tissue and the tumor stroma was remodeled upon inhibition of STAT3. Tumor stroma density was not changed but the collagen fibers were rearranged leading to reduction of tumor volume and size. Furthermore, blood supply was increased in tumors treated with STAT3 inhibitor and gemcitabine (Nagathihalli et al., 2015). Manipulation of the tumor stroma may represent a new therapeutic option. By the use of the dual-recombination system targeted stromal cells can be influenced and possible effects on the tumor microenvironment and the tumor itself can be investigated. The tumor stroma is known be a pool for diverse growth factors like TGFβ, VEGF, FGF and PDGF. The growth factors and other chemokines/cytokines are released by stromal cells which can induce tumor cell proliferation (Polanska and Orimo, 2013). One option for remodeling the tumor microenvironment using the dual-recombination system would be inactivation of growth factor receptors in stromal cells. The influence of the knockout of the TGFβ type 2 receptor in Fsp1-positive cells was already under investigation. It was reported that this knockout of the growth factor receptor in these cells led to an autoimmune pancreatitis phenotype (Boomershine et al., 2009) or even to carcinoma of the forestomach (Bhowmick et al., 2004). The effect of the knockout of other growth factor receptors in Fsp1-Cre cells needs to be examined as well as in different stromal cell types.

The tumor microenvironment and how it influences the tumor growth and development can only be analyzed with the help of genetic models. Therefore, it is necessary to clearly identify stromal subpopulations by specific marker proteins. This will furthermore allow the inactivation of different signaling pathways in these subtypes and reveal their role in development and progression as well as possible therapeutic target options of stroma-rich tumors.

6 SUMMARY

Pancreatic ductal adenocarcinoma (PDAC) is predicted to be the second leading cause of cancer-related death in 2030. Currently, the 5-year survival rate is still around 7 % despite newly developed treatments. Genetic engineered mouse models were used to investigate the tumor development and its progression. So far, the established mouse models are limited in recapitulating the human disease. Further, over the last years new insight was gained regarding the tumor microenvironment. PDAC is known to have a dense desmoplastic stroma containing activated fibroblasts, pancreatic stellate cells, and infiltrating immune cells.

The aim of this study was to characterize a novel, newly generated dual-recombination system allowing sequential manipulation of pancreatic cancer cells to study the development and progression of PDAC. Expression of oncogenic $Kras^{G12D}$, silenced by a frt-STOP-frt (FSF) cassette, was activated in the *Pdx1-Flp* lineage directed to the pancreas. Thereby, invasive and highly metastatic PDACs were induced. For secondary manipulation of cancer cells a tamoxifen-inducible Flp-dependent $CreER^{T2}$ allele was introduced into the *R26* locus. Upon tamoxifen treatment genes can be selectively activated or inactivated. Cre efficiency and specificity was determined using the Cre reporter $R26^{mT\text{-}mG}$. Cre activity could be only observed in tissues expressing Pdx1 and no leaky Cre activity could be detected. A mouse model for whole body recombination was characterized as well and revealed recombination in all tissues. Secondary manipulation was proven by restoration of p53 wild type protein in isolated primary pancreatic cancer cell lines.

In a second step, the tumor microenvironment was investigated for its different stromal cell types. Therefore, various Cre driver lines were used in $Pdx1\text{-}Flp;FSF\text{-}Kras^{G12D/+}$ mice (*KF*) to examine targeted stromal cells. Here, it was shown that the development and maintenance of PDAC was independent of mast cells. Furthermore, there was no significant difference in survival of mast-cell proficient and mast-cell deficient *KF* mice. Targeting of activated pancreatic stellate cells was performed using two different *GFAP-Cre* lines. The Cre under control of the human GFAP promoter resulted in unspecific recombination targeting pancreatic cancer cells as well whereas the murine *GFAP-Cre* line appears to target pancreatic stellate cells as demonstrated by immunofluorescence staining for GFAP and nestin. Fibroblasts were targeted using two different *Sm22-Cre* lines and the *Fsp1-Cre* line. Only a few cells co-localize with αSMA or vimentin, indicating that these Cre lines only target a small subpopulation of fibroblasts in the tumor stroma. Furthermore, it could be shown, by CK19 staining and by a dual Flp/Cre reporter line, that these Cre lines are partly expressed in cancer cells as well.

These data show that the dual-recombination system is a novel mouse model which is capable of recapitulating the human disease as a multi-step, sequential process. This model is a useful tool not only to manipulate host-cell specific genes but to analyze the tumor microenvironment. By this dual-recombination system new knowledge of the tumor progression/maintenance and its surrounding microenvironment can be gained and possible therapeutic targets identified for this fatal disease.

7 ZUSAMMENFASSUNG

Das duktale Pankreaskarzinom (PDAC) ist eine der aggressivsten und tödlichsten Krebserkrankungen der Welt. Trotz neuer Erkenntnisse und Therapieansätze liegt die 5-Jahres-Überlebensrate bei nur 7 %. Mit Hilfe von Mausmodellen kann die Tumorentstehung und Entwicklung untersucht werden. PDAC ist durch eine starke Fibrose und viel Stroma gekennzeichnet, in dem neben Immunzellen auch aktivierte Fibroblasten und Pankreasstellatzellen vorkommen.

In der vorliegenden Arbeit wurde ein neues duales Rekombinationsmodell charakterisiert, welches das Flp/frt und das Cre/loxP System kombiniert. Die Flp-Rekombinase ist durch den *Pdx1*-Promotor im Pankreas aber auch in Haut, Duodenum und Gallengang aktiv. Die Expression des Onkogens $Kras^{G12D}$ wird durch eine frt-STOP-frt (FSF) Kassette verhindert und erst nach Rekombination durch Flp exprimiert (*KF*). Hierdurch entstehen invasive, metastasierende Pankreaskarzinome. Um eine Zell- und Zeit-spezifische Cre-Aktivität zu erhalten, wurde ein Tamoxifen-induzierbares $CreER^{T2}$-Fusionsprotein generiert, dass unter der Kontrolle des ubiquitären CAG-Promotors in den *R26* Lokus inseriert wurde (*FSF-R26*$^{CAG\text{-}CreERT2}$). Ebenfalls durch eine FSF-Kassette geblockt, wird $CreER^{T2}$ nur in Pdx1-Flp-exprimierenden Zellen aktiviert. Mittels des Cre-Reporters *R26*$^{mT\text{-}mG}$ konnte die Spezifität und Effizienz der Cre-Rekombinase im Pankreas nachgewiesen werden. Die damit mögliche zeit- und zellspezifische Inaktivierung bzw. Aktivierung weitere Gene konnte anhand der Rekonstitution des p53-Wildtyp Proteins in Pankreastumorzellen gezeigt werden. Durch die Deletion der FSF-Kassette des *FSF-R26*$^{CAG\text{-}CreERT2}$ Konstrukts ergibt sich die Möglichkeit die Auswirkung einer Inaktivierung/Aktivierung eines Zielgens auf den gesamten Organismus zu untersuchen. Die Effektivität des *R26*$^{CAG\text{-}CreERT2}$ Konstrukts wurde ebenfalls mittels dem *R26*$^{mT\text{-}mG}$ Cre-Reporters nachgewiesen.

Im zweiten Teil der Arbeit wurde das duale Rekombinationssystem verwendet um das Tumormikromilieu zu analysieren. Dazu wurden Zelltyp-spezifische Cre-Linien in *KF*-Tiere gekreuzt. Es konnte gezeigt werden, dass die Tumorentstehung und die Aufrechterhaltung des PDAC unabhängig von Mastzellen sind. Aktivierte Stellatzellen des Pankreas wurden mittels zweier *GFAP-Cre* Linien untersucht. Unter der Kontrolle des humanen GFAP-Promotors wurde Cre-Aktivitität hauptsächlich in Tumorzellen beobachtet, während die Cre-Rekombinase unter der Kontrolle des murinen GFAP-Promotors eine Subpoplulation der pankreatischen Stellatzellen identifiziert. Neben aktivierten Stellatzellen wurden auch Fibroblasten im Stroma des PDAC analysiert. Die verwendeten Cre-Linien um Fibroblasten zu identifizieren, *Sm22-Cre*,

Sm22^{Cre} und *Fsp1-Cre*, rekombinierten jeweils Subpopulationen von Fibroblasten. Allerdings rekombinierten die Cre-Linien *Sm22-Cre* und *Sm22*^{Cre} teilweise auch in Pankreastumorzellen, was anhand der CK19-Co-Lokalisation gezeigt werden konnte. Auch die Fsp1-Cre wird in wenigen Tumorzellen exprimiert, was anhand einer dualen Flp/Cre Reporterlinie nachgewiesen werden konnte.

Mit dem neuen dualen Rekombinationssystem lässt sich der sequentielle Prozess der humanen Tumorentwicklung und -aufrechterhaltung nachempfinden. Es erlaubt die Analyse neuer Therapieansätze sowohl gezielt in den Tumorzellen selbst als auch in der Tumormikroumgebung des duktalen Pankreaskarzinoms.

8 REFERENCES

Aichler, M., Seiler, C., Tost, M., Siveke, J., Mazur, P. K., Da Silva-Buttkus, P., Bartsch, D. K., Langer, P., Chiblak, S., Durr, A., *et al.* (2012). Origin of pancreatic ductal adenocarcinoma from atypical flat lesions: a comparative study in transgenic mice and human tissues. The Journal of pathology *226*, 723-734.

Almoguera, C., Shibata, D., Forrester, K., Martin, J., Arnheim, N., and Perucho, M. (1988). Most human carcinomas of the exocrine pancreas contain mutant c-K-ras genes. Cell *53*, 549-554.

Ammendola, M., Sacco, R., Sammarco, G., Donato, G., Zuccala, V., Luposella, M., Patruno, R., Marech, I., Montemurro, S., Zizzo, N., *et al.* (2014). Mast cells density positive to tryptase correlates with angiogenesis in pancreatic ductal adenocarcinoma patients having undergone surgery. Gastroenterol Res Pract *2014*, 951957.

Amundadottir, L., Kraft, P., Stolzenberg-Solomon, R. Z., Fuchs, C. S., Petersen, G. M., Arslan, A. A., Bueno-de-Mesquita, H. B., Gross, M., Helzlsouer, K., Jacobs, E. J., *et al.* (2009). Genome-wide association study identifies variants in the ABO locus associated with susceptibility to pancreatic cancer. Nature genetics *41*, 986-990.

Andea, A., Sarkar, F., and Adsay, V. N. (2003). Clinicopathological correlates of pancreatic intraepithelial neoplasia: a comparative analysis of 82 cases with and 152 cases without pancreatic ductal adenocarcinoma. Modern pathology : an official journal of the United States and Canadian Academy of Pathology, Inc *16*, 996-1006.

Apte, M., Pirola, R., and Wilson, J. (2011). The fibrosis of chronic pancreatitis: new insights into the role of pancreatic stellate cells. Antioxidants & redox signaling *15*, 2711-2722.

Apte, M. V., Haber, P. S., Applegate, T. L., Norton, I. D., McCaughan, G. W., Korsten, M. A., Pirola, R. C., and Wilson, J. S. (1998). Periacinar stellate shaped cells in rat pancreas: identification, isolation, and culture. Gut *43*, 128-133.

Apte, M. V., Park, S., Phillips, P. A., Santucci, N., Goldstein, D., Kumar, R. K., Ramm, G. A., Buchler, M., Friess, H., McCarroll, J. A., *et al.* (2004). Desmoplastic reaction in pancreatic cancer: role of pancreatic stellate cells. Pancreas *29*, 179-187.

Apte, M. V., and Wilson, J. S. (2012). Dangerous liaisons: pancreatic stellate cells and pancreatic cancer cells. Journal of gastroenterology and hepatology *27 Suppl 2*, 69-74.

Arumugam, T., Ramachandran, V., Fournier, K. F., Wang, H., Marquis, L., Abbruzzese, J. L., Gallick, G. E., Logsdon, C. D., McConkey, D. J., and Choi, W. (2009). Epithelial to mesenchymal transition contributes to drug resistance in pancreatic cancer. Cancer research *69*, 5820-5828.

Augsten, M. (2014). Cancer-associated fibroblasts as another polarized cell type of the tumor microenvironment. Front Oncol *4*, 62.

Bachem, M. G., Schneider, E., Gross, H., Weidenbach, H., Schmid, R. M., Menke, A., Siech, M., Beger, H., Grunert, A., and Adler, G. (1998). Identification, culture, and characterization of pancreatic stellate cells in rats and humans. Gastroenterology *115*, 421-432.

Bachem, M. G., Schunemann, M., Ramadani, M., Siech, M., Beger, H., Buck, A., Zhou, S., Schmid-Kotsas, A., and Adler, G. (2005). Pancreatic carcinoma cells induce fibrosis by stimulating proliferation and matrix synthesis of stellate cells. Gastroenterology *128*, 907-921.

Bailey, J. M., Swanson, B. J., Hamada, T., Eggers, J. P., Singh, P. K., Caffery, T., Ouellette, M. M., and Hollingsworth, M. A. (2008). Sonic hedgehog promotes desmoplasia in pancreatic cancer. Clinical cancer research : an official journal of the American Association for Cancer Research *14*, 5995-6004.

Bailey, P., Chang, D. K., Nones, K., Johns, A. L., Patch, A. M., Gingras, M. C., Miller, D. K., Christ, A. N., Bruxner, T. J., Quinn, M. C., *et al.* (2016). Genomic analyses identify molecular subtypes of pancreatic cancer. Nature *531*, 47-52.

Bardeesy, N., Aguirre, A. J., Chu, G. C., Cheng, K. H., Lopez, L. V., Hezel, A. F., Feng, B., Brennan, C., Weissleder, R., Mahmood, U., *et al.* (2006). Both p16(Ink4a) and the p19(Arf)-p53 pathway constrain progression of pancreatic adenocarcinoma in the mouse. Proceedings of the National Academy of Sciences of the United States of America *103*, 5947-5952.

Bardeesy, N., and DePinho, R. A. (2002). Pancreatic cancer biology and genetics. Nature reviews Cancer *2*, 897-909.

Beppu, K., Jaboine, J., Merchant, M. S., Mackall, C. L., and Thiele, C. J. (2004). Effect of imatinib mesylate on neuroblastoma tumorigenesis and vascular endothelial growth factor expression. Journal of the National Cancer Institute *96*, 46-55.

Berlin, J. D., Catalano, P., Thomas, J. P., Kugler, J. W., Haller, D. G., and Benson, A. B., 3rd (2002). Phase III study of gemcitabine in combination with fluorouracil versus gemcitabine alone in patients with advanced pancreatic carcinoma: Eastern Cooperative Oncology Group Trial E2297. Journal of clinical oncology : official journal of the American Society of Clinical Oncology *20*, 3270-3275.

Berrozpe, G., Timokhina, I., Yukl, S., Tajima, Y., Ono, M., Zelenetz, A. D., and Besmer, P. (1999). The W(sh), W(57), and Ph Kit expression mutations define tissue-specific control elements located between -23 and -154 kb upstream of Kit. Blood *94*, 2658-2666.

Bever, K. M., Sugar, E. A., Bigelow, E., Sharma, R., Laheru, D., Wolfgang, C. L., Jaffee, E. M., Anders, R. A., De Jesus-Acosta, A., and Zheng, L. (2015). The prognostic value of stroma in pancreatic cancer in patients receiving adjuvant therapy. HPB (Oxford) *17*, 292-298.

Bhowmick, N. A., Chytil, A., Plieth, D., Gorska, A. E., Dumont, N., Shappell, S., Washington, M. K., Neilson, E. G., and Moses, H. L. (2004). TGF-beta signaling in fibroblasts modulates the oncogenic potential of adjacent epithelia. Science *303*, 848-851.

Boomershine, C. S., Chamberlain, A., Kendall, P., Afshar-Sharif, A. R., Huang, H., Washington, M. K., Lawson, W. E., Thomas, J. W., Blackwell, T. S., and Bhowmick, N. A. (2009). Autoimmune pancreatitis results from loss of TGFbeta signalling in S100A4-positive dendritic cells. Gut *58*, 1267-1274.

Bradford, M. M. (1976). A rapid and sensitive method for the quantitation of microgram quantities of protein utilizing the principle of protein-dye binding. Analytical biochemistry *72*, 248-254.

Bramhall, S. R., Rosemurgy, A., Brown, P. D., Bowry, C., Buckels, J. A., and Marimastat Pancreatic Cancer Study, G. (2001). Marimastat as first-line therapy for patients with unresectable pancreatic cancer: a randomized trial. Journal of clinical oncology : official journal of the American Society of Clinical Oncology *19*, 3447-3455.

Bramhall, S. R., Schulz, J., Nemunaitis, J., Brown, P. D., Baillet, M., and Buckels, J. A. (2002). A double-blind placebo-controlled, randomised study comparing gemcitabine and marimastat with gemcitabine and placebo as first line therapy in patients with advanced pancreatic cancer. British journal of cancer *87*, 161-167.

Brugge, W. R., Lauwers, G. Y., Sahani, D., Fernandez-del Castillo, C., and Warshaw, A. L. (2004). Cystic neoplasms of the pancreas. The New England journal of medicine *351*, 1218-1226.

Burris, H. A., 3rd, Moore, M. J., Andersen, J., Green, M. R., Rothenberg, M. L., Modiano, M. R., Cripps, M. C., Portenoy, R. K., Storniolo, A. M., Tarassoff, P., *et al.* (1997). Improvements in survival and clinical benefit with gemcitabine as first-line therapy for patients with advanced pancreas cancer: a randomized trial. Journal of clinical oncology : official journal of the American Society of Clinical Oncology *15*, 2403-2413.

Butturini, G., Stocken, D. D., Wente, M. N., Jeekel, H., Klinkenbijl, J. H., Bakkevold, K. E., Takada, T., Amano, H., Dervenis, C., Bassi, C., *et al.* (2008). Influence of resection margins and treatment on survival in patients with pancreatic cancer: meta-analysis of randomized controlled trials. Archives of surgery *143*, 75-83; discussion 83.

Cai, S. W., Yang, S. Z., Gao, J., Pan, K., Chen, J. Y., Wang, Y. L., Wei, L. X., and Dong, J. H. (2011). Prognostic significance of mast cell count following curative resection for pancreatic ductal adenocarcinoma. Surgery *149*, 576-584.

Caicedo-Granados, E., Lin, R., Fujisawa, C., Yueh, B., Sangwan, V., and Saluja, A. (2014). Wild-type p53 reactivation by small-molecule Minnelide in human papillomavirus (HPV)-positive head and neck squamous cell carcinoma. Oral Oncol *50*, 1149-1156.

Castor, C. W., Wilson, S. M., Heiss, P. R., and Seidman, J. C. (1979). Activation of lung connective tissue cells in vitro. The American review of respiratory disease *120*, 101-106.

Chames, P., Kerfelec, B., and Baty, D. (2010). Therapeutic antibodies for the treatment of pancreatic cancer. TheScientificWorldJournal *10*, 1107-1120.

Chang, D. Z., Ma, Y., Ji, B., Wang, H., Deng, D., Liu, Y., Abbruzzese, J. L., Liu, Y. J., Logsdon, C. D., and Hwu, P. (2011). Mast cells in tumor microenvironment promotes the in vivo growth of pancreatic ductal adenocarcinoma. Clinical cancer research : an official journal of the American Association for Cancer Research *17*, 7015-7023.

Chang, H. Y., Chi, J. T., Dudoit, S., Bondre, C., van de Rijn, M., Botstein, D., and Brown, P. O. (2002). Diversity, topographic differentiation, and positional memory in human fibroblasts. Proceedings of the National Academy of Sciences of the United States of America *99*, 12877-12882.

Cheng, N., Bhowmick, N. A., Chytil, A., Gorksa, A. E., Brown, K. A., Muraoka, R., Arteaga, C. L., Neilson, E. G., Hayward, S. W., and Moses, H. L. (2005). Loss of TGF-beta type II receptor in fibroblasts promotes mammary carcinoma growth and invasion through upregulation of TGF-alpha-, MSP- and HGF-mediated signaling networks. Oncogene *24*, 5053-5068.

Chu, G. C., Kimmelman, A. C., Hezel, A. F., and DePinho, R. A. (2007). Stromal biology of pancreatic cancer. Journal of cellular biochemistry *101*, 887-907.

Collisson, E. A., Trejo, C. L., Silva, J. M., Gu, S., Korkola, J. E., Heiser, L. M., Charles, R. P., Rabinovich, B. A., Hann, B., Dankort, D., *et al.* (2012). A central role for RAF-->MEK-->ERK signaling in the genesis of pancreatic ductal adenocarcinoma. Cancer discovery *2*, 685-693.

Conroy, T., Desseigne, F., Ychou, M., Bouche, O., Guimbaud, R., Becouarn, Y., Adenis, A., Raoul, J. L., Gourgou-Bourgade, S., de la Fouchardiere, C., *et al.* (2011). FOLFIRINOX versus gemcitabine for metastatic pancreatic cancer. The New England journal of medicine *364*, 1817-1825.

Cowley, M. J., Chang, D. K., Pajic, M., Johns, A. L., Waddell, N., Grimmond, S. M., and Biankin, A. V. (2013). Understanding pancreatic cancer genomes. Journal of hepato-biliary-pancreatic sciences *20*, 549-556.

Desmouliere, A., Guyot, C., and Gabbiani, G. (2004). The stroma reaction myofibroblast: a key player in the control of tumor cell behavior. Int J Dev Biol *48*, 509-517.

DiGiuseppe, J. A., Hruban, R. H., Goodman, S. N., Polak, M., van den Berg, F. M., Allison, D. C., Cameron, J. L., and Offerhaus, G. J. (1994a). Overexpression of p53 protein in adenocarcinoma of the pancreas. American journal of clinical pathology *101*, 684-688.

DiGiuseppe, J. A., Hruban, R. H., Offerhaus, G. J., Clement, M. J., van den Berg, F. M., Cameron, J. L., and van Mansfeld, A. D. (1994b). Detection of K-ras mutations in mucinous pancreatic duct hyperplasia from a patient with a family history of pancreatic carcinoma. The American journal of pathology *144*, 889-895.

Dvorak, H. F. (1986). Tumors: wounds that do not heal. Similarities between tumor stroma generation and wound healing. The New England journal of medicine *315*, 1650-1659.

Erkan, M., Kleeff, J., Gorbachevski, A., Reiser, C., Mitkus, T., Esposito, I., Giese, T., Buchler, M. W., Giese, N. A., and Friess, H. (2007). Periostin creates a tumor-supportive microenvironment in the pancreas by sustaining fibrogenic stellate cell activity. Gastroenterology *132*, 1447-1464.

Erkan, M., Michalski, C. W., Rieder, S., Reiser-Erkan, C., Abiatari, I., Kolb, A., Giese, N. A., Esposito, I., Friess, H., and Kleeff, J. (2008). The activated stroma index is a novel and independent prognostic marker in pancreatic ductal adenocarcinoma. Clin Gastroenterol Hepatol *6*, 1155-1161.

Erkan, M., Reiser-Erkan, C., Michalski, C. W., Deucker, S., Sauliunaite, D., Streit, S., Esposito, I., Friess, H., and Kleeff, J. (2009). Cancer-stellate cell interactions perpetuate the hypoxia-fibrosis cycle in pancreatic ductal adenocarcinoma. Neoplasia *11*, 497-508.

Eser, S., Reiff, N., Messer, M., Seidler, B., Gottschalk, K., Dobler, M., Hieber, M., Arbeiter, A., Klein, S., Kong, B., *et al.* (2013). Selective requirement of PI3K/PDK1 signaling for Kras oncogene-driven pancreatic cell plasticity and cancer. Cancer cell *23*, 406-420.

Esposito, I., Konukiewitz, B., Schlitter, A. M., and Kloppel, G. (2012). [New insights into the origin of pancreatic cancer. Role of atypical flat lesions in pancreatic carcinogenesis]. Der Pathologe *33 Suppl 2*, 189-193.

Esposito, I., Menicagli, M., Funel, N., Bergmann, F., Boggi, U., Mosca, F., Bevilacqua, G., and Campani, D. (2004). Inflammatory cells contribute to the generation of an angiogenic phenotype in pancreatic ductal adenocarcinoma. Journal of clinical pathology *57*, 630-636.

Evan, G. I., and Vousden, K. H. (2001). Proliferation, cell cycle and apoptosis in cancer. Nature *411*, 342-348.

Everhart, J., and Wright, D. (1995). Diabetes mellitus as a risk factor for pancreatic cancer. A meta-analysis. Jama *273*, 1605-1609.

Feig, C., Gopinathan, A., Neesse, A., Chan, D. S., Cook, N., and Tuveson, D. A. (2012). The pancreas cancer microenvironment. Clinical cancer research : an official journal of the American Association for Cancer Research *18*, 4266-4276.

Feil, R., Brocard, J., Mascrez, B., LeMeur, M., Metzger, D., and Chambon, P. (1996). Ligand-activated site-specific recombination in mice. Proceedings of the National Academy of Sciences of the United States of America *93*, 10887-10890.

Feil, R., Wagner, J., Metzger, D., and Chambon, P. (1997). Regulation of Cre recombinase activity by mutated estrogen receptor ligand-binding domains. Biochemical and biophysical research communications *237*, 752-757.

Feldmann, G., and Maitra, A. (2008). Molecular genetics of pancreatic ductal adenocarcinomas and recent implications for translational efforts. The Journal of molecular diagnostics : JMD *10*, 111-122.

Feldmann, G., Mishra, A., Hong, S. M., Bisht, S., Strock, C. J., Ball, D. W., Goggins, M., Maitra, A., and Nelkin, B. D. (2010). Inhibiting the cyclin-dependent kinase CDK5 blocks pancreatic cancer formation and progression through the suppression of Ras-Ral signaling. Cancer research *70*, 4460-4469.

Feyerabend, T. B., Weiser, A., Tietz, A., Stassen, M., Harris, N., Kopf, M., Radermacher, P., Moller, P., Benoist, C., Mathis, D., *et al.* (2011). Cre-mediated cell ablation contests mast cell contribution in models of antibody- and T cell-mediated autoimmunity. Immunity *35*, 832-844.

Fuchs, C. S., Colditz, G. A., Stampfer, M. J., Giovannucci, E. L., Hunter, D. J., Rimm, E. B., Willett, W. C., and Speizer, F. E. (1996). A prospective study of cigarette smoking and the risk of pancreatic cancer. Archives of internal medicine *156*, 2255-2260.

Fukuda, A., Kawaguchi, Y., Furuyama, K., Kodama, S., Kuhara, T., Horiguchi, M., Koizumi, M., Fujimoto, K., Doi, R., Wright, C. V., and Chiba, T. (2006). Loss of the major duodenal papilla results in brown pigment biliary stone formation in pdx1 null mice. Gastroenterology *130*, 855-867.

Galinsky, D. S., and Nechushtan, H. (2008). Mast cells and cancer--no longer just basic science. Critical reviews in oncology/hematology *68*, 115-130.

Galli, S. J. (2000). Mast cells and basophils. Current opinion in hematology *7*, 32-39.

Gapstur, S. M., Gann, P. H., Lowe, W., Liu, K., Colangelo, L., and Dyer, A. (2000). Abnormal glucose metabolism and pancreatic cancer mortality. Jama *283*, 2552-2558.

Garcia, A. D., Doan, N. B., Imura, T., Bush, T. G., and Sofroniew, M. V. (2004). GFAP-expressing progenitors are the principal source of constitutive neurogenesis in adult mouse forebrain. Nature neuroscience *7*, 1233-1241.

Gilfillan, A. M., and Beaven, M. A. (2011). Regulation of mast cell responses in health and disease. Critical reviews in immunology *31*, 475-529.

Gooch, J. L., Lee, A. V., and Yee, D. (1998). Interleukin 4 inhibits growth and induces apoptosis in human breast cancer cells. Cancer research *58*, 4199-4205.

Gopinathan, A., Morton, J. P., Jodrell, D. I., and Sansom, O. J. (2015). GEMMs as preclinical models for testing pancreatic cancer therapies. Disease models & mechanisms *8*, 1185-1200.

Gore, J., and Korc, M. (2014). Pancreatic cancer stroma: friend or foe? Cancer cell *25*, 711-712.

Grimbaldeston, M. A., Chen, C. C., Piliponsky, A. M., Tsai, M., Tam, S. Y., and Galli, S. J. (2005). Mast cell-deficient W-sash c-kit mutant Kit W-sh/W-sh mice as a model for investigating mast cell biology in vivo. The American journal of pathology *167*, 835-848.

Guerra, C., Schuhmacher, A. J., Canamero, M., Grippo, P. J., Verdaguer, L., Perez-Gallego, L., Dubus, P., Sandgren, E. P., and Barbacid, M. (2007). Chronic pancreatitis is essential for induction of pancreatic ductal adenocarcinoma by K-Ras oncogenes in adult mice. Cancer cell *11*, 291-302.

Gupta, S., and El-Rayes, B. F. (2008). Small molecule tyrosine kinase inhibitors in pancreatic cancer. Biologics : targets & therapy *2*, 707-715.

Hahn, S. A., Hoque, A. T., Moskaluk, C. A., da Costa, L. T., Schutte, M., Rozenblum, E., Seymour, A. B., Weinstein, C. L., Yeo, C. J., Hruban, R. H., and Kern, S. E. (1996). Homozygous deletion map at 18q21.1 in pancreatic cancer. Cancer research *56*, 490-494.

Hanahan, D., and Coussens, L. M. (2012). Accessories to the crime: functions of cells recruited to the tumor microenvironment. Cancer cell *21*, 309-322.

Hanahan, D., and Weinberg, R. A. (2000). The hallmarks of cancer. Cell *100*, 57-70.

Hanahan, D., and Weinberg, R. A. (2011). Hallmarks of cancer: the next generation. Cell *144*, 646-674.

Hedstrom, G., Berglund, M., Molin, D., Fischer, M., Nilsson, G., Thunberg, U., Book, M., Sundstrom, C., Rosenquist, R., Roos, G., *et al.* (2007). Mast cell infiltration is a favourable prognostic factor in diffuse large B-cell lymphoma. British journal of haematology *138*, 68-71.

Herrmann, R., Bodoky, G., Ruhstaller, T., Glimelius, B., Bajetta, E., Schuller, J., Saletti, P., Bauer, J., Figer, A., Pestalozzi, B., *et al.* (2007). Gemcitabine plus capecitabine compared with gemcitabine alone in advanced pancreatic cancer: a randomized, multicenter, phase III trial of the Swiss Group for Clinical Cancer Research and the Central

European Cooperative Oncology Group. Journal of clinical oncology : official journal of the American Society of Clinical Oncology *25*, 2212-2217.

Hezel, A. F., Kimmelman, A. C., Stanger, B. Z., Bardeesy, N., and Depinho, R. A. (2006). Genetics and biology of pancreatic ductal adenocarcinoma. Genes & development *20*, 1218-1249.

Hingorani, S. R., Harris, W. P., Beck, J. T., Berdov, B. A., Wagner, S. A., Pshevlotsky, E. M., Tjulandin, S. A., Gladkov, O. A., Holcombe, R. F., Korn, R.*, et al.* (2016). Phase Ib Study of PEGylated Recombinant Human Hyaluronidase and Gemcitabine in Patients with Advanced Pancreatic Cancer. Clinical cancer research : an official journal of the American Association for Cancer Research *22*, 2848-2854.

Hingorani, S. R., Petricoin, E. F., Maitra, A., Rajapakse, V., King, C., Jacobetz, M. A., Ross, S., Conrads, T. P., Veenstra, T. D., Hitt, B. A.*, et al.* (2003). Preinvasive and invasive ductal pancreatic cancer and its early detection in the mouse. Cancer cell *4*, 437-450.

Hingorani, S. R., Wang, L., Multani, A. S., Combs, C., Deramaudt, T. B., Hruban, R. H., Rustgi, A. K., Chang, S., and Tuveson, D. A. (2005). Trp53R172H and KrasG12D cooperate to promote chromosomal instability and widely metastatic pancreatic ductal adenocarcinoma in mice. Cancer cell *7*, 469-483.

Hinz, B., Phan, S. H., Thannickal, V. J., Galli, A., Bochaton-Piallat, M. L., and Gabbiani, G. (2007). The myofibroblast: one function, multiple origins. The American journal of pathology *170*, 1807-1816.

Hodges, K., Kennedy, L., Meng, F., Alpini, G., and Francis, H. (2012). Mast cells, disease and gastrointestinal cancer: A comprehensive review of recent findings. Translational gastrointestinal cancer *1*, 138-150.

Holtwick, R., Gotthardt, M., Skryabin, B., Steinmetz, M., Potthast, R., Zetsche, B., Hammer, R. E., Herz, J., and Kuhn, M. (2002). Smooth muscle-selective deletion of guanylyl cyclase-A prevents the acute but not chronic effects of ANP on blood pressure. Proceedings of the National Academy of Sciences of the United States of America *99*, 7142-7147.

Hruban, R. H., Adsay, N. V., Albores-Saavedra, J., Anver, M. R., Biankin, A. V., Boivin, G. P., Furth, E. E., Furukawa, T., Klein, A., Klimstra, D. S.*, et al.* (2006). Pathology of genetically engineered mouse models of pancreatic exocrine cancer: consensus report and recommendations. Cancer research *66*, 95-106.

Hruban, R. H., Adsay, N. V., Albores-Saavedra, J., Compton, C., Garrett, E. S., Goodman, S. N., Kern, S. E., Klimstra, D. S., Kloppel, G., Longnecker, D. S.*, et al.* (2001). Pancreatic intraepithelial neoplasia: a new nomenclature and classification system for pancreatic duct lesions. The American journal of surgical pathology *25*, 579-586.

Hruban, R. H., Goggins, M., Parsons, J., and Kern, S. E. (2000a). Progression model for pancreatic cancer. Clinical cancer research : an official journal of the American Association for Cancer Research *6*, 2969-2972.

Hruban, R. H., Takaori, K., Klimstra, D. S., Adsay, N. V., Albores-Saavedra, J., Biankin, A. V., Biankin, S. A., Compton, C., Fukushima, N., Furukawa, T.*, et al.* (2004). An illustrated consensus on the classification of pancreatic intraepithelial neoplasia and intraductal papillary mucinous neoplasms. The American journal of surgical pathology *28*, 977-987.

Hruban, R. H., Wilentz, R. E., and Kern, S. E. (2000b). Genetic progression in the pancreatic ducts. The American journal of pathology *156*, 1821-1825.

Hwang, R. F., Moore, T., Arumugam, T., Ramachandran, V., Amos, K. D., Rivera, A., Ji, B., Evans, D. B., and Logsdon, C. D. (2008). Cancer-associated stromal fibroblasts promote pancreatic tumor progression. Cancer research *68*, 918-926.

Ishii, G., Sangai, T., Oda, T., Aoyagi, Y., Hasebe, T., Kanomata, N., Endoh, Y., Okumura, C., Okuhara, Y., Magae, J., *et al.* (2003). Bone-marrow-derived myofibroblasts contribute to the cancer-induced stromal reaction. Biochemical and biophysical research communications *309*, 232-240.

Iwano, M., Plieth, D., Danoff, T. M., Xue, C., Okada, H., and Neilson, E. G. (2002). Evidence that fibroblasts derive from epithelium during tissue fibrosis. The Journal of clinical investigation *110*, 341-350.

Jackson, E. L., Willis, N., Mercer, K., Bronson, R. T., Crowley, D., Montoya, R., Jacks, T., and Tuveson, D. A. (2001). Analysis of lung tumor initiation and progression using conditional expression of oncogenic K-ras. Genes & development *15*, 3243-3248.

Jacobetz, M. A., Chan, D. S., Neesse, A., Bapiro, T. E., Cook, N., Frese, K. K., Feig, C., Nakagawa, T., Caldwell, M. E., Zecchini, H. I., *et al.* (2013). Hyaluronan impairs vascular function and drug delivery in a mouse model of pancreatic cancer. Gut *62*, 112-120.

Johnson, C., Huynh, V., Hargrove, L., Kennedy, L., Graf-Eaton, A., Owens, J., Trzeciakowski, J. P., Hodges, K., DeMorrow, S., Han, Y., *et al.* (2016). Inhibition of Mast Cell-Derived Histamine Decreases Human Cholangiocarcinoma Growth and Differentiation via c-Kit/Stem Cell Factor-Dependent Signaling. The American journal of pathology *186*, 123-133.

Jones, S., Zhang, X., Parsons, D. W., Lin, J. C., Leary, R. J., Angenendt, P., Mankoo, P., Carter, H., Kamiyama, H., Jimeno, A., *et al.* (2008). Core signaling pathways in human pancreatic cancers revealed by global genomic analyses. Science *321*, 1801-1806.

Jones, S. N., Hancock, A. R., Vogel, H., Donehower, L. A., and Bradley, A. (1998). Overexpression of Mdm2 in mice reveals a p53-independent role for Mdm2 in tumorigenesis. Proceedings of the National Academy of Sciences of the United States of America *95*, 15608-15612.

Jonkers, J., Meuwissen, R., van der Gulden, H., Peterse, H., van der Valk, M., and Berns, A. (2001). Synergistic tumor suppressor activity of BRCA2 and p53 in a conditional mouse model for breast cancer. Nature genetics *29*, 418-425.

Kalluri, R., and Zeisberg, M. (2006). Fibroblasts in cancer. Nature reviews Cancer *6*, 392-401.

Kanda, M., Matthaei, H., Wu, J., Hong, S. M., Yu, J., Borges, M., Hruban, R. H., Maitra, A., Kinzler, K., Vogelstein, B., and Goggins, M. (2012). Presence of somatic mutations in most early-stage pancreatic intraepithelial neoplasia. Gastroenterology *142*, 730-733 e739.

Karamitopoulou, E., Shoni, M., and Theoharides, T. C. (2014). Increased number of non-degranulated mast cells in pancreatic ductal adenocarcinoma but not in acute pancreatitis. Int J Immunopathol Pharmacol *27*, 213-220.

Kawaguchi, Y., Cooper, B., Gannon, M., Ray, M., MacDonald, R. J., and Wright, C. V. (2002). The role of the transcriptional regulator Ptf1a in converting intestinal to pancreatic progenitors. Nature genetics *32*, 128-134.

Kellendonk, C., Tronche, F., Casanova, E., Anlag, K., Opherk, C., and Schutz, G. (1999). Inducible site-specific recombination in the brain. Journal of molecular biology *285*, 175-182.

Kikuta, K., Masamune, A., Watanabe, T., Ariga, H., Itoh, H., Hamada, S., Satoh, K., Egawa, S., Unno, M., and Shimosegawa, T. (2010). Pancreatic stellate cells promote epithelial-mesenchymal transition in pancreatic cancer cells. Biochemical and biophysical research communications *403*, 380-384.

Kim, H. W., Lee, J. C., Paik, K. H., Lee, Y. S., Hwang, J. H., and Kim, J. (2015). Initial Metastatic Site as a Prognostic Factor in Patients With Stage IV Pancreatic Ductal Adenocarcinoma. Medicine (Baltimore) *94*, e1012.

Kim, S. K., and MacDonald, R. J. (2002). Signaling and transcriptional control of pancreatic organogenesis. Current opinion in genetics & development *12*, 540-547.

Kitamura, Y., Go, S., and Hatanaka, K. (1978). Decrease of mast cells in W/Wv mice and their increase by bone marrow transplantation. Blood *52*, 447-452.

Klein, A. P., Brune, K. A., Petersen, G. M., Goggins, M., Tersmette, A. C., Offerhaus, G. J., Griffin, C., Cameron, J. L., Yeo, C. J., Kern, S., and Hruban, R. H. (2004). Prospective risk of pancreatic cancer in familial pancreatic cancer kindreds. Cancer research *64*, 2634-2638.

Klein, S., Seidler, B., Kettenberger, A., Sibaev, A., Rohn, M., Feil, R., Allescher, H. D., Vanderwinden, J. M., Hofmann, F., Schemann, M., *et al.* (2013). Interstitial cells of Cajal integrate excitatory and inhibitory neurotransmission with intestinal slow-wave activity. Nature communications *4*, 1630.

Klimstra, D. S., and Longnecker, D. S. (1994). K-ras mutations in pancreatic ductal proliferative lesions. The American journal of pathology *145*, 1547-1550.

Korc, M. (2007). Pancreatic cancer-associated stroma production. American journal of surgery *194*, S84-86.

Kozuka, S., Sassa, R., Taki, T., Masamoto, K., Nagasawa, S., Saga, S., Hasegawa, K., and Takeuchi, M. (1979). Relation of pancreatic duct hyperplasia to carcinoma. Cancer *43*, 1418-1428.

Krapp, A., Knofler, M., Frutiger, S., Hughes, G. J., Hagenbuchle, O., and Wellauer, P. K. (1996). The p48 DNA-binding subunit of transcription factor PTF1 is a new exocrine pancreas-specific basic helix-loop-helix protein. The EMBO journal *15*, 4317-4329.

Kuhbandner, S., Brummer, S., Metzger, D., Chambon, P., Hofmann, F., and Feil, R. (2000). Temporally controlled somatic mutagenesis in smooth muscle. Genesis *28*, 15-22.

Laemmli, U. K. (1970). Cleavage of structural proteins during the assembly of the head of bacteriophage T4. Nature *227*, 680-685.

Lampiasi, N., Azzolina, A., Montalto, G., and Cervello, M. (2007). Histamine and spontaneously released mast cell granules affect the cell growth of human hepatocellular carcinoma cells. Experimental & molecular medicine *39*, 284-294.

Lee, C. L., Moding, E. J., Huang, X., Li, Y., Woodlief, L. Z., Rodrigues, R. C., Ma, Y., and Kirsch, D. G. (2012). Generation of primary tumors with Flp recombinase in FRT-flanked p53 mice. Disease models & mechanisms *5*, 397-402.

Lee, J. J., Perera, R. M., Wang, H., Wu, D. C., Liu, X. S., Han, S., Fitamant, J., Jones, P. D., Ghanta, K. S., Kawano, S., *et al.* (2014). Stromal response to Hedgehog signaling restrains pancreatic cancer progression. Proceedings of the National Academy of Sciences of the United States of America *111*, E3091-3100.

Leone, D. P., Genoud, S., Atanasoski, S., Grausenburger, R., Berger, P., Metzger, D., Macklin, W. B., Chambon, P., and Suter, U. (2003). Tamoxifen-inducible glia-specific Cre mice for somatic mutagenesis in oligodendrocytes and Schwann cells. Mol Cell Neurosci *22*, 430-440.

Li, X., Sterling, J. A., Fan, K. H., Vessella, R. L., Shyr, Y., Hayward, S. W., Matrisian, L. M., and Bhowmick, N. A. (2012). Loss of TGF-beta responsiveness in prostate stromal cells alters chemokine levels and facilitates the development of mixed osteoblastic/osteolytic bone lesions. Molecular cancer research : MCR *10*, 494-503.

Lim, K. H., Baines, A. T., Fiordalisi, J. J., Shipitsin, M., Feig, L. A., Cox, A. D., Der, C. J., and Counter, C. M. (2005). Activation of RalA is critical for Ras-induced tumorigenesis of human cells. Cancer cell *7*, 533-545.

Louvet, C., Labianca, R., Hammel, P., Lledo, G., Zampino, M. G., Andre, T., Zaniboni, A., Ducreux, M., Aitini, E., Taieb, J., *et al.* (2005). Gemcitabine in combination with oxaliplatin compared with gemcitabine alone in locally advanced or metastatic pancreatic cancer: results of a GERCOR and GISCAD phase III trial. Journal of clinical oncology : official journal of the American Society of Clinical Oncology *23*, 3509-3516.

Lowenfels, A. B., and Maisonneuve, P. (2006). Epidemiology and risk factors for pancreatic cancer. Best practice & research Clinical gastroenterology *20*, 197-209.

Lowenfels, A. B., Maisonneuve, P., Cavallini, G., Ammann, R. W., Lankisch, P. G., Andersen, J. R., Dimagno, E. P., Andren-Sandberg, A., and Domellof, L. (1993). Pancreatitis and the risk of pancreatic cancer. International Pancreatitis Study Group. The New England journal of medicine *328*, 1433-1437.

Lowery, M. A., and O'Reilly, E. M. (2015). Novel Therapeutics for Pancreatic Adenocarcinoma. Hematology/oncology clinics of North America *29*, 777-787.

Lu, J., McEachern, D., Li, S., Ellis, M. J., and Wang, S. (2016). Reactivation of p53 by MDM2 inhibitor MI-77301 for the treatment of endocrine-resistant breast cancer. Molecular cancer therapeutics.

Lu, J., Zhou, S., Siech, M., Habisch, H., Seufferlein, T., and Bachem, M. G. (2014). Pancreatic stellate cells promote hapto-migration of cancer cells through collagen I-mediated signalling pathway. British journal of cancer *110*, 409-420.

Luttges, J., Galehdari, H., Brocker, V., Schwarte-Waldhoff, I., Henne-Bruns, D., Kloppel, G., Schmiegel, W., and Hahn, S. A. (2001). Allelic loss is often the first hit in the biallelic inactivation of the p53 and DPC4 genes during pancreatic carcinogenesis. The American journal of pathology *158*, 1677-1683.

Ma, Y., Hwang, R. F., Logsdon, C. D., and Ullrich, S. E. (2013). Dynamic mast cell-stromal cell interactions promote growth of pancreatic cancer. Cancer research *73*, 3927-3937.

Madisen, L., Garner, A. R., Shimaoka, D., Chuong, A. S., Klapoetke, N. C., Li, L., van der Bourg, A., Niino, Y., Egolf, L., Monetti, C.*, et al.* (2015). Transgenic mice for intersectional targeting of neural sensors and effectors with high specificity and performance. Neuron *85*, 942-958.

Maitra, A., Fukushima, N., Takaori, K., and Hruban, R. H. (2005). Precursors to invasive pancreatic cancer. Advances in anatomic pathology *12*, 81-91.

Malumbres, M., and Barbacid, M. (2003). RAS oncogenes: the first 30 years. Nature reviews Cancer *3*, 459-465.

Mantoni, T. S., Schendel, R. R., Rodel, F., Niedobitek, G., Al-Assar, O., Masamune, A., and Brunner, T. B. (2008). Stromal SPARC expression and patient survival after chemoradiation for non-resectable pancreatic adenocarcinoma. Cancer Biol Ther *7*, 1806-1815.

Marino, S., Vooijs, M., van Der Gulden, H., Jonkers, J., and Berns, A. (2000). Induction of medulloblastomas in p53-null mutant mice by somatic inactivation of Rb in the external granular layer cells of the cerebellum. Genes & development *14*, 994-1004.

Masamune, A., Kikuta, K., Watanabe, T., Satoh, K., Hirota, M., and Shimosegawa, T. (2008). Hypoxia stimulates pancreatic stellate cells to induce fibrosis and angiogenesis in pancreatic cancer. American journal of physiology Gastrointestinal and liver physiology *295*, G709-717.

Massague, J., Blain, S. W., and Lo, R. S. (2000). TGFbeta signaling in growth control, cancer, and heritable disorders. Cell *103*, 295-309.

Masso-Valles, D., Jauset, T., Serrano, E., Sodir, N. M., Pedersen, K., Affara, N. I., Whitfield, J. R., Beaulieu, M. E., Evan, G. I., Elias, L.*, et al.* (2015). Ibrutinib exerts potent antifibrotic and antitumor activities in mouse models of pancreatic adenocarcinoma. Cancer research *75*, 1675-1681.

McAllister, S. S., and Weinberg, R. A. (2014). The tumour-induced systemic environment as a critical regulator of cancer progression and metastasis. Nature cell biology *16*, 717-727.

McKay, C. J., Glen, P., and McMillan, D. C. (2008). Chronic inflammation and pancreatic cancer. Best practice & research Clinical gastroenterology *22*, 65-73.

Metzger, D., Clifford, J., Chiba, H., and Chambon, P. (1995). Conditional site-specific recombination in mammalian cells using a ligand-dependent chimeric Cre recombinase. Proceedings of the National Academy of Sciences of the United States of America *92*, 6991-6995.

Micke, P., Basrai, M., Faldum, A., Bittinger, F., Ronnstrand, L., Blaukat, A., Beeh, K. M., Oesch, F., Fischer, B., Buhl, R., and Hengstler, J. G. (2003). Characterization of c-kit expression in small cell lung cancer: prognostic and therapeutic implications. Clinical cancer research : an official journal of the American Association for Cancer Research *9*, 188-194.

Moir, J. A., Mann, J., and White, S. A. (2015). The role of pancreatic stellate cells in pancreatic cancer. Surgical oncology *24*, 232-238.

Moore, M. J., Goldstein, D., Hamm, J., Figer, A., Hecht, J. R., Gallinger, S., Au, H. J., Murawa, P., Walde, D., Wolff, R. A.*, et al.* (2007). Erlotinib plus gemcitabine compared with gemcitabine alone in patients with advanced pancreatic cancer: a phase III trial of the National Cancer Institute of Canada Clinical Trials Group. Journal of clinical oncology : official journal of the American Society of Clinical Oncology *25*, 1960-1966.

Moore, M. J., Hamm, J., Dancey, J., Eisenberg, P. D., Dagenais, M., Fields, A., Hagan, K., Greenberg, B., Colwell, B., Zee, B.*, et al.* (2003). Comparison of gemcitabine versus the matrix metalloproteinase inhibitor BAY 12-9566 in patients with advanced or metastatic adenocarcinoma of the pancreas: a phase III trial of the National Cancer Institute of Canada Clinical Trials Group. Journal of clinical oncology : official journal of the American Society of Clinical Oncology *21*, 3296-3302.

Muzumdar, M. D., Tasic, B., Miyamichi, K., Li, L., and Luo, L. (2007). A global double-fluorescent Cre reporter mouse. Genesis *45*, 593-605.

Nagathihalli, N. S., Castellanos, J. A., Shi, C., Beesetty, Y., Reyzer, M. L., Caprioli, R., Chen, X., Walsh, A. J., Skala, M. C., Moses, H. L., and Merchant, N. B. (2015). Signal Transducer and Activator of Transcription 3, Mediated Remodeling of the Tumor Microenvironment Results in Enhanced Tumor Drug Delivery in a Mouse Model of Pancreatic Cancer. Gastroenterology *149*, 1932-1943 e1939.

Neesse, A., Algul, H., Tuveson, D. A., and Gress, T. M. (2015). Stromal biology and therapy in pancreatic cancer: a changing paradigm. Gut *64*, 1476-1484.

Neesse, A., Krug, S., Gress, T. M., Tuveson, D. A., and Michl, P. (2013). Emerging concepts in pancreatic cancer medicine: targeting the tumor stroma. OncoTargets and therapy *7*, 33-43.

Neesse, A., Michl, P., Frese, K. K., Feig, C., Cook, N., Jacobetz, M. A., Lolkema, M. P., Buchholz, M., Olive, K. P., Gress, T. M., and Tuveson, D. A. (2011). Stromal biology and therapy in pancreatic cancer. Gut *60*, 861-868.

Nishitani, Y., Iwano, M., Yamaguchi, Y., Harada, K., Nakatani, K., Akai, Y., Nishino, T., Shiiki, H., Kanauchi, M., Saito, Y., and Neilson, E. G. (2005). Fibroblast-specific protein 1 is a specific prognostic marker for renal survival in patients with IgAN. Kidney international *68*, 1078-1085.

Offield, M. F., Jetton, T. L., Labosky, P. A., Ray, M., Stein, R. W., Magnuson, M. A., Hogan, B. L., and Wright, C. V. (1996). PDX-1 is required for pancreatic outgrowth and differentiation of the rostral duodenum. Development *122*, 983-995.

Oft, M., Heider, K. H., and Beug, H. (1998). TGFbeta signaling is necessary for carcinoma cell invasiveness and metastasis. Current biology : CB *8*, 1243-1252.

Olive, K. P., Jacobetz, M. A., Davidson, C. J., Gopinathan, A., McIntyre, D., Honess, D., Madhu, B., Goldgraben, M. A., Caldwell, M. E., Allard, D*., et al.* (2009). Inhibition of Hedgehog signaling enhances delivery of chemotherapy in a mouse model of pancreatic cancer. Science *324*, 1457-1461.

Omary, M. B., Lugea, A., Lowe, A. W., and Pandol, S. J. (2007). The pancreatic stellate cell: a star on the rise in pancreatic diseases. The Journal of clinical investigation *117*, 50-59.

Orban, P. C., Chui, D., and Marth, J. D. (1992). Tissue- and site-specific DNA recombination in transgenic mice. Proceedings of the National Academy of Sciences of the United States of America *89*, 6861-6865.

Osterreicher, C. H., Penz-Osterreicher, M., Grivennikov, S. I., Guma, M., Koltsova, E. K., Datz, C., Sasik, R., Hardiman, G., Karin, M., and Brenner, D. A. (2011). Fibroblast-specific protein 1 identifies an inflammatory subpopulation of macrophages in the liver. Proceedings of the National Academy of Sciences of the United States of America *108*, 308-313.

Otranto, M., Sarrazy, V., Bonte, F., Hinz, B., Gabbiani, G., and Desmouliere, A. (2012). The role of the myofibroblast in tumor stroma remodeling. Cell adhesion & migration *6*, 203-219.

Ozdemir, B. C., Pentcheva-Hoang, T., Carstens, J. L., Zheng, X., Wu, C. C., Simpson, T. R., Laklai, H., Sugimoto, H., Kahlert, C., Novitskiy, S. V*., et al.* (2014). Depletion of carcinoma-associated fibroblasts and fibrosis induces immunosuppression and accelerates pancreas cancer with reduced survival. Cancer cell *25*, 719-734.

Pandol, S. J., and Edderkaoui, M. (2015). What are the macrophages and stellate cells doing in pancreatic adenocarcinoma? Frontiers in physiology *6*, 125.

Pasca di Magliano, M., and Hebrok, M. (2003). Hedgehog signalling in cancer formation and maintenance. Nature reviews Cancer *3*, 903-911.

Phillips, P. A., McCarroll, J. A., Park, S., Wu, M. J., Pirola, R., Korsten, M., Wilson, J. S., and Apte, M. V. (2003). Rat pancreatic stellate cells secrete matrix metalloproteinases: implications for extracellular matrix turnover. Gut *52*, 275-282.

Polanska, U. M., and Orimo, A. (2013). Carcinoma-associated fibroblasts: non-neoplastic tumour-promoting mesenchymal cells. Journal of cellular physiology *228*, 1651-1657.

Poplin, E., Feng, Y., Berlin, J., Rothenberg, M. L., Hochster, H., Mitchell, E., Alberts, S., O'Dwyer, P., Haller, D., Catalano, P*., et al.* (2009). Phase III, randomized study of gemcitabine and oxaliplatin versus gemcitabine (fixed-dose rate infusion) compared with gemcitabine (30-minute infusion) in patients with pancreatic carcinoma E6201: a trial of the Eastern Cooperative Oncology Group. Journal of clinical oncology : official journal of the American Society of Clinical Oncology *27*, 3778-3785.

Provenzano, P. P., Cuevas, C., Chang, A. E., Goel, V. K., Von Hoff, D. D., and Hingorani, S. R. (2012). Enzymatic targeting of the stroma ablates physical barriers to treatment of pancreatic ductal adenocarcinoma. Cancer cell *21*, 418-429.

Quante, M., Tu, S. P., Tomita, H., Gonda, T., Wang, S. S., Takashi, S., Baik, G. H., Shibata, W., Diprete, B., Betz, K. S*., et al.* (2011). Bone marrow-derived myofibroblasts contribute to the mesenchymal stem cell niche and promote tumor growth. Cancer cell *19*, 257-272.

Rahib, L., Smith, B. D., Aizenberg, R., Rosenzweig, A. B., Fleshman, J. M., and Matrisian, L. M. (2014). Projecting cancer incidence and deaths to 2030: the unexpected burden of thyroid, liver, and pancreas cancers in the United States. Cancer research *74*, 2913-2921.

Rajput, A. B., Turbin, D. A., Cheang, M. C., Voduc, D. K., Leung, S., Gelmon, K. A., Gilks, C. B., and Huntsman, D. G. (2008). Stromal mast cells in invasive breast cancer are a marker of favourable prognosis: a study of 4,444 cases. Breast cancer research and treatment *107*, 249-257.

Redston, M. S., Caldas, C., Seymour, A. B., Hruban, R. H., da Costa, L., Yeo, C. J., and Kern, S. E. (1994). p53 mutations in pancreatic carcinoma and evidence of common involvement of homocopolymer tracts in DNA microdeletions. Cancer research *54*, 3025-3033.

Reichert, M., and Rustgi, A. K. (2011). Pancreatic ductal cells in development, regeneration, and neoplasia. The Journal of clinical investigation *121*, 4572-4578.

Rhim, A. D., Mirek, E. T., Aiello, N. M., Maitra, A., Bailey, J. M., McAllister, F., Reichert, M., Beatty, G. L., Rustgi, A. K., Vonderheide, R. H., *et al.* (2012). EMT and dissemination precede pancreatic tumor formation. Cell *148*, 349-361.

Rhim, A. D., Oberstein, P. E., Thomas, D. H., Mirek, E. T., Palermo, C. F., Sastra, S. A., Dekleva, E. N., Saunders, T., Becerra, C. P., Tattersall, I. W., *et al.* (2014). Stromal elements act to restrain, rather than support, pancreatic ductal adenocarcinoma. Cancer cell *25*, 735-747.

Riley, T., Sontag, E., Chen, P., and Levine, A. (2008). Transcriptional control of human p53-regulated genes. Nature reviews Molecular cell biology *9*, 402-412.

Rodemann, H. P., and Muller, G. A. (1991). Characterization of human renal fibroblasts in health and disease: II. In vitro growth, differentiation, and collagen synthesis of fibroblasts from kidneys with interstitial fibrosis. American journal of kidney diseases : the official journal of the National Kidney Foundation *17*, 684-686.

Rodewald, H. R., and Feyerabend, T. B. (2012). Widespread immunological functions of mast cells: fact or fiction? Immunity *37*, 13-24.

Ronnov-Jessen, L., and Petersen, O. W. (1993). Induction of alpha-smooth muscle actin by transforming growth factor-beta 1 in quiescent human breast gland fibroblasts. Implications for myofibroblast generation in breast neoplasia. Laboratory investigation; a journal of technical methods and pathology *68*, 696-707.

Ronnov-Jessen, L., Petersen, O. W., and Bissell, M. J. (1996). Cellular changes involved in conversion of normal to malignant breast: importance of the stromal reaction. Physiological reviews *76*, 69-125.

Rozenblum, E., Schutte, M., Goggins, M., Hahn, S. A., Panzer, S., Zahurak, M., Goodman, S. N., Sohn, T. A., Hruban, R. H., Yeo, C. J., and Kern, S. E. (1997). Tumor-suppressive pathways in pancreatic carcinoma. Cancer research *57*, 1731-1734.

Samoszuk, M., Kanakubo, E., and Chan, J. K. (2005). Degranulating mast cells in fibrotic regions of human tumors and evidence that mast cell heparin interferes with the growth of tumor cells through a mechanism involving fibroblasts. BMC cancer *5*, 121.

Santos, A. M., Jung, J., Aziz, N., Kissil, J. L., and Pure, E. (2009). Targeting fibroblast activation protein inhibits tumor stromagenesis and growth in mice. The Journal of clinical investigation *119*, 3613-3625.

Schmitt, C. A., Fridman, J. S., Yang, M., Lee, S., Baranov, E., Hoffman, R. M., and Lowe, S. W. (2002). A senescence program controlled by p53 and p16INK4a contributes to the outcome of cancer therapy. Cell *109*, 335-346.

Schneider, G., Siveke, J. T., Eckel, F., and Schmid, R. M. (2005). Pancreatic Cancer: Basic and Clinical Aspects. Gastroenterology *128*, 1606-1625.

Schonhuber, N., Seidler, B., Schuck, K., Veltkamp, C., Schachtler, C., Zukowska, M., Eser, S., Feyerabend, T. B., Paul, M. C., Eser, P., *et al.* (2014). A next-generation dual-recombinase system for time- and host-specific targeting of pancreatic cancer. Nature medicine *20*, 1340-1347.

Sclafani, F., Iyer, R., Cunningham, D., and Starling, N. (2015). Management of metastatic pancreatic cancer: Current treatment options and potential new therapeutic targets. Critical reviews in oncology/hematology *95*, 318-336.

Selivanova, G. (2014). Wild type p53 reactivation: from lab bench to clinic. FEBS Lett *588*, 2628-2638.

Shen, Z., Li, C., Frieler, R. A., Gerasimova, A. S., Lee, S. J., Wu, J., Wang, M. M., Lumeng, C. N., Brosius, F. C., 3rd, Duan, S. Z., and Mortensen, R. M. (2012). Smooth muscle protein 22 alpha-Cre is expressed in myeloid cells in mice. Biochemical and biophysical research communications *422*, 639-642.

Sherman, M. H., Yu, R. T., Engle, D. D., Ding, N., Atkins, A. R., Tiriac, H., Collisson, E. A., Connor, F., Van Dyke, T., Kozlov, S., *et al.* (2014). Vitamin d receptor-mediated stromal reprogramming suppresses pancreatitis and enhances pancreatic cancer therapy. Cell *159*, 80-93.

Shi, C., Klein, A. P., Goggins, M., Maitra, A., Canto, M., Ali, S., Schulick, R., Palmisano, E., and Hruban, R. H. (2009). Increased Prevalence of Precursor Lesions in Familial Pancreatic Cancer Patients. Clinical cancer research : an official journal of the American Association for Cancer Research *15*, 7737-7743.

Shiga, K., Hara, M., Nagasaki, T., Sato, T., Takahashi, H., and Takeyama, H. (2015). Cancer-Associated Fibroblasts: Their Characteristics and Their Roles in Tumor Growth. Cancers *7*, 2443-2458.

Shu, H. K., Kim, M. M., Chen, P., Furman, F., Julin, C. M., and Israel, M. A. (1998). The intrinsic radioresistance of glioblastoma-derived cell lines is associated with a failure of p53 to induce p21(BAX) expression. Proceedings of the National Academy of Sciences of the United States of America *95*, 14453-14458.

Siegel, P. M., and Massague, J. (2003). Cytostatic and apoptotic actions of TGF-beta in homeostasis and cancer. Nature reviews Cancer *3*, 807-821.

Siegel, R. L., Miller, K. D., and Jemal, A. (2015). Cancer statistics, 2015. CA: a cancer journal for clinicians *65*, 5-29.

Sinnamon, M. J., Carter, K. J., Sims, L. P., Lafleur, B., Fingleton, B., and Matrisian, L. M. (2008). A protective role of mast cells in intestinal tumorigenesis. Carcinogenesis *29*, 880-886.

Smith, B. N., and Bhowmick, N. A. (2016). Role of EMT in Metastasis and Therapy Resistance. Journal of clinical medicine *5*.

Soucek, L., Lawlor, E. R., Soto, D., Shchors, K., Swigart, L. B., and Evan, G. I. (2007). Mast cells are required for angiogenesis and macroscopic expansion of Myc-induced pancreatic islet tumors. Nature medicine *13*, 1211-1218.

Stoker, M. G., Shearer, M., and O'Neill, C. (1966). Growth inhibition of polyoma-transformed cells by contact with static normal fibroblasts. Journal of cell science *1*, 297-310.

Stolzenberg-Solomon, R. Z., Graubard, B. I., Chari, S., Limburg, P., Taylor, P. R., Virtamo, J., and Albanes, D. (2005). Insulin, glucose, insulin resistance, and pancreatic cancer in male smokers. Jama *294*, 2872-2878.

Stolzenberg-Solomon, R. Z., Pietinen, P., Barrett, M. J., Taylor, P. R., Virtamo, J., and Albanes, D. (2001). Dietary and other methyl-group availability factors and pancreatic cancer risk in a cohort of male smokers. American journal of epidemiology *153*, 680-687.

Strobel, O., Dor, Y., Alsina, J., Stirman, A., Lauwers, G., Trainor, A., Castillo, C. F., Warshaw, A. L., and Thayer, S. P. (2007). In vivo lineage tracing defines the role of acinar-to-ductal transdifferentiation in inflammatory ductal metaplasia. Gastroenterology *133*, 1999-2009.

Strouch, M. J., Cheon, E. C., Salabat, M. R., Krantz, S. B., Gounaris, E., Melstrom, L. G., Dangi-Garimella, S., Wang, E., Munshi, H. G., Khazaie, K., and Bentrem, D. J. (2010). Crosstalk between mast cells and pancreatic cancer cells contributes to pancreatic tumor progression. Clinical cancer research : an official journal of the American Association for Cancer Research *16*, 2257-2265.

Strutz, F., Okada, H., Lo, C. W., Danoff, T., Carone, R. L., Tomaszewski, J. E., and Neilson, E. G. (1995). Identification and characterization of a fibroblast marker: FSP1. J Cell Biol *130*, 393-405.

Sugimoto, H., Mundel, T. M., Kieran, M. W., and Kalluri, R. (2006). Identification of fibroblast heterogeneity in the tumor microenvironment. Cancer Biol Ther *5*, 1640-1646.

Taeger, J., Moser, C., Hellerbrand, C., Mycielska, M. E., Glockzin, G., Schlitt, H. J., Geissler, E. K., Stoeltzing, O., and Lang, S. A. (2011). Targeting FGFR/PDGFR/VEGFR impairs tumor growth, angiogenesis, and metastasis by effects on tumor cells, endothelial cells, and pericytes in pancreatic cancer. Molecular cancer therapeutics *10*, 2157-2167.

Thayer, S. P., di Magliano, M. P., Heiser, P. W., Nielsen, C. M., Roberts, D. J., Lauwers, G. Y., Qi, Y. P., Gysin, S., Fernandez-del Castillo, C., Yajnik, V.*, et al.* (2003). Hedgehog is an early and late mediator of pancreatic cancer tumorigenesis. Nature *425*, 851-856.

Theoharides, T. C. (2008). Mast cells and pancreatic cancer. The New England journal of medicine *358*, 1860-1861.

Tian, H., Callahan, C. A., DuPree, K. J., Darbonne, W. C., Ahn, C. P., Scales, S. J., and de Sauvage, F. J. (2009). Hedgehog signaling is restricted to the stromal compartment during pancreatic carcinogenesis. Proceedings of the National Academy of Sciences of the United States of America *106*, 4254-4259.

Tinge, B., Molin, D., Bergqvist, M., Ekman, S., and Bergstrom, S. (2010). Mast cells in squamous cell esophageal carcinoma and clinical parameters. Cancer genomics & proteomics *7*, 25-29.

Towbin, H., Staehelin, T., and Gordon, J. (1979). Electrophoretic transfer of proteins from polyacrylamide gels to nitrocellulose sheets: procedure and some applications. Proceedings of the National Academy of Sciences of the United States of America *76*, 4350-4354.

Tsutsumi, R., Xie, C., Wei, X., Zhang, M., Zhang, X., Flick, L. M., Schwarz, E. M., and O'Keefe, R. J. (2009). PGE2 signaling through the EP4 receptor on fibroblasts upregulates RANKL and stimulates osteolysis. Journal of bone and mineral research : the official journal of the American Society for Bone and Mineral Research *24*, 1753-1762.

van Heek, N. T., Meeker, A. K., Kern, S. E., Yeo, C. J., Lillemoe, K. D., Cameron, J. L., Offerhaus, G. J., Hicks, J. L., Wilentz, R. E., Goggins, M. G.*, et al.* (2002). Telomere shortening is nearly universal in pancreatic intraepithelial neoplasia. The American journal of pathology *161*, 1541-1547.

Ventura, A., Kirsch, D. G., McLaughlin, M. E., Tuveson, D. A., Grimm, J., Lintault, L., Newman, J., Reczek, E. E., Weissleder, R., and Jacks, T. (2007). Restoration of p53 function leads to tumour regression in vivo. Nature *445*, 661-665.

Vincent, A., Herman, J., Schulick, R., Hruban, R. H., and Goggins, M. (2011). Pancreatic cancer. Lancet *378*, 607-620.

Von Hoff, D. D., Ervin, T., Arena, F. P., Chiorean, E. G., Infante, J., Moore, M., Seay, T., Tjulandin, S. A., Ma, W. W., Saleh, M. N.*, et al.* (2013). Increased survival in pancreatic cancer with nab-paclitaxel plus gemcitabine. The New England journal of medicine *369*, 1691-1703.

Vonlaufen, A., Joshi, S., Qu, C., Phillips, P. A., Xu, Z., Parker, N. R., Toi, C. S., Pirola, R. C., Wilson, J. S., Goldstein, D., and Apte, M. V. (2008). Pancreatic stellate cells: partners in crime with pancreatic cancer cells. Cancer research *68*, 2085-2093.

Waddell, N., Pajic, M., Patch, A. M., Chang, D. K., Kassahn, K. S., Bailey, P., Johns, A. L., Miller, D., Nones, K., Quek, K.*, et al.* (2015). Whole genomes redefine the mutational landscape of pancreatic cancer. Nature *518*, 495-501.

Weissmueller, S., Manchado, E., Saborowski, M., Morris, J. P. t., Wagenblast, E., Davis, C. A., Moon, S. H., Pfister, N. T., Tschaharganeh, D. F., Kitzing, T., *et al.* (2014). Mutant p53 drives pancreatic cancer metastasis through cell-autonomous PDGF receptor beta signaling. Cell *157*, 382-394.

Wendling, O., Bornert, J. M., Chambon, P., and Metzger, D. (2009). Efficient temporally-controlled targeted mutagenesis in smooth muscle cells of the adult mouse. Genesis *47*, 14-18.

Wilentz, R. E., Geradts, J., Maynard, R., Offerhaus, G. J., Kang, M., Goggins, M., Yeo, C. J., Kern, S. E., and Hruban, R. H. (1998). Inactivation of the p16 (INK4A) tumor-suppressor gene in pancreatic duct lesions: loss of intranuclear expression. Cancer research *58*, 4740-4744.

Wilentz, R. E., Iacobuzio-Donahue, C. A., Argani, P., McCarthy, D. M., Parsons, J. L., Yeo, C. J., Kern, S. E., and Hruban, R. H. (2000). Loss of expression of Dpc4 in pancreatic intraepithelial neoplasia: evidence that DPC4 inactivation occurs late in neoplastic progression. Cancer research *60*, 2002-2006.

Witkiewicz, A. K., McMillan, E. A., Balaji, U., Baek, G., Lin, W. C., Mansour, J., Mollaee, M., Wagner, K. U., Koduru, P., Yopp, A., *et al.* (2015). Whole-exome sequencing of pancreatic cancer defines genetic diversity and therapeutic targets. Nature communications *6*, 6744.

Wolpin, B. M., Chan, A. T., Hartge, P., Chanock, S. J., Kraft, P., Hunter, D. J., Giovannucci, E. L., and Fuchs, C. S. (2009). ABO blood group and the risk of pancreatic cancer. Journal of the National Cancer Institute *101*, 424-431.

Xu, Z., Pothula, S. P., Wilson, J. S., and Apte, M. V. (2014). Pancreatic cancer and its stroma: a conspiracy theory. World journal of gastroenterology : WJG *20*, 11216-11229.

Xue, W., Zender, L., Miething, C., Dickins, R. A., Hernando, E., Krizhanovsky, V., Cordon-Cardo, C., and Lowe, S. W. (2007). Senescence and tumour clearance is triggered by p53 restoration in murine liver carcinomas. Nature *445*, 656-660.

Yamano, M., Fujii, H., Takagaki, T., Kadowaki, N., Watanabe, H., and Shirai, T. (2000). Genetic progression and divergence in pancreatic carcinoma. The American journal of pathology *156*, 2123-2133.

Yasuda, A., Sawai, H., Takahashi, H., Ochi, N., Matsuo, Y., Funahashi, H., Sato, M., Okada, Y., Takeyama, H., and Manabe, T. (2006). The stem cell factor/c-kit receptor pathway enhances proliferation and invasion of pancreatic cancer cells. Molecular cancer *5*, 46.

Zavoral, M., Minarikova, P., Zavada, F., Salek, C., and Minarik, M. (2011). Molecular biology of pancreatic cancer. World journal of gastroenterology : WJG *17*, 2897-2908.

Zeisberg, E. M., Potenta, S., Xie, L., Zeisberg, M., and Kalluri, R. (2007). Discovery of endothelial to mesenchymal transition as a source for carcinoma-associated fibroblasts. Cancer research *67*, 10123-10128.

Zhang, J., Zhong, W., Cui, T., Yang, M., Hu, X., Xu, K., Xie, C., Xue, C., Gibbons, G. H., Liu, C., *et al.* (2006). Generation of an adult smooth muscle cell-targeted Cre recombinase mouse model. Arteriosclerosis, thrombosis, and vascular biology *26*, e23-24.

Zhang, Y., Riesterer, C., Ayrall, A. M., Sablitzky, F., Littlewood, T. D., and Reth, M. (1996). Inducible site-directed recombination in mouse embryonic stem cells. Nucleic acids research *24*, 543-548.

Zheng, B., Zhang, Z., Black, C. M., de Crombrugghe, B., and Denton, C. P. (2002). Ligand-dependent genetic recombination in fibroblasts : a potentially powerful technique for investigating gene function in fibrosis. The American journal of pathology *160*, 1609-1617.

Zhu, X., Hill, R. A., Dietrich, D., Komitova, M., Suzuki, R., and Nishiyama, A. (2011). Age-dependent fate and lineage restriction of single NG2 cells. Development *138*, 745-753.

Zhu, X. D., Pan, G., Luetke, K., and Sadowski, P. D. (1995). Homology requirements for ligation and strand exchange by the FLP recombinase. The Journal of biological chemistry *270*, 11646-11653.

Zhuo, L., Theis, M., Alvarez-Maya, I., Brenner, M., Willecke, K., and Messing, A. (2001). hGFAP-cre transgenic mice for manipulation of glial and neuronal function in vivo. Genesis *31*, 85-94.

Zimnoch, L., Szynaka, B., and Puchalski, Z. (2002). Mast cells and pancreatic stellate cells in chronic pancreatitis with differently intensified fibrosis. Hepatogastroenterology *49*, 1135-1138.

9 ACKNOWLEDGEMENT

First of all, I want to thank Prof. Roland M. Schmid for giving me the opportunity to do my PhD research in his department, the II. Medizinische Klinik at Klinikum rechts der Isar.

Above all, I thank Prof. Dieter Saur for giving me the opportunity to perform my PhD research in his group. By proposing such an exciting, interesting, and promising project to me and by his support of me and my project, he contributed to the successful outcome of my dissertation.

I am very grateful to Prof. Angelika Schnieke for being my second advisor. Furthermore, I thank Dr. Günter Schneider for being my mentor during my PhD research. Also, I want to thank both of them for their outstanding scientific input and fruitful discussions.

I am thankful to all members of the Saur, Schneider, Rad and Reichert groups for the great working atmosphere in the lab, their constant help and support throughout the years. I would like to thank Barbara Seidler for her scientific contribution and for sharing her methodical knowledge, especially concerning cloning, with me. I further thank Juliana Götzfried and Magdalena Zukowska for their excellent technical support.

For critical reading, giving suggestions and corrections of my thesis manuscript I want to thank Dr. Mariel Paul which contributed to completion of this work.

Finally, I want to thank all my friends and my family for their support. I especially want to thank my husband Sebastian for his support and advice, his patience and help during the last years. Without him and my friends and my family, my dissertation would not have been possible.